Journal of the
OPTICAL SOCIETY *of* AMERICA

VOLUME 35; NUMBER 11 NOVEMBER, 1945

A Photoelectric Instrument for Direct Spectrochemical Analysis

J. L. SAUNDERSON, V. J. CALDECOURT, AND E. W. PETERSON
The Dow Chemical Company, Midland, Michigan

(Received September 4, 1945)

A direct reading spectrometer for spectrochemical analysis, combining great speed, simplicity of operation, and exceptionally good analytical results, is described. The grating spectrometer is equipped with eleven electron multiplier photo-tubes allowing the determination of ten elements using the internal standard method. The light intensities are integrated over a sparking period of 20 seconds by storing the photo-currents in suitable condensers. Direct-current amplifiers of novel design perform the function of measuring the stored charges, and the results are recorded on a strip chart of electrical marking paper. A method is discussed for making a background correction which materially increases the sensitivity and accuracy for trace elements. Analytical results having a standard deviation of the order of 2 percent of the amount present on alloying constituents are regularly obtained by routine operators.

INTRODUCTION

THE direct reading spectrometer herein described has been in use for nearly one year in a commercial alloy plant producing magnesium alloys. The instrument was installed in an air-conditioned laboratory directly in the alloy plant in order to make routine analytical determinations on the composition of the metal during the alloying process. Samples are currently run at the rate of about 4000 per month, representing roughly 20,000 quantitative determinations. The apparatus is operated entirely with non-technical personnel, and the analytical results are equal and in some cases superior to those obtained with conventional photographic methods. The operation of the instrument is completely automatic from the time the sample electrodes are loaded into the clamps until a record is obtained (forty seconds later) from which the analysis for seven elements can be read with the aid of calibrated scales.

FUNDAMENTALS OF THE METHOD

A simplified description of the method may be given by reference to Fig. 1. Light from a spark passing between the two electrodes of the sample being analyzed enters the spectrometer through the entrance slit and falls on a concave grating. The concave grating forms images of the entrance slit along the Rowland circle, the positions of the images being dependent upon the wave-lengths present in the incident light. Exit slits appropriately located permit the spectral lines thus formed to fall upon light sensitive tubes. In Fig. 1, one line is considered as arising from an element in the sample for which a quantitative analysis is desired, and the other line is ascribed to the internal standard element.

During the time the sample is being sparked, the condensers C_1 and C_2 are charged with the photo-currents resulting from the light intensities of the two spectral lines. After the spark excitation period, the switches *Sw* are closed simul-

BOSTON UNIVERSITY
COLLEGE OF LIBERAL ARTS
LIBRARY

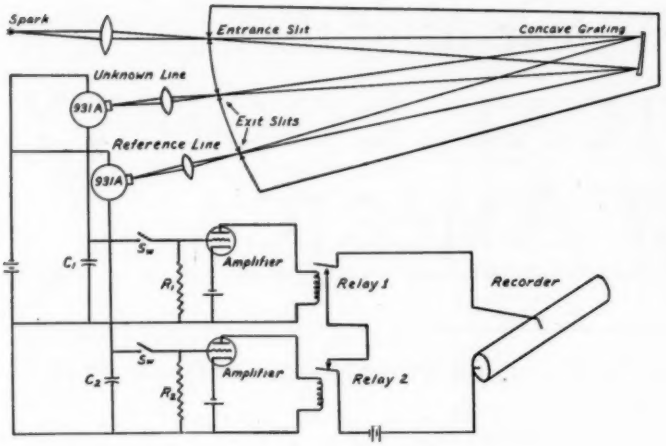

FIG. 1. Simplified schematic diagram illustrating the method of operation of the direct reading spectrometer.

taneously and the condensers discharge slowly through the resistances R_1 and R_2. The grids of the triodes, intended schematically to represent d.c. amplifiers, follow the voltage on the discharging condensers. Each d.c. amplifier is set to operate the plate relay when the potential of the grid falls to some small voltage, for example, one volt. The initial voltage on C_2 is arranged to be greater than that on C_1, so that upon discharging, the potential of C_1 reaches one volt before that of C_2. If relay *2* is normally closed and relay *1* normally open, the recorder circuit is closed when the voltage of C_1 reaches one volt and is opened again when the voltage of C_2 reaches one volt. Thus a strip of recording paper moving at uniform speed will contain a line whose length is proportional to the difference in time required for the two condensers to discharge from their initial voltage down to the same small voltage. As shown below, this difference in time, Δt, is a measure of the relative intensity of the two spectral lines, and hence can be used for calibration with the percent of the unknown element in the sample being analyzed.

The discharge of a condenser of capacity C through a resistance R is described by the equation

$$E = E_0 e^{-t/RC},$$

where E_0 is the initial voltage and E is the voltage at any time t. Considering two condensers C_1 and C_2, having initial voltages E_1 and E_2, and discharging through the resistances R_1 and R_2, the time required for each condenser to reach a voltage E_s is

$$t_1 = R_1 C_1 \log E_1/E_s,$$

$$t_2 = R_2 C_2 \log E_2/E_s.$$

If $R_1C_1 = R_2C_2 = RC$, and $t_2 - t_1 = \Delta t$, then

$$\Delta t = RC \log E_2/E_1.$$

The initial voltages E_1, E_2 are proportional to the original charges Q_1, Q_2, which are in turn proportional to the light intensities I_1, I_2 of the two spectral lines averaged over the sparking period. Thus

$$\Delta t = RC \log (I_2/I_1) + K,$$

indicating that a plot of Δt *vs.* $\log I_2/I_1$ is a straight line of slope RC and intercept K. An empirical plot of Δt *vs.* the log of the concentration of an unknown element thus gives an approximately linear calibration curve.

The fact that Δt is proportional to the logarithm of the relative intensities, thus resulting in approximately logarithmic concentration scales, has several inherent advantages. In the first place, the spectrochemical method in general tends to have a rather constant relative accuracy for the quantitative determination of an element over a fairly wide range of concentration. For example, the absolute error in the determination of an element at 10 percent concentration is in general about ten times as great as the absolute error at 1 percent concentration. A logarithmic scale is similar in this respect, since it may be

read with constant relative accuracy over the entire scale. The use of a logarithmic working curve according to the method described above is particularly advantageous from the standpoint of standardization of the analytical results. It is evident from the above equations that all proportionality factors fall in the constant K. Thus a change in the sensitivity of a photo-tube or dirt collected in the optical path will shift the calibration curve parallel to itself but will not change the slope. Standardization is therefore possible by running only one standard, and the same calibration curve, or a projection of it in the form of a calibrated scale, can be used indefinitely.

Variations of the total intensity of the spark and variations in the time of sparking, which do not affect the integrated relative intensity of the spectral lines, have no effect upon Δt. The internal standard method so well-known in the field of photographic spectrochemical work is retained in the electrical method for these reasons.

Preliminary work done on this project using a bridge method for the determination of the relative intensity of two spectral lines[1] of two different elements was disappointing. Electrodes of a magnesium alloy were used with the ordinary type high voltage condensed spark. With a galvanometer having a two-second period to balance the bridge, it was found that the variation in the relative intensity of the two spectral lines was too great to permit a sufficiently accurate balance to be made. In view of this work, the method just described for integrating the light intensities over a larger sparking period was adopted.

OPTICAL DETAILS

The grating frame and housing was specially designed for this application, and was supplied by Baird Associates with a two-meter 15,000-line per inch aluminized grating. The grating was ruled such that the light is concentrated in one first order near 3000 Angstroms, and has a ruled area about $1\frac{1}{2}\times 3\frac{1}{2}$ inches. The wave-length range accessible is from 2000 to 5500 Angstroms in the first order, with a dispersion of about 8 Angstroms per millimeter. The instrument has a fairly airtight case and has an internal heater, fan, and thermostat. The inside temperature is maintained at 90 ± 2 degrees F. With the instrument mounted on a solid block of concrete, the position of the spectral lines at the exit slits is constant to within 0.01 mm. In spite of the fact that the instrument is in a location subject to almost continuous vibration and numerous heavy jars, no precautions in this respect have been required.

Light from the spark is focused on the grating with an external condensing lens mounted about 8 inches in front of the 0.1-mm entrance slit. The exit slits were made up singly, or in small groups when several spectral lines fell close together, and were mounted over holes cut in a brass plate bent along the focal curve. The alignment of the exit slits with respect to the positions of the spectral lines was done photographically by exposing the film both to the line and to a small tungsten light located near the position of the grating. Figure 2 shows two arrangements used for the exit slits, depending upon whether a background correction is required for any particular line. Whenever a strong line, well above background, was available, the exit slit was made twice as wide as the entrance slit, or 0.2 mm, and the line was centered in the slit. There is thus a 0.05-mm tolerance on either side of the line, as shown in (*a*) of Fig. 2. Figure 2(*b*) illustrates the optical arrangement used with weak lines where a background correction is desirable. In this case the line is centered in one half of a 0.4-mm slit, leaving the other half of the slit for the background. The alignment tolerances in this case are

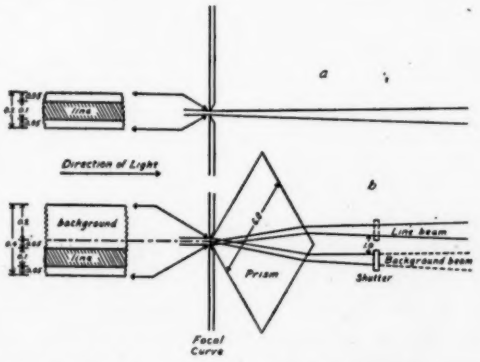

FIG. 2. Exit slit details, (*a*) without background correction, and (*b*) with background correction. All dimensions in millimeters.

[1] See also E. A. Boettner and G. P. Brewington, J. Opt. Soc. Am. **34**, 6 (1944).

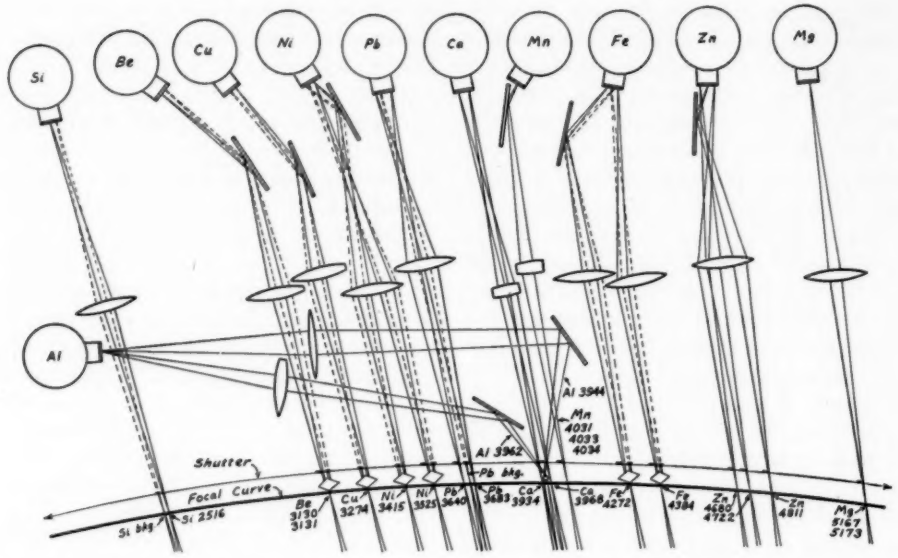

FIG. 3. Optical details in the photo-tube compartment, showing the arrangement of exit slits on the focal curve, prisms, shutter, mirrors, lenses, and multiplier photo-tubes.

the same as in the previous case. Light passing through the two halves of the slit is separated into two beams by a small prism. The two beams are sufficiently far apart upon emerging from the prism to allow a shutter, shown in Fig. 2(*b*), to cut off one or the other. The functions of the shutter and an explanation of the background correction method are given in a later section.

Details of the optical arrangement in the photo-tube compartment are shown in Fig. 3. Twenty exit slits are mounted along the focal curve. Spectral lines of ten elements in addition to Mg, the internal standard, are used. Background correction prisms 25 mm long are used for Be, Cu, two Ni lines, and two Fe lines. A separate slit is used to pass background in the case of Si and Pb, since the region next to these lines contains interfering lines of other elements. In the case of Si, the background slit has the same width as the slit passing the Si line, 0.2 mm, while for Pb, the background slit is 0.4 mm wide, which balances the widths of the two slits for the two Pb lines used. The Mg and Mn slits pass more than one line through the same slit, and hence are wider than the usual 0.2 mm. The two Al lines falling between the two Ca lines, and separated from the latter by 10 and 6 Angstroms, presented a special problem. A small prism about 3 mm wide and 25 mm long was inserted between the two Ca lines so that the Al lines passed through the prism and were bent away from the Ca lines. If necessary, lines about 2 Angstroms apart could be separated without difficulty by inserting prisms of the type used for separating the line and adjacent background. The height of the spectral lines at the focal curve is limited by a diaphram at the entrance slit to about 22 mm. The intensity of illumination from top to bottom along the spectral lines is fairly constant.

A shutter is shown in Fig. 3 about 1 cm behind the focal curve. The shutter has a sidewise motion of about 2 mm, and carries numerous strips of brass about 30 mm long mounted vertically. In one position all lines are transmitted and all background beams blocked out; in the opposite position all background beams are passed and all lines are stopped, regardless of whether or not a background correction is actually made on the line. The shutter is moved by means of solenoids mounted on each end.

After passing through the shutter, the beams are focused onto ground glass or quartz plates mounted on the envelopes of the photo-multiplier tubes. In most cases an auxiliary mirror is re-

quired to direct the light onto the proper multiplier. The lines of one element and associated background beams are focused onto the same tube. Front surface aluminized mirrors are used throughout. The lenses and prisms for use with light of wave-length less than 3800 Angstroms are of fused quartz, and the multipliers are equipped with special ultraviolet transmitting glass. In the visible region glass optics and standard 931A multiplier tubes are used.

The lenses used in the photo-tube compartment are required for accurate analytical results. From Fig. 1 it is evident that a change in the position of the spark on the electrodes or of the electrodes themselves is accompanied by a change in the position of illumination on the grating. The positions of the spectral lines is of course fixed, but after passing the exit slits the light beams move with every motion of the light source. When lenses are used to refocus the light back to line images of the exit slits, the effects of motions of the source are eliminated except for aberrations produced by using different portions of the lens. Unless a receiver having constant sensitivity with position is available, even the motions due to lens aberrations are of importance. Tests described below have shown that the usual multiplier photo-tube is extremely sensitive to position, and a device intended to minimize this effect was developed. It is evident that here is a problem peculiar to the direct reading method and not encountered in ordinary photographic spectroscopy. Although a spark tends to average out fairly well in respect to position during an exposure of several seconds, some arrangement to refocus the light from the exit slit onto the photo-tubes is a necessity in order to eliminate the need for controlling exactly the position and diameter of the sample electrodes.

The optical arrangement in the photo-tube compartment was adopted following a study made of the sensitivity characteristics of several 931A photo-multiplier tubes. In Fig. 4, two curves, typical of the results obtained on several multiplier tubes, show the change in sensitivity with varying position of illumination on the cathode. In obtaining data for these curves, light from a projection type tungsten lamp with a concentrated filament was placed 50 cm from a 0.2-mm slit. The light from the lamp passed through the slit and fell on the photo-sensitive cathode of the multiplier. The cathode was thus illuminated with a beam of light about 2 cm high and 0.3 mm wide. A screw feed on the slit made it possible to move the light in small steps across the cathode surface. The light source was held fairly constant, and the sensitivity of the tube was measured as a function of the position of the light on the cathode. The two curves of Fig. 4 show the tremendous variation in sensitivity for different positions on the cathode. The millimeter scale shown as the abscissa in Fig. 4 corresponds to the actual movement in the position of the light entering the multiplier. In most cases, positions of secondary maxima in the sensitivity could be traced to reflections occurring within the tube, for example, from one or the other of the two posts supporting the wire grid through which the light must pass. It seems likely that the true sensitivity for the cathode surface is everywhere

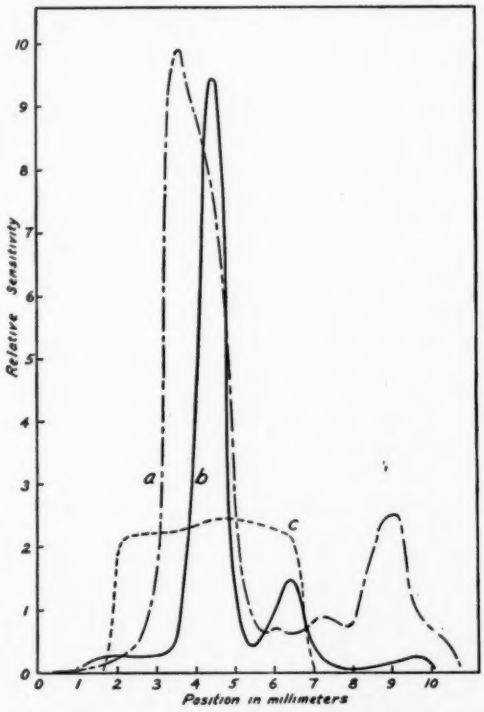

FIG. 4. Variation in the sensitivity of multiplier phototubes with position of illumination on the light sensitive cathode. Curves (*a*) and (*b*) are for two typical multiplier tubes. Curve (*c*) is for a tube equipped with a diffusing plate.

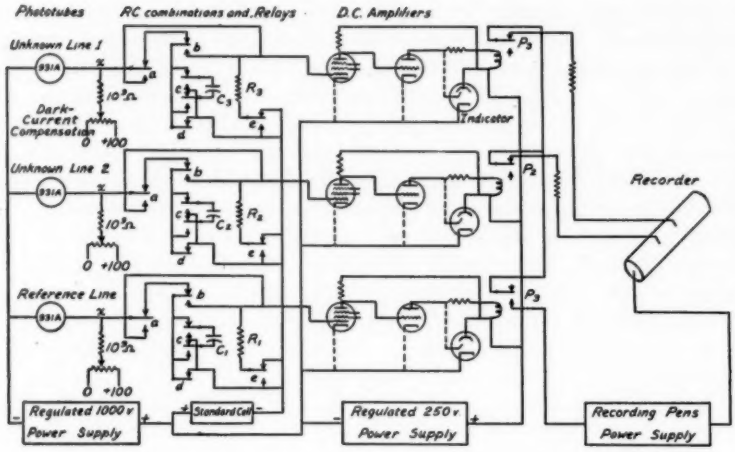

FIG. 5. Simplified schematic diagram of the electrical system, considering one internal standard line and only two lines of unknown elements. (*a*), Dark-current check switches; (*b*), (*e*), measuring relays; (*c*), reversing relays; (*d*), shorting relays; (*p*), plate relays; (*C*), charge-storage condensers; (*R*), discharge resistors.

zero except for a region a millimeter or two wide, located such that electrons emitted from this region are focused properly to pass through the opening between the first and second dynodes.[2] The small photo-current observed with the light beam apparently directed at some point other than on the "hot spot" is probably caused by light scattered in passing through the envelope or reflected from the wires of the entrance grid and finally falling upon the narrow sensitive region of the cathode. The position of the sensitive spot on the cathode changes for different accelerating voltages between the cathode and the first dynode, and broadens out somewhat at lower voltages. The curves in Fig. 4 were obtained with 100 volts between the cathode and the first dynode. Curves obtained by focusing an illuminated slit onto the cathode surface with a condensing lens were similar to those in Fig. 4 but considerably flatter. This difference was thought to be caused by the difficulty of obtaining a sharp focus upon the inclined cathode, and also to more scattered light.

The third curve in Fig. 4 was obtained with a ground quartz plate mounted on the multiplier and exposed to the moving slit as before. The sensitivity curve is fairly flat over more than 4 mm, and falls rapidly to zero at the two sides where the light is obstructed by the support for the ground plate. The design adopted was to separate the ground plate and the tube envelope with a metal tube $\frac{1}{4}''$ long having an internal cross section of about $\frac{1}{4}''\times 1''$. This arrangement has equivalent efficiency and somewhat better constancy of sensitivity (for a change in position of the light) than mounting the ground plate directly on the tube envelope.

Several different types of integrating boxes smoked on the inside with MgO were constructed and tested in a similar manner. Some boxes were made with the photo-tube partially or entirely within the enclosure, and others were made smaller and mounted on the front of the tubes. These boxes all had excellent properties in respect to constancy of photo-current with change of position of illumination, but the sacrifice in intensity was too great for use with the weaker spectral lines. Presumably a large fraction of the light entered the photo-tube but only a small fraction fell on the narrow sensitive region of the cathode. The much better efficiency of the ground quartz plate is probably caused by the predominance of forward scattering and incomplete diffusion produced by the plate. The arrangement finally adopted has been entirely satisfactory and has eliminated the necessity for critical positioning of the multiplier tubes.

Early in the design of the direct reading spectrometer, an extensive study was made of the most advantageous spectral lines for use with the elements desired. This preliminary study was done photographically, by inspecting spectra taken of alloys containing elements varying over the ranges of interest. Lines were selected on the

[2] See, for example, the RCA descriptive literature on the 931A multiplier tube.

basis of intensity and freedom from interferences, and regions for making the background corrections were checked for the presence of other lines. In most cases it was possible to use the most persistent line for an element. For a few elements the most sensitive line fell close to an interfering line or in the region of high background due to magnesium, in which case a weaker line had to be chosen. The use of the principle lines of the various elements insofar as possible is advantageous since the same lines can be used over the entire range of concentrations encountered. For example, the aluminum pair at 3944 and 3962 Angstroms can be used from less than 0.01 percent up to 12 percent. Whenever a group of favorable lines of an element was found, with the lines fairly close together in wave-length, an attempt was made to use all the lines of the group, rather than selecting only one, in order to have the increased intensity available. Since such groups of lines are usually doublets or triplets arising from different levels of the same terms, it is not to be expected that the sum of the intensities of the several lines in a group would be any less sensitive to variations in sparking conditions than would be the intensity of a single line. If "non-homologous" lines could be combined, increased accuracy in analytical results might be obtained.

The spectral lines chosen all originate from transitions either to the ground state of the atom or to the lowest level in the series, so that the possibility of self absorption arises. The shape of the calibration curves obtained for some of the elements tends to indicate that some reversal does take place. However, there is little, if any, indication that the analytical accuracy is impaired in these cases.

ELECTRICAL DETAILS

A simplified electrical system is shown in Fig. 5 in order to illustrate the operation of the instrument. The diagram shows three multiplier tubes and three separate measuring circuits, which would mean a system for measuring the intensity of two unknown lines relative to the same internal standard line. Only the contacts of the various relays involved are included. The d.c. amplifiers are shown in simplified fashion in Fig. 5, and are described in greater detail later.

The circuit is shown in its normal position before a sample is run. The condensers C which are to store the current from the multipliers are normally shorted by the relays d. The input grids of the d.c. amplifiers are all at the potential of the standard cell and are considered "balanced" for this condition. That is, the "magic eye" or indicator tubes are just closed, and the plate relays p are in the normal or non-activated condition. When a voltage more negative than $-E_s$, the voltage of the standard cell, is applied to the input grid, the relays p operate, and for an increasing grid voltage the relays are set to drop out again when the grid potential becomes equal to $-E_s$. At this instant also the indicator tubes are just closed. Because of the differential between "pull in" and "drop out" currents for the relays p, the input grid voltage can be returned to $-E_s$ following a measurement without operating the relays.

The manually operated switches a are used for making a dark current correction on the multipliers. With the switches a in the lower positions the input grids will be at a potential different from $-E_s$ until the dark-current compensation potentiometers are set such that the potential of the points x are at $-E_s$. When the dark current is balanced in this manner, the indicator tubes are just closed and all the dark currents flow through the 10^9-ohm resistors.

With the dark-current check switches in the upper or normal position, the circuit is ready for use. At the beginning of the spark discharge period, relays d are operated thus unshorting the condensers C. The condensers C then accumulate the current from the multiplier tubes during the whole sparking period. During the sparking period, the reversing relays c are operated periodically with a cam system. The relays c are reversed once a second, and synchronized with this reversing is the motion of the shutter of Fig. 3. With the shutter in position to pass the spectral lines, the relays c are in one position, and with the shutter in the background position, the relays are reversed. Thus the condensers C are alternately charged with the photo-current from the intensity of the line + background and then discharged with the photo-current from the intensity of the background. The time spent by the shutter in each position is made equal to one second, so that a completed cycle takes two

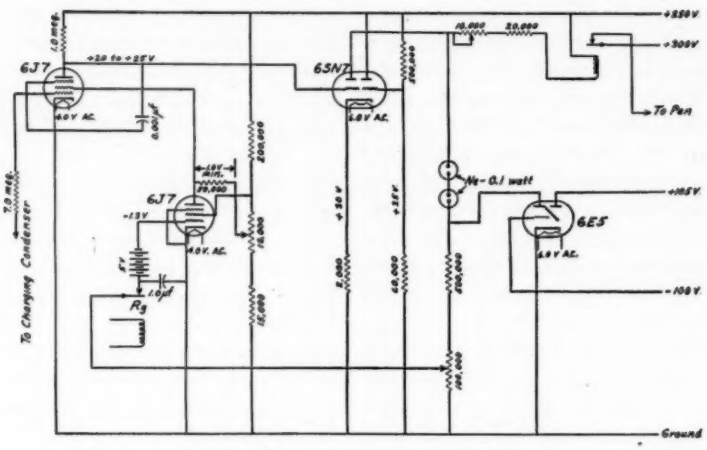

FIG. 6. Direct-current amplifier design.*

seconds, and ten such cycles occur in the normal sparking time of 20 seconds. It will be noticed that this method eliminates the effect of dark current upon the final charge on the condenser. It is therefore not necessary in practice to make frequent nor critical dark-current adjustments on all the multiplier tubes, and it is for this reason that the reversing method is used also on the strong lines for which no background correction is actually made.

When the sparking period ends, the measuring relays b and e are operated, thus connecting the condensers C to their respective discharge resistors R, and disconnecting the grids of the amplifiers from the standard cell. Assuming that the voltages on the condensers C are greater than E_s, the grids of the amplifiers are now more negative than $-E_s$ and the relays p operate. The pen circuit was normally open because of p_1, and after operation of all the relays, the circuit is still open because of p_2 and p_3. The strip recorder, equipped with electrical marking paper,[3] is set in motion at the same time relays b and e are operated, and as long as p_2 or p_3 remain operated, no lines appear on the chart. With several volts on the condensers C, the indicator tubes are wide open, but at the instant the voltage becomes greater than $-E_s$ (nearer to zero) the indicator tubes suddenly close and the relays p drop out. Relays p_2 and p_3 drop out before p_1, so that two lines appear on the strip chart. These two lines have lengths which measure the difference in time required to discharge C_2 or C_3 and C_1 down to the same voltage, $-E_s$. The relay p_1 is also used to stop the recorder, and relays d are released thus shorting the condensers C in preparation for the next operating cycle. Relays b and e are also returned to the original positions.

The d.c. amplifier is shown in detail in Fig. 6. The first 6J7 and the 6SN7 comprise a two stage amplifier, while the second 6J7 is in the feed-back circuit. The relay R_g shown in the diagram allows operation of the amplifier either with or without degeneration. The operating conditions chosen for the 6J7's are such as to insure low grid current, as indicated by Roberts.[4] Under the proper conditions, the grid current in an ordinary 6J7 can be reduced to 10^{-11} ampere. With the relay R_g in the normal position as shown, the amplifier is degenerative. In the degenerative position, the amplifier has almost no drift and requires adjustment of the 100,000-ohm potentiometer only occasionally, about once a week. In the degenerative position, however, the amplifier has a d.c. sensitivity of about 200 millivolts input per milliampere output. To overcome this low sensitivity, the amplifier is switched out of the degenerative position into the high gain position, by means of the relay R_g, during the time that a measurement is required. The gain of the

[3] Obtained from the Western Union Telegraph Company.

* *Note added in proof:* The first stage resistor in Fig. 6 should be labeled 10 meg. instead of 1.0 meg.

[4] Shepard Roberts, Rev. Sci. Inst. **10**, 181 (1939).

amplifier in the high gain position is about 5 millivolts per milliampere, but the rate of drift in this condition is considerably greater than in the low gain position. The 1 μf condenser plays a particularly important part during the time that the amplifier is in the high gain position. In the degenerative position the amplifier remains balanced almost indefinitely, and the 1 μf condenser acquires a potential consistent with the conditions of balance prevailing in the degenerative state. When the amplifier is switched to high gain, the feed-back network is broken but the 1 μf condenser tends to hold its original charge (except for grid current and leakage) thus holding the amplifier to the balanced condition obtained previously in the degenerative position. Thus only the drift occurring within a measuring period of about 15 seconds, when the amplifier is in high gain, is of any concern. It turns out that this drift can be made sufficiently small so as to cause negligible errors in the analytical results.

In use, then, the amplifiers are maintained at balance by the degenerative circuit during the sparking period, and in this condition are much less subject to disturbance by spark interference. After the spark stops, relay R_g in each amplifier is operated simultaneously with relays b and e of Fig. 5 so that the amplifiers are put into high gain for the measurement. After the measurement interval, R_g is released at the same time relays b and e are released, and the amplifiers immediately correct for any drift which may have occurred during the measurement interval and are thus ready for the next measurement. The drift of a typical amplifier in high gain position is of the order of one millivolt in from 5 to 30 seconds. Over a measurement period of 15 seconds, the drift is thus not greater than 3 millivolts, or about 0.3 percent of the standard cell voltage (about one volt). This means that relative intensities can be measured to better than 0.5 percent and accuracy tests have proved this to be the case.

The setting of the amplifier is not critical, and a change in the plate relay characteristics is not serious. The relays are originally set to drop out at a current of 3 milliamperes. If the relay characteristics changed by 30 percent, so that the drop out current were 2 milliamperes, there would be an error of 5 millivolts in 1 volt, or about $\frac{1}{2}$ percent. Similarly, the amplifier setting can change by the same magnitude and still cause a negligible error in analytical results.

Accuracy data on the measuring apparatus were obtained by placing a small tungsten lamp in front of the grating and measuring the intensity of the light beams passing through the exit slits of the unknown elements relative to the light passing through the magnesium slit. Repeated runs showed a standard deviation of less than 0.5 percent in the measurement of the relative intensities, which is about the accuracy to which the record could be read. This figure represents the error to be expected insofar as the variation in performance of the multiplier tubes, amplifiers, and remaining electrical equipment is concerned. The actual analytical results are of course less accurate, mainly because of sample inhomogeneity and variation of the characteristics of the spark discharge. Figures on over-all analytical accuracy are given later.

In checking the dark currents of the multipliers, the amplifiers are put into high gain by a manual control on the relays R_g. In this position, a 1-millivolt difference in potential of the input grid is readable on the indicator tube. With a grid resistor R (Fig. 5) of 10^7 ohms, the smallest used, a current of 10^{-10} ampere can be detected. This is of the order of from 50 to 1000 times smaller than the dark currents usually encountered with the 931A multiplier tube, so that dark-current corrections can be made in most cases to 1 percent or better. This method of dark-current balance is limited by the dark-current fluctuation. The background correction method involving the reversal of the charge storing condenser greatly reduces the effect of these fluctuations.

The regulated 250-volt power supply was constructed according to the design of Miller,[5] and the 1000-volt supply is based upon the same design but modified for the higher voltage. The d.c. amplifiers are also used for checking the adjustment of the 1000-volt supply for the voltage divider used with the multiplier tubes. Although the ratio method of calibration (or internal standard method) is used, it is desirable to keep the voltage on the multiplier tubes as constant as possible, inasmuch as the gain of

[5] Stewart E. Miller, Electronics (November, 1941).

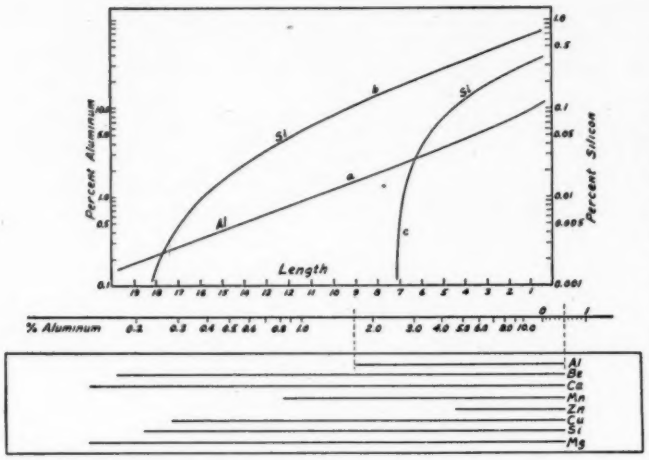

FIG. 7. Calibration details. Curve (*a*) is a calibration curve for aluminum. Curves (*b*) and (*c*) are calibration curves for silicon, with and without the background correction. Below the calibration curves is a projected scale for Al, and below that a typical record from which the analysis for seven elements can be read with the use of calibrated scales.

these tubes varies so rapidly with voltage. In checking the high voltage, the amplifiers are switched manually to high gain, and a second switch connects the grids of all the amplifiers to a small test resistance in series with the resistors of the voltage divider. When the high voltage is 1000 volts, the magnitude of the test resistance is such that the voltage across it is equal to the voltage of the standard cell, for which the amplifiers are in balance. Since a voltage change across the test resistor of 0.1 percent can be seen on the indicator tubes, the voltage on the divider is measurable to the same accuracy, or within 1 volt in 1000 volts. Because of the ratio method used, fluctuations in the high voltage less than the amount measurable have no detrimental effect upon the accuracy of the analytical results.

The condensers used for storing the charge during the sparking period were selected after a study of various types of dielectric materials. As used in the direct reading spectrometer, it is important that the charge retained by the condenser after a brief period of shorting be small in order that the succeeding measurement not be affected. In testing, the condensers were charged to 10 volts, shorted for twenty seconds, left open for 30 seconds, and then connected to a ballistic galvanometer to measure the remaining charge. Three sizes of charge-storing condensers are used in the spectrometer, 1 μf, 0.5 μf, and 0.1 μf. Of the numerous commercially available condensers tested, those containing a mineral oil impregnated paper dielectric were found to be better than any other type except mica. It was found that the mineral oil type condenser retained about 0.4 percent of its original charge under the conditions of test mentioned above. This would cause an error of 4 percent in the measurement of the intensity of a spectral line having one tenth the intensity of the line measured 20 seconds previously. Since new electrodes can be loaded into the clamps as soon as the previous sparking period is over, that is, during the measurement time, it is possible that in routine operation the time of short could be less than 10 seconds. Since mica condensers were not greatly better than the mineral oil type, a special condenser using polystyrene as the dielectric was constructed and tested. This condenser was found to retain only 0.02 percent of its original charge under the conditions of test, and was therefore about 20 times better in this respect than the mineral oil type and 10 times better than the mica. Thus a polystyrene condenser can be shorted for only 5 seconds without affecting the succeeding measurement. Several sizes of polystyrene condensers were obtained on special order from the John E. Fast Company, and have been very satisfactory in this application.

The timing system of the spectrometer is rather involved, and will be discussed here only briefly. Timing of the various operations required for the analysis of one sample is controlled by a system of eight cams, several relays, and two timers. The

cams are mounted on a shaft rotating once every two seconds, driven by a synchronous motor, and are left running continuously. One timer is set for 5 seconds and the second for 20 seconds. The run is begun by pushing the "start" button on the front of the spark unit. This operation starts the spark and also the first timer. During the first 5 seconds of the sparking interval, the shutter on the spark unit is closed, thus preventing light from entering the spectrometer. At the end of the period for which the first timer is set, the shutter on the source is ready to open when allowed to do so by the cam system. The delay between the time the first timer is "timed out" and the time the cam system opens the shutter may be anywhere between 0 and 2 seconds, depending upon the position of the cams when the run was started. At the same time the shutter opens, the second timer is started, and also the charging condensers are unshorted and thus begin collecting the currents from the multipliers. The background correction shutter at this time is in position to pass the lines, and remains so for one second until moved by the cam system. Thus a full one-second "line exposure" is assured at the beginning, and thereafter the cam system reverses the shutter alternately from the line to the background positions at one-second intervals. When the second timer, set at about 20 seconds, is timed out, the cam system stops the spark at the end of the next "background exposure," so that the number of line and background exposures is always equal, independent of the setting of the second timer. As soon as the sparking period has ended, the recorder is started and is allowed about one-half second to get up to synchronous speed before relays *b* and *e* (Fig. 5) and the high gain relays R_g (Fig. 6) operate to begin the measurement period. The measurement period is then completed as previously described. After completion of the measurement period, a time delay relay keeps the recorder running about two seconds longer to give the record space in which to be torn off. The entire operating cycle requires about 40 seconds, and is completely automatic from the time the starting button is pushed until the record strip may be removed from the recorder. Thus, in addition to speed, another advantage of the direct reading spectrometer over the photographic method is in the elimination of intermediate steps and the consequent probability for mistakes on the part of the operators.

CALIBRATION CURVES

A typical record obtained from the recorder after having run a sample is shown in Fig. 7. The record contains eight parallel lines of varying length, but all ending at the same place on the right. Each line is associated with one of the eight amplifiers. From the record can be read the percentages of seven elements, since the Mg is the internal standard. The lowest line on the record, for Mg, has a different significance than the other seven lines. The recorder is connected so that this line begins drawing (at the left end) when the discharge of all the storage condensers begins, and ends (at the right end) when the voltage of the Mg condenser falls to E_s. The length of this line controls the length of the record and is a measure of the integrated intensity of the Mg line alone. The lengths of the other seven lines is a measure of relative intensities, as explained previously. The length of the Ca line, which began writing as soon as the Mg line, indicates that the Ca condenser was charged during the spark exposure to some voltage less than E_s, and therefore means a Ca content in the sample less than the lower limit of the calibration.

Above the record in Fig. 7 is shown a projected calibration scale for aluminum, and above this is a calibration curve for aluminum and two for silicon. The calibration curve for aluminum is seen to be essentially linear over the entire range covered. A calibration curve of this sort is constructed by running standards, and plotting the length of the Al line on the record against the logarithm of the concentration. The projected scale shown for Al is marked off in percentage units according to the calibration curve directly above. The small linear scale at the right end of the projected scale is called a "standardization" scale, and is used for keeping the instrument in calibration. In use, a record on a standard sample containing a known amount of aluminum, say 4 percent, is obtained. The Al scale is placed next to the Al line on the record, with the 4.0 percent opposite the left end of the line. The position of the right end of the line is noted on the standardization scale, for example 0.5. In running an

unknown, then, the Al scale is lined up with the end of the Al line at 0.5, and the percent Al can then be read directly from the scale. For example, the record in Fig. 7 would indicate 1.7 percent aluminum. Once a complete calibration curve has been established, subsequent calibration can be done in this manner by running only one standard. This method of calibration is possible because the slope of the calibration curve remains constant indefinitely, and depends only upon the choice of the RC constant (of the storage condenser—discharge resistor combination) relative to the speed of the recorder.

Two calibration curves for silicon are given in Fig. 7 to show the effect of the background correction method on the slope of the curves. The two curves approach the same straight line at the higher silicon concentrations, and the slope of curve (b) at low concentrations depends entirely upon how much background correction is made. With a "perfect" background correction, the calibration curve would be straight over its entire length. By a "perfect" or 100 percent background correction is meant that for zero silicon the "line" and background beams are exactly balanced and the condenser thus acquires zero net charge at the end of the sparking period. Under such circumstances, however, an extension of the straight line portion of curve b shows that about 0.009 percent silicon would be required to get the silicon condenser charged to E_s so as to be in the region covered by the record. By weakening the background beam, it is evident that the calibration curve b can be made to take any shape between a straight line and the position occupied by curve c, representing no background correction. The amount of background subtracted can be adjusted such that zero silicon is just "on scale," or the silicon condenser is charged slightly greater than E_s during the spark exposure. This is the case for curve b in Fig. 7. Data for curve c were obtained without reversing and one-half the spark exposure time used for curve b, so that the two curves are comparable. Calculation shows that the condenser voltage for 0.1 percent silicon was 12.0 volts for curve c and 5.4 volts for curve b. Thus a background voltage of 6.6 volts was subtracted under the conditions obtaining for curve b. Curve c at 0.001 percent silicon is essentially background, and this voltage is calculated to be 7.8 volts. The amount of background correction made in curve b is therefore 6.6/7.8 or about 85 percent. Curve b at 0.001 percent silicon shows a voltage of 1.28, which is in approximate agreement with the difference between 7.8 and 6.6. It is possible, of course, to make more than an 85 percent background correction and thus have a calibration curve more nearly linear at the low end. The point for 0.001 percent silicon could then be brought on scale, or above E_s, by using either a higher gain on the multiplier or a smaller storage condenser. This would mean, however, that a longer record would be required to reach 1 percent silicon, since the slope at the upper end would be essentially unchanged.

The advantages of the background correction method are several. The unimportance of the dark-current balance with the reversing method has been mentioned above. Without reversing, the background of curve c, Fig. 7, is 7.82 volts, and the point for 0.01 percent silicon is 8.10 volts, so that the silicon itself is responsible for 0.28 volts, or 3.8 percent of the total. These voltages are stored in a 0.1 μf condenser over a charging period of 10 seconds, which means that the current due to the 0.01 percent silicon alone is only 2.8×10^{-9} ampere. Great constancy of dark current or very frequent checks on the dark current would be required in order to obtain significant results on silicon between 0.001 percent and 0.01 percent without the background correction method. Furthermore, different types of alloys tend to have different intensities of background relative to the intensity of the magnesium line, so that the 0.28 volt due to the 0.01 percent silicon would be lost in the greater variation of the background itself. This latter effect is 85 percent removed by the background correction employed in curve b. The calibration curve is also spread out more by the background correction, thus facilitating reading of the projected scale.

It is possible to make some predictions concerning the shapes of calibration curves. The relative intensity equation for all elements is

$$\Delta t = RC \log I_2/I_1 + K,$$

where I_2 is the intensity of the magnesium line (internal standard) and I_1 is the intensity of the unknown line. I_1 is a function of the concentration X of the unknown element, and the shape of the

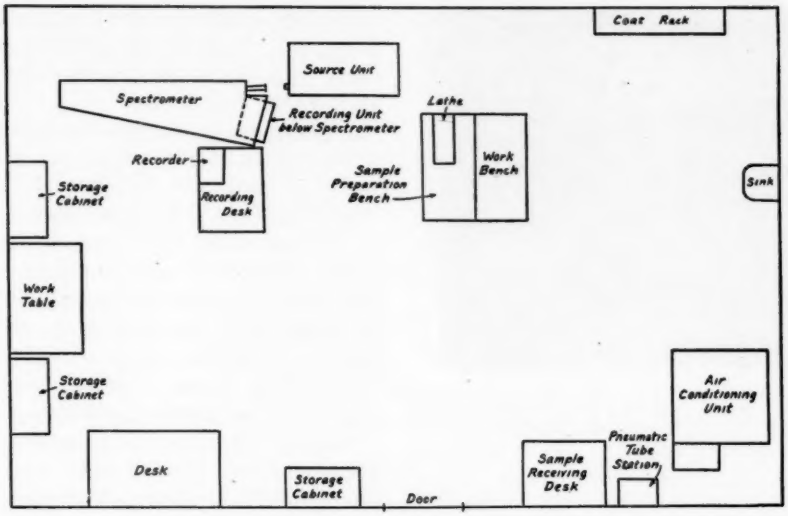

FIG. 8. Layout of the spectrochemical laboratory, measuring 20×30 feet, using the direct reading spectrometer.

calibration curve is entirely dependent upon the nature of this function. The simplest case is one of proportionality,

$$I_1 = \alpha X.$$

Neglecting the effect of dilution, considering I_2 as a constant,

$$\Delta t = -RC \log X + K'.$$

A plot of t *vs.* $\log X$ is thus a straight line of slope $-RC$. The calibration curve for zinc is found to agree with this equation in regard to linearity and slope.

Many elements have a calibration curve differing from this ideal case. The factors governing the deviation from the theoretical calibration curve in any particular case are several: intensity of background, self-absorption, effect of concentration of an element upon its own rate of volatilization from the sample, and effect of concentration of an element upon the discharge characteristics of the spark. The effect of the background intensity is to bend the calibration curve downward at low concentrations, as in curve *b*, Fig. 7. At high concentrations, in the absence of the other factors given above, the calibration curve should gradually approach a straight line of slope $-RC$. Such is the case for zinc. The effect of self-absorption is to bend the calibration curve upward at the higher concentrations. There is a slight indication of this effect in the calibration curve for aluminum. The calibration curve observed for manganese appears to combine both background and self-absorption effects, giving a calibration curve bent at both ends with a very short straight line portion. The nearly linear aluminum curve and the perfectly linear curve observed for calcium are more difficult to explain, inasmuch as both curves have a slope significantly smaller (steeper, in Fig. 7) than $-RC$. Apparently these cases can be explained only by assuming effects due to the last two factors mentioned.

The choice of RC constant for the storage condenser—discharge resistor combination may vary considerably. RC must not be too large, since then the discharge period would be too long and the amplifiers would have a longer period in which to drift. RC also must not be too small mainly because of the difficulties encountered in starting and stopping rapidly a strip recorder containing a large roll of recording paper. An RC value of about 5 seconds was arbitrarily chosen, which represents a distance of 12 cm on the record. The magnesium condenser during the run is charged to about 20 volts, so that the usual record length is about 36 cm, and the recording time is about 15 seconds. The RC constant could undoubtedly be reduced at least to 2 seconds, in

FIG. 9. View of the direct reading spectrometer, showing the spark source unit, grating housing, recording chassis, and recorder.

which case only 6 seconds would be required for a record of the same length. With an RC constant of 12 cm in terms of the speed of the chart, it can be shown that a distance of 1.2 mm on the chart represents a change of 1 percent in the measurement of the voltage ratios, or relative intensity. Hence it is desirable to read the record to the nearest millimeter.

The necessity for having all RC constants equal will now be explained. Let

$$t = RC \log E/E_s$$

for the internal standard line, and

$$t_1 = R_1C_1 \log E_1/E_s$$

for the unknown line. Then

$$\Delta t = t - t_1 = RC \log E/E_s - R_1C_1 \log E_1/E_s.$$

If $R_1C_1 = RC + \Delta(RC)$, then

$$\Delta t = RC \log E/E_1 - \Delta(RC) \log E_1/E_s.$$

If E is constant, Δt changes only with E_1, and hence this equation would provide the basis for a valid calibration between Δt and the concentration of the unknown. For a change in the total intensity of the discharge, however, Δt changes even though E/E_1 remains constant. For a change in total intensity (with E/E_1 constant),

$$\delta(\Delta t) = -\Delta(RC)\delta E_1/E.$$

If $\delta E_1/E = 25$ percent, about the maximum to be expected,

$$\Delta(RC) = 4\delta(\Delta t).$$

If it be required that $\delta(\Delta t)$ be less than 0.6 mm, so that the relative intensity is accurate to better than $\frac{1}{2}$ percent, $\Delta(RC)$ must be less than 2.4 mm. Since $RC = 12$ cm, the RC constants must vary by less than 2 percent.

The sizes of the storage condensers used in the direct reading spectrometer vary from 0.1 μf to 1 μf, depending upon the intensity of the spectral lines. With the 1 μf-size condenser, a grid resistor or discharge resistor of 5 megohms is used, and hence a 50-megohm resistor is used with a 0.1-μf condenser. It is an advantage from the standpoint of leakage and absorbed charge to work with fairly low voltages on the storage condensers. The highest voltage used is obtained on the magnesium condenser; a 1-μf condenser is charged to twenty volts in the ten-second exposure period (extending over 20 seconds), and the largest photo-current employed is therefore 2 microamperes. The smallest photo-currents used are of the order of 10^{-8} ampere. No fatigue effects have been observed at these light levels during the operation of the spectrometer.

DESCRIPTION OF THE INSTALLATION

The floor plan of the spectrochemical laboratory showing the arrangement of the necessary

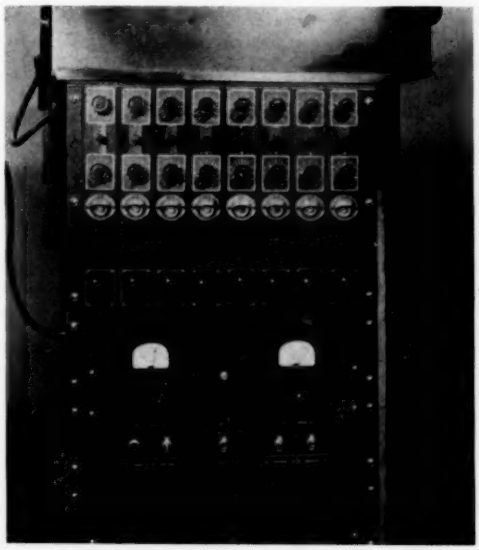

FIG. 10. Front view of the recording chassis, showing the eight relay drawers, eight amplifier drawers, and control panel.

equipment is given in Fig. 8. The laboratory is located in the basement of the alloy plant which it serves, and is connected with pneumatic tubes to three stations on the floor above. Samples are received and results returned through these tubes. Temperature and humidity are controlled within the laboratory.

Samples cast in a special mold[6] are turned down to a uniform size in a simplified lathe previously described,[7] forming two electrodes about 1 inch long and 4 mm in diameter, with a 10° bevel on the ends to be sparked. The electrodes thus prepared are placed in electrode clamps[7] located in a compartment in the upper left-hand corner of the source unit. Details of the source unit will be given in another paper.[8] Optimum speed under the present conditions of operation is obtained with two people, one preparing and loading the electrodes and the other reading and reporting results. At present, each sample is run twice, reversing the ends of the electrodes for the second run, so that the effect of non-homogeneity of sample is minimized. Under these conditions, results are usually returned in less than five minutes from the time the sample is received.

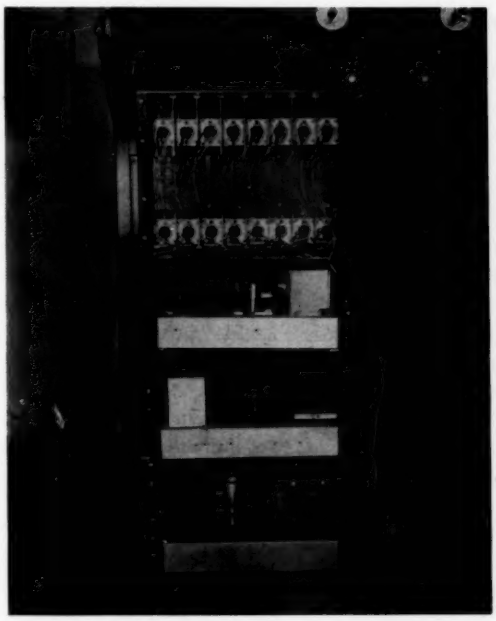

FIG. 11. Rear view of the recording chassis.

FIG. 12. View of the amplifier (left) and relay (right) drawers removed from the recording chassis.

Figure 9 is a photograph showing the arrangement of the direct reading spectrometer. The electrode preparation table is partially included at the right. The source unit is shown with the door, at the upper left-hand corner of the unit, closed to the compartment containing the electrode clamps. The height of the clamps and hence also of the optical axis of the spectrometer was made 55 inches from the floor, considerably higher than usual, partly to get the clamps up to a more convenient height and partly because of the space required for the recording chassis. The recording chassis is shown below the photo-tube compartment of the spectrometer. The recorder is placed at the side of the recording chassis upon a table of sufficient height to allow an operator to write conveniently while standing.

Figures 10 and 11 show front and rear views of the recording chassis, illustrating the unique construction. The unit has eight "relay drawers" across the top, each with two dark-current correction potentiometers and a lever switch. The eight "amplifier drawers" are located directly below, each with an indicator tube and a balancing potentiometer. A relay drawer and an amplifier drawer are shown removed from the chassis in Fig. 12. Each drawer has an eleven-pronged plug at the rear, through which most of the electrical connections are made. The corresponding sockets are shown in Fig. 11, as well as the "bus bar" system used for connections. Each relay drawer contains four relays and two charging condenser

[6] T. M. Hess and L. G. Reinhardt, J. Opt. Soc. Am. **34**, 104 (1944).
[7] J. L. Saunderson and V. J. Caldecourt, J. Opt. Soc. Am. **34**, 116 (1944).
[8] V. J. Caldecourt and J. L. Saunderson, Combination Arc-Spark Source for Magnesium Alloys, J. Opt. Soc. Am., to be published.

FIG. 13. Recorder with eight pens using electrical marking paper. Also shown is a record, projected scale, report pad, and carrier for pneumatic tube system.

—discharge resistor combinations. The two condensers allow the use of one drawer for two elements, but not simultaneously. Eight relay and amplifier drawers limit the number of elements determinable in one single run to seven, but a second run would permit the determination of seven more, if the total capacity of the apparatus were utilized. Connections from the multiplier tubes in the compartment directly above the recording chassis are made through the spring contacts on top of the relay drawers, and connections from the latter to the amplifiers are made in the same manner. Thus the drawers are easily removable and all are interchangeable, except for relay drawers having different sized charging condensers. The lever switches on the front of the relay drawers allow the dark currents of the two multipliers feeding into the two charging condensers to be balanced with the same amplifier. Relays inside the relay drawers determine which of the two elements is to record at any particular time. The amplifier and relay drawers fit between vertical plates of $\frac{1}{8}$-inch iron, giving the unit the required stability and shielding. The "control chassis," on which the cam system may be seen in Fig. 11, is located beneath the amplifier drawers. The next chassis contains the high voltage power supply, and the lowest chassis contains the low voltage power supply. These three shelves are interconnected with a system of cables, so that any chassis may be removed from the front of the unit by pulling out two or three plugs. The meters on the front of the recording chassis are connected with the 1000-volt and the 250-volt power supplies. Switches are provided for manually changing the amplifiers to high gain, checking the high voltage, turning

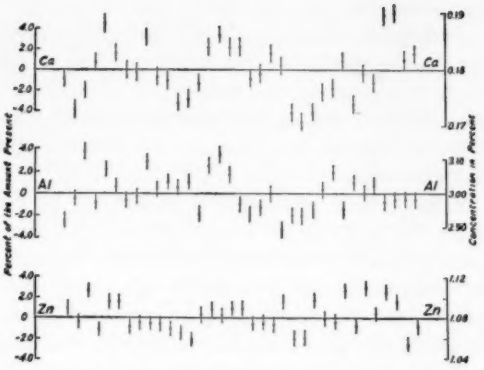

FIG. 14. Calibration constancy data for a period of six days, showing the results of standardization at four-hour intervals for three elements.

on the indicator tubes, and making the instrument operate either with or without the reversing feature. The recorder is shown in Fig. 13, equipped with eight "pens" and a roll of electrical recording paper.

PRECISION DATA

The data studied here were taken over a period of six days during which the instrument was operated continuously. The standardization was checked at four-hour intervals by running a standard sample four times. The average of these four runs was used as the standardization for the next four-hour period. The fluctuations in the standardization for Al, Ca, and Zn over this period are shown in Fig. 14, in which the units of the left ordinate are in percent of the amount present and those of the right ordinate are in actual concentration of the element. The position of the average of the four determinations is plotted, and a vertical line of length $\sigma_1/2$, where σ_1 is the standard deviation for a single determination, is drawn above and below the point. For these elements, σ_1 was calculated by finding the standard deviations for each of the 35 groups of four determinations[9] and averaging all 35 results. This method eliminates from σ_1 the effect of drift from one four-hour period to the next.

Table I summarizes these and other data obtained during the same six-day period. σ_1 is con-

[9] The formula $\sigma = (\Sigma d^2/3)^{\frac{1}{2}}$ was used, where d = deviation of each of the four individual determinations from the mean of the same four.

sidered to be the standard deviation of a single determination, calculated as described above, for conditions of no drift. In addition to the 140 runs entering into the calculation of σ_1, the same standard sample was run 60 more times, well spread out over the six-day period, and these 200 runs have been used to calculate σ_2, the standard deviation obtainable by operating without periodic standardization, which of course includes instrument drift. From the data of Fig. 14, σ_3 was calculated. σ_3 is the root mean square of the shifts in standardization over a four-hour period. The quantity $(\sigma_2^2-\sigma_1^2)^{\frac{1}{2}}$ represents the part of the over-all standard deviation, σ_2, which is caused by the drift under conditions for no periodic standardization. The next quantity in Table I, $(\sigma_1^2+\sigma_3^2/4+\sigma_1^2/4)^{\frac{1}{2}}$, represents the standard deviation of a single run with the four-hour standardization method, assuming on the average that the error caused by drift is $\sigma_3/2$ and the error in the standardization itself (four runs) is $\sigma_1/2$. The last quantity, $(\sigma_1^2/2+\sigma_3^2/4+\sigma_1^2/4)^{\frac{1}{2}}$, indicates the standard deviation using the four-hour standardization method and running the unknown sample in duplicate.

The above considerations indicate that the drift of the apparatus is real. The drift for Al and Zn is about equal to σ_1, and for Ca is about twice as large as σ_1. These data were obtained with an unregulated power supply to the spark excitation source, and the line voltage is known to fluctuate widely. Furthermore, since obtaining these data, the importance of very careful adjustment of the electrode shaping tool has been realized. It is believed at present that control of the line voltage to the spark source and better reproducibility of the electrode shape would materially reduce the magnitude of observed drift, and that the direct reading spectrometer itself is essentially free from drift. Additional data will be examined to test this belief.

TABLE I. Standard deviations describing the precision of analytical results. The standard deviations are given in percent of the amount present.

Element	σ_1	σ_2	σ_3	$(\sigma_2^2-\sigma_1^2)^{\frac{1}{2}}$	$\left(\frac{5\sigma_1^2}{4}+\frac{\sigma_3^2}{4}\right)^{\frac{1}{2}}$	$\left(\frac{3\sigma_1^2}{4}+\frac{\sigma_3^2}{4}\right)^{\frac{1}{2}}$
Al (at 3%)	1.68	2.38	2.22	1.69	2.28	1.83
Ca (at 0.18%)	1.90	3.07	2.47	2.41	2.45	2.06
Zn (at 1%)	1.43	1.92	2.00	1.28	1.89	1.59

TABLE II. Standard deviations for individual determinations in percent of the amount present.

Element	Concentration	Standard deviation
Mn	0.30%	1.9
Si	0.008%	15.4
	0.046%	8.0
	0.13%	2.7
Cu	0.008%	5.4
	0.04%	3.1
	0.21%	3.5
Be	0.0001%	21.1
	0.0025%	5.8

Table II gives additional precision data on four more elements, Mn, Si, Cu, and Be. Standardization data for these elements were not available, so the standard deviation σ_1' for a single determination was found from a series of thirty repeat determinations in the usual manner. σ_1' has the same meaning as σ_1, but comes from a different set of data. These data of course include errors caused by non-uniformity in the sample which is of considerable importance for some elements, particularly at higher concentrations. The precision data for the low concentrations of Si and Be indicate that the direct reading spectrometer is at least equal to photographic methods both in regard to sensitivity and accuracy. At the higher concentrations, the instrument has equal or superior accuracy than is usually claimed in the literature for the photographic method on magnesium alloys.

JOURNAL OF THE OPTICAL SOCIETY OF AMERICA VOLUME 35, NUMBER 11 NOVEMBER, 1945

Optics of Distilled and Natural Water

E. O. HULBURT
Naval Research Laboratory, Washington, D. C.
(Received September 6, 1945)

INTRODUCTION

THE sea viewed in the daytime by an observer looking downward from a ship or an airplane has a certain color and brightness which, apart from the surface reflection, is caused by the portion of the daylight that has penetrated into the sea and has returned upward. The character and intensity of the up-welling light depends on the optical properties of the sea water. It is the purpose here to describe laboratory measurements of the absorption and scattering of distilled water and of the water of the Chesapeake Bay and the Atlantic Ocean, and to relate these through theory with observations of the Bay and the Ocean.

MEASUREMENTS IN THE LABORATORY

Apparatus was arranged for measuring the attenuation and scattering of samples of water for light of the visible spectrum. For the attenuation a glass tube was used 364 cm (12 feet) in length and 4.2 cm in internal diameter, closed with glass end-plates that were flat and perpendicular to the axis of the tube. A beam of light from a tungsten lamp, rendered parallel by a lens, passed through the tube being limited by diaphragms to a circular cross section of 2.5 cm so that it did not touch the walls of the tube. The beam passed through a Nutting photometer and came to a focus on the slit of a glass prism spectrograph. The long glass tube could be moved out of the beam and replaced by a short tube 20 cm in length, both tubes being filled with water from the same sample. In this way the attenuation κ of the water was determined throughout the visible spectrum from 420 to 700$\mu\mu$.

κ is defined by

$$i = i_0 e^{-\kappa x}, \tag{1}$$

where i and i_0 are the respective intensities of a parallel beam of light of wave-length λ that enters and emerges from a thickness χ cm of the water.

Now

$$\kappa = \beta + \sigma, \tag{2}$$

where β and σ are the attenuations due to true absorption and to scattering, respectively.

In order to measure the scattering σ the water was placed in a spherical flask of 8 cm radius. A parallel beam of tungsten light was passed through the center of the flask and the brightness of the beam at various angles ϕ to the forward direction of the beam was measured with a Macbeth illuminometer. The flask was removed and replaced by a diffusing white plaque normal to the beam and in the position previously occupied by the center of the flask. The brightness of the white plaque was measured. From these measurements the values of σ_ϕ were determined, where σ_ϕ is the fraction of the light of the beam that was scattered per unit volume of water per unit solid angle in the direction ϕ.

The attenuation σ of parallel, or collimated, light due to scattering is given by

$$\sigma = 2\pi \int_0^\pi \sigma_\phi \sin\phi d\phi. \tag{3}$$

Of the light that is scattered from the parallel beam portions σ_F and σ_B are scattered in the forward and backward directions, respectively, where

$$\sigma = \sigma_F + \sigma_B, \tag{4}$$

$$\sigma_F = 2\pi \int_0^{\pi/2} \sigma_\phi \sin\phi d\phi, \tag{5}$$

$$\sigma_B = 2\pi \int_{\pi/2}^\pi \sigma_\phi \sin\phi d\phi. \tag{6}$$

Quantities of interest here are η and $1-\eta$, the fractions of the light scattered in the forward and backward directions, respectively. Then

$$\eta = \sigma_F/\sigma, \qquad 1-\eta = \sigma_B/\sigma. \tag{7}$$

If the values of β, σ, and η are known throughout the visible spectrum for a sample of water the upcoming daylight from a uniform sea of such water may be calculated.

Distilled water was investigated first, because earlier measurements of its optical properties were not in complete agreement, and a knowledge of pure water was important to an understanding of natural waters. The preparation of approximately chemically pure water is relatively simple, but to prepare it free from optical impurities, that is, "dust free," is well known to be difficult. A good way is by slow distillation in quartz. There was no opportunity to do this in the case of the considerable quantity of water required in the present experiments. The procedure used was to allow distilled water to stand for several weeks in five-gallon bottles. The upper two-thirds of the water in a bottle was siphoned directly into the absorption tube and scattering flask for rinsing and finally for filling. Motes were visible in the settled-out distilled water in the tube and flask, especially when viewed by forward scattering, but after standing for several days many, but not all, settled out. After ten days $\sigma_{\pi/2}$, the scattering coefficient at right angles for tungsten light, diminished to

$$\sigma_{\pi/2}=1.44\times10^{-6},$$

and did not decrease any more with further standing in the flask.

The theoretical value for water for tungsten light viewed with the light adapted eye is

$$\sigma_{\pi/2}=1.21\times10^{-6},$$

as calculated from the density fluctuation expression with polarization defect.[1]

The observed values of σ_ϕ for distilled water for tungsten light are plotted as $(\sigma_\phi/\sigma_{\pi/2})\sin\phi$ as ordinate against ϕ as abscissa in Fig. 3. From these values the scattering attenuation σ_t for tungsten light and η were calculated from (3), (5) –(7). One obtained

$$\sigma_t=0.931\times10^{-4},$$
$$\eta=0.864.$$

The theoretical values for water[1] for tungsten light were

$$\sigma_t=0.194,$$
$$\eta=0.50.$$

It is seen that the dust content of the distilled water was reduced until the scattering at right angles was only about 20 percent in excess of the theoretical value. The total scattering, however, was over 4 times the theoretical value because of the forward scattering. However, there is no compelling reason why the scattering of water should conform with a simple theory.

From the observed value of $\sigma_t=0.931\times10^{-4}$ for tungsten light the values of σ, the scattering attenuation coefficient at wave-length λ, was derived by assuming that σ varied with the inverse fourth power of λ. Earlier measurements[2] supported the assumption and some experimental justification for it was afforded by the observation that the beam of tungsten light in the scattering flask was distinctly bluish. It would have been more satisfactory to have measured σ directly throughout the visible spectrum, but there was no opportunity for such a program. The values of σ are given in Table I, Column 3, and are plotted in the dotted curves of Fig. 1 and Fig. 2.

The values of $\kappa=\beta+\sigma$ for distilled water were measured throughout the visible spectrum. They

TABLE I. Absorption and scattering of distilled water and Chesapeake Bay.

	Distilled water			Chesapeake Bay		
λ	κ	σ	β	κ	β	plankton β
400$\mu\mu$	8.0×10^{-4}	3.57×10^{-4}	4.4×10^{-4}	—	—	—
410	7.0	3.23	3.8	—	—	—
420	6.1	2.95	3.1	80.5×10^{-4}	62.5×10^{-4}	60×10^{-4}
430	5.3	2.69	2.6	70.5	52.5	49
440	4.6	2.45	2.1	62.8	44.8	43
450	4.0	2.25	1.7	55.6	37.6	36
460	3.6	2.04	1.6	51.2	33.2	31
470	3.6	1.89	1.7	47.5	29.5	28
480	3.65	1.72	1.8	44.7	26.7	25
490	3.7	1.59	2.1	41.9	23.9	22
500	3.8	1.47	2.3	38.8	20.8	18
510	3.9	1.35	2.6	36.8	18.8	16
520	4.0	1.25	2.8	35.1	17.1	14
530	4.2	1.17	3.0	33.7	15.7	13
540	4.4	1.09	3.3	33.1	15.1	12
550	4.7	1.00	3.7	32.3	14.3	11
560	5.3	.932	4.4	32.3	14.3	10
570	6.6	.868	5.7	32.3	14.3	9
580	8.4	.810	8.6	33.1	15.1	8
590	12.0	.756	11.2	36.5	18.5	7
600	19.7	.708	19.0	42.9	24.9	6
610	24.3	.662	23.6	46.5	28.5	5
620	26.5	.618	25.9	47.6	29.6	4
630	28.0	.581	27.4	48.8	30.8	4
640	29.2	.535	28.7	50.0	32.0	4
650	30.8	.507	30.3	51.8	33.8	4
660	33.5	.483	33.0	54.2	36.2	4
670	37.5	.455	37.0	56.3	38.3	2
680	40.6	.429	40.2	58.9	40.9	1
690	46.7	.404	46.3	63.	45.	0
700	57.6	.380	57.2	74.	56.	0

[1] L. H. Dawson and E. O. Hulburt, J. Opt. Soc. Am. **31**, 554–557 (1941).

[2] L. H. Dawson and E. O. Hulburt, J. Opt. Soc. Am. **27**, 199–201 (1937).

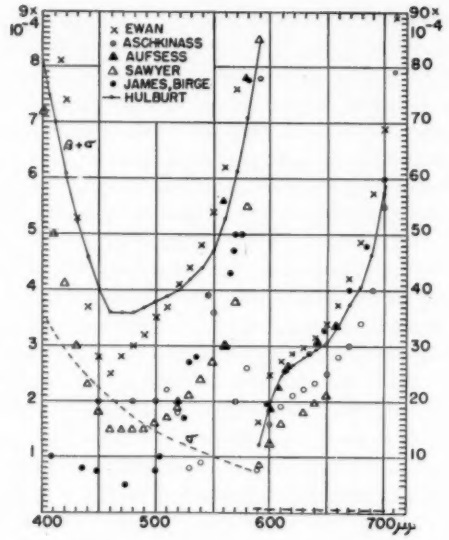

FIG. 1. Absorption and scattering of distilled water.

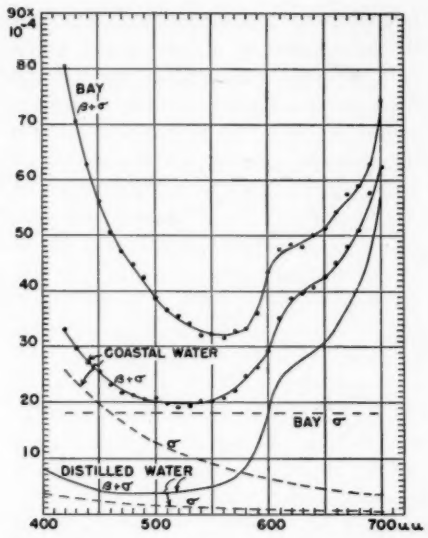

FIG. 2. Absorption and scattering of water samples.

are listed in Table I, Column 2, and are plotted in Fig. 1 in which for clarity the scale of ordinate for $\lambda < 580\mu\mu$ is 10 times the scale for $\lambda > 580\mu\mu$. By reflecting the beam of light back through the 12-foot absorption tube, so that the beam traversed 24 feet of distilled water, the shallow minimum of absorption in the blue green could be seen visually to lie in the region 460 to $470\mu\mu$. For comparison, the values of κ obtained by a number of earlier observers[3] are plotted in Fig. 1. It is seen that there is considerable variance among the measurements. Whether the variations were caused by differences in preparation of water or in spectrographic and photometric techniques is not known.

Subtracting the values of σ, Table I, Column 3, from the respective values of κ, Column 2, gave the values of β, Column 4. These are the first data of the absorption coefficients of distilled water throughout the visible spectrum that have been obtained, for the present case is the only one in which σ was measured simultaneously with κ, thereby permitting β to be evaluated.

The sample of Atlantic Ocean water was taken on February 11 from the sea 2.5 miles east of the Florida coast near Hollywood.* The depth was about 70 fathoms and a 5-gallon bottle was used with an automatic stopper that opened about one fathom below the surface. The water might be described as "coastal Gulf Stream" water. The bottle was received at the laboratory on February 24. It was shaken vigorously and the water poured into the scattering flask and absorption tube. A few large heavy particles were visible which settled out almost immediately leaving motes visible for the most part only by forward scattering. The observed values of $\sigma_{\pi/2}$ for tungsten light are shown in Table II. Comparing these values with the value 1.44×10^{-6} for carefully settled out distilled water it is seen that the scattering of the coastal water was somewhat greater. But when compared with tap water, or with un-settled-out distilled water, the coastal water seemed astonishingly dust free.

TABLE II. Values of $\sigma_{\pi/2}$ of coastal water.

Date	$\sigma_{\pi/2}$
February 24	12.2×10^{-6}
27	8.8
March 1	8.6
5	6.7

[3] N. E. Dorsey, *Properties of Ordinary Water-Substance* (Reinhold Publishing Corporation, New York, 1940), Table 161.

* Lieutenant E. R. F. Johnson kindly obtained the sample for me.

The values of σ_ϕ of the coastal water were measured on February 24 and are plotted as $(\sigma_\phi/\sigma_{\pi/2})\sin\phi$ in Fig. 3. From these values and $\sigma_{\pi/2}=12.2\times10^{-6}$ the scattering attenuation σ_t for tungsten light and η were calculated from (3), (5)–(7). One found

$$\sigma_t=8.69\times10^{-4},$$
$$\eta=0.866.$$

The scattered beam was bluish in color, justifying the assumption that σ was proportional approximately to λ^{-4}. With this assumption and with $\sigma_t=8.69\times10^{-4}$ the values of σ were calculated throughout the visible spectrum; they are plotted in Fig. 2.

The attenuation $\kappa=\beta+\sigma$ of the coastal water was measured on February 25 and 26, and is plotted in Fig. 2. In the absorption tube the ocean water was slightly, but distinctly, greener than the distilled water. In keeping with this was the fact that the κ or $\beta+\sigma$ curve of the coastal water showed relatively greater attenuation for the shorter wave-lengths than the curve of distilled water.

The sample of Chesapeake Bay water was taken on October 18 from the surface about a mile from Bloody Point, the depth being about 15 fathoms. Measurements were begun the following day. The water was shaken up and poured into the scattering flask and absorption tube. It showed considerable scattering especially in the forward direction, the beam being whitish in color with many motes. Some of the larger motes were alive and moved about; the larger ones soon settled out. Measurements on October 19 resulted in

$$\sigma_{\pi/2}=15.6\times10^{-6}$$

and the $(\sigma_\phi,\ \sigma_{\pi/2})\sin\phi$ curve of Fig. 3. From these data and (3), (5), and (6) one found

$$\sigma_t=18\times10^{-4},$$
$$\eta=0.93.$$

The whiteness of the beam indicated that σ was approximately constant with λ. Therefore the σ,λ curve is drawn in Fig. 2 as a straight line parallel to the X axis.

The attenuation $\kappa=\beta+\sigma$ curve, measured on October 20, is given in Fig. 2, and shows a maximum of transmission in the yellow green. A

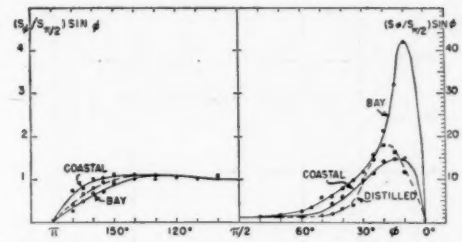

FIG. 3. Scattering of water samples. (The "S's" in the figure should be σ's.)

white plaque observed through the Bay water in the 12-foot tube appeared yellow green. The values of κ for the Bay water are in Table I, Column 5. Subtracting $\sigma=18\times10^{-4}$ from these gave the absorption β of the Bay water in Column 6, which may be considered made up of two parts, one due to the water and the other due to the colored material in the water, the material being plankton. Subtracting β for distilled water from the respective values of Column 6 gave in Table I, Column 7, the absorption of the Bay plankton. The values are plotted in Fig. 4.

The Bay water remained in the absorption tube for several weeks. It gradually lost its green color and approached the color of distilled water, indicating that with lack of air and light the plankton material slowly changed and disappeared.

A filter whose absorption coefficient increased rapidly with decreasing wave-length, as that of the Chesapeake Bay plankton, would be yellow, or even amber. Thus we may say that the color of the plankton was yellow. When the plankton are in water, which absorbs the red end of the spectrum, the result is a green or yellow-green color. The fact that the color of the Bay material, which we have vaguely referred to as "plankton," is yellow is in keeping with an earlier conclusion[4] that pigments of a yellow color are present in water of the North Sea. The slight absorption in the blue of the coastal water of Fig. 2 may be regarded as due to a very slight amount of the yellow material, similar as far as color is concerned to that of the Chesapeake Bay considerably diluted. However, one cannot generalize too broadly, for not all planktonic materials are the same in color, various types being described as green, muddy, brownish, reddish, and so forth.

[4] K. Kalle, Ann. d. Hydrogr. u. Mar. Met. 66, 1–13 (1938).

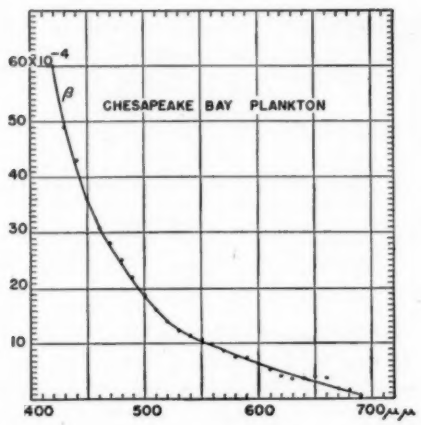

FIG. 4. Absorption of Chesapeake plankton.

THEORETICAL

A general expression for the light coming out of the sea in terms of the optical constants of the sea water was worked out for a sea of any depth in sunny and cloudy weather.[5] It is of interest to apply the expression to the present measurements. Let a_0 and i_0 be the illuminations from the sky and the sun, respectively, that fall on the surface of the sea, and b_0 the light that emerges from the sea outside of the sun path. The general expression is Eq. (16),[5] and may be written

$$b_0 = a_0\Gamma + i_0\Gamma', \tag{8}$$

where Γ and Γ' are functions of β, σ, η, ζ, the depth of the water and the reflectivity of the bottom; ζ is the zenith angle of the sun. All quantities of (8) refer to wave-length λ. In (8) no surface reflection is assumed. With surface reflection r_c for collimated light and r_d for diffuse light (8) becomes

$$b_0 = a_0[(1-r_c)(1-r_d)\Gamma + r_c] + i_0(1-r_c)^2\Gamma'. \tag{9}$$

For a calm surface of water $r_c = 0.021$ for $\lambda = 5600$A and $\zeta = 0°$ and for other values of λ and ζ is given by Fresnel's equations. For $\lambda = 5600$A $r_d = 0.066$. The reflectivity r_λ of the sea for wave-length λ is defined as the ratio of the downward light to the upward light seen by an observer looking vertically downward. Then

$$r_\lambda = b_0/(a_0 + i_0). \tag{10}$$

[5] E. O. Hulburt, J. Opt. Soc. Am. **33**, 42–45 (1943), Eq. (16).

For skylight and sunlight seen with the eye, the visible reflectivity R is given by

$$R = \frac{\int b_0\psi d\lambda}{\int (a_0 + i_0)\psi d\lambda}, \tag{11}$$

where ψ is the visibility function and the integrals are taken over the visible spectrum.

In order to calculate from (11) the color of the up-welling light and the values of R for the three samples of water, we consider a simple case of an infinite depth and a uniformly cloudy sky. For no surface reflection R is given by (11) with

$$b_0 = a_0\Gamma, \tag{12}$$

and with surface reflection R is given by (11) with

$$b_0 = a_0[(1-r_c)(1-r_d)\Gamma + r_c]. \tag{13}$$

The b_0, λ curves were calculated for the three samples of water from (12) with the data of Fig. 2 and the observed values of η; they are plotted in Fig. 5 together with a_0 the spectral distribution of daylight for a cloudy sky.[6] Likewise, the b_0, λ curves from (13) were drawn. The $b_0\psi$, λ curves were then plotted but are not given here. From the areas under the curves and from (11) the reflectivities were determined and are given in Table III.

It appears from Table III that about 60 percent of the brightness of the Gulf Stream or Chesapeake Bay viewed in calm cloudy weather by an observer looking vertically downward is caused by light up-welling from the depths and about 40 percent is caused by surface reflection. The curves of Fig. 5 show that the light coming up from the Gulf Stream off the coast of Florida

TABLE III. Calculated reflectivity R of a calm sea of infinite depth for a cloudy sky.

	No surface reflection	With surface reflection
Distilled water	0.018	0.036
Gulf Stream	0.047	0.063
Chesapeake Bay	0.035	0.052

[6] A. C. Hardy, *Handbook of Colorimetry* (The Technology Press, Massachusetts Institute of Technology, Cambridge, Massachusetts, 1936), p. 17.

and from distilled water is very blue and from Chesapeake Bay is green. This is in agreement with familiar observation. The case of distilled water may be of interest in connection with observations of very pure fresh water lakes.

In order to bring out the change in the reflectivity of the sea with the state of the sky and the altitude of the sun, it is sufficiently accurate for the present purpose to use (11) with values averaged over the visible spectrum rather than to perform the indicated integrations. Let f define the state of the sky, where

$$i_0 = f a_0. \tag{14}$$

Values of f observed for various states of the sky are given in Table IV. Then (11) becomes

$$R = \frac{[(1-r_c)(1-r_d)\Gamma + r_c] + f(1-r_c)^2\Gamma'}{1+f}, \tag{15}$$

where now the quantities are values averaged over the visible spectrum for the spectral distributions of the illuminants and the visibility function. Average values for the Chesapeake Bay sample are

$$\sigma_c = 18\times10^{-4},$$

$$\beta_c = 16.7\times10^{-4},$$

$$\eta = 0.93.$$

With these the values of R were calculated from (15) for ζ from 0° to 90° for the values of f of Table IV. The R, ζ curves are plotted in Fig. 6; corresponding curves for the Gulf Stream were very similar to those of Fig. 6. The curves show the theoretical changes in the Bay and the Gulf Stream with the state of the sky and the altitude of the sun. For example, R increases by about 60 percent as the sky changes from cloudless to cloudy for altitudes of the sun above 50°.

OBSERVATIONS IN THE OPEN

Measurements of the reflectivity of Chesapeake Bay were made from a boat and from an airplane

TABLE IV.

State of Sky	f
All sun, no sky	infinity
Sunny, clear sky	7
Sunny, hazy sky	3
Sun through thin clouds	1
No sun, cloudy	0

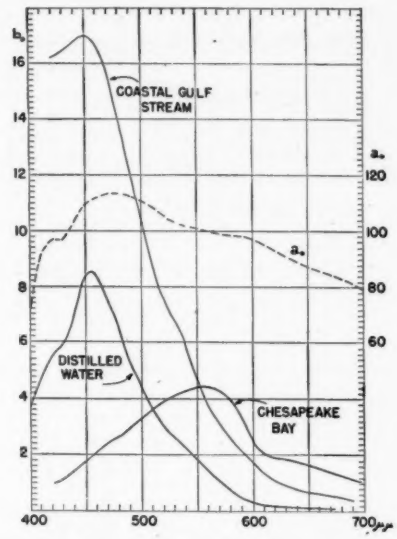

FIG. 5. Spectral curves of surface light from deep water.

and of the sea from an airplane. Macbeth illuminometers were used and in each experiment three quantities were determined, the brightness W of the water surface outside of the sun path and the brightness P_1 of a horizontal, white, mat plaque exposed to the illumination of the sky plus the sun and P_2 to the sky alone. A pale blue, calibrated filter was placed over the illuminometer lamp in order to obtain a color match when bluish areas were observed. From W, P_1, and P_2, the reflectivity R and sun-to-sky ratio f were calculated by means of

$$R = W/P_1, \tag{16}$$

$$f = (P_1 - P_2)/P_2. \tag{17}$$

An interesting series of observations made from a boat on Chesapeake Bay is given in Table V. In this case the boat was becalmed in the middle of the Bay while dark clouds, which covered the sun and a portion of the sky, slowly moved away to expose the sun in a clear blue sky. During this time the altitude of the sun varied from 67° to 72°. The observed values of R are in Table V, Column 3, the theoretical values from Fig. 6 are in Column 4, and are in fair agreement with the observations.

Similarly, values of R of the Bay measured from an airplane changed from 0.025 to 0.06 when

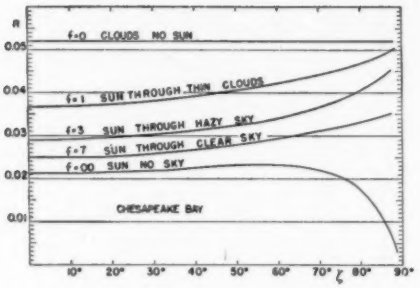

FIG. 6. Theoretical reflectivity of Chesapeake Bay.

the plane passed from sunshine into regions under clouds. In fact the decrease in R with the change in the illumination from diffuse, i.e., cloudy, to collimated, i.e., sunshine, was easily noticeable without accurate measurement. This was done with a large card painted a mat dark green and held horizontally against the Bay surface as background. The card matched the Bay surface approximately when the sun was behind clouds, and when the sun came out the card was observed to brighten much more than the Bay surface.

Observations of the reflectivity of the Atlantic Ocean made from an airplane on August 10, 1943, are recorded in Table VI. The sea was moderate and the air fairly clear. The plane flew at an altitude of about 1000 feet from the Maryland coast eastward about 150 miles out to sea. The plane passed under a cloudy area on the outward flight; on the return flight the sky became nearly cloudless. It is seen from Table VI that R was from 0.022 to 0.034 outside of the sun path for a sunny sky and about 0.05 for a cloudy sky for distances from shore beyond 12 miles where the depths were greater than 10 fathoms. The corresponding theoretical values, from Fig. 6, are 0.025 and 0.052. As the shore was approached, the depth decreasing from 8 fathoms to zero, R in sunshine increased from 0.025 to 0.05, due no doubt to the bottom and to considerable scattering material in the shoal water. A few observations indicated that R increased by one or two units in the second decimal place with the roughness of the sea. The above results are in approximate agreement with some earlier observations[7] off the coast of New England of the change in the reflectivity of the sea with the state of the sky. It was found that for the sun above

[7] W. M. Powell and G. L. Clarke, J. Opt. Soc. Am. **26**, 111–120 (1936).

TABLE V. Reflectivity R of Chesapeake Bay.

State of sky	f	R observed	R theoretical
Cloudy	0	0.054	0.052
	0	0.056	0.052
Sun through edge of cloud	1.2	0.036	0.037
	1.7	0.023	0.035
	2.8	0.023	0.032
	5.3	0.017	0.027
Sunny	6.1	0.019	0.026

TABLE VI. Reflectivity R of the Atlantic Ocean.

Time EST	Altitude of sun	Distance from shore, nautical miles	Depth of sea, fathoms	R Sunny	R Cloudy
9.50	51°	4	5	0.033	
9.53				0.031	
9.56		17	16		0.037
9.58				0.023	
10.00		25	20	0.026	
10.05					0.047
10.07					0.052
10.09		45	40		0.052
10.23	60°	75	800	0.030	
10.25				0.028	
10.27		85	1100	0.029	
10.32				0.027	
10.35		100	1400	0.029	
10.52				0.026	
10.54		140	1800	0.025	
10.59	68°	150	1800	0.025	
11.33		110	1500	0.034	
11.35				0.033	
11.37				0.022	
11.56		70	600	0.030	
11.59	69°			0.025	
12.01		50	50	0.024	
12.02				0.024	
12.08				0.022	
12.09				0.025	
12.10		30	25	0.024	
12.11				0.024	
12.12				0.027	
12.13		20	15	0.025	
12.16				0.027	
12.17	68°			0.026	
12.18		10	8	0.025	
12.19		8	8	0.027	
12.20		6	7	0.030	
		5	6	0.032	
		4	5	0.032	
		3	5	0.037	
		2	4	0.040	
		1	3	0.044	
12.23		0	0	0.051	

30° altitude the reflectivity was about 0.065 for cloudy days and 0.04 for clear days.

In general, it is seen that there was fair agreement between the observed values of the sea and the Bay reflectivity and the values of Table III and Fig. 6 which were calculated from the optical constants of samples of the sea and the Bay measured in the laboratory. This was not entirely anticipated, for the suspicion was entertained that the optical properties of samples, particularly the scattering, would change with time and with handling and would not be representative of the water from which they were taken. It appears that in the present case the suspicion was without much foundation. However, it is certain that the procedure of measuring samples transported to a laboratory is not a best procedure. Measurement of the water *in situ* is much to be preferred, or at least of samples carefully taken and not more than a few hours old.

In voyages on the Atlantic Ocean I have often observed that the color of the up-coming light of the open sea far from land is a beautiful turquoise blue in low latitudes, but in higher and colder latitudes is less blue in color, being a blue-black or a dark gray almost devoid of color. The explanation of the color difference is suggested in the results of the present experiments. A slight amount of yellow or green or brown coloring material in pure sea water will reduce the blue color and make the water appear less blue and more gray. Now it is well known that pelagic planktonic material is more abundant in the colder than in the warmer areas of the sea. For example the *Encyclopaedia Britannica*[8] states, "In general the temperate and cold waters are rich in plankton, while the tropical and warm waters are relatively poor. The richest plankton in any part of the world ocean is that found on the borders of the polar seas in the regions of melting ice." Therefore it is reasonable to suppose that the turquoise blue color of the ocean in low latitudes is that of nearly pure sea water, and that the blacker or grayer color of high latitude seas is to be attributed to a more or less amount of yellow or green or brown coloring due to the planktonic content.

[8] *Encyclopaedia Britannica*, fourteenth edition, Vol. 17, p. 1004.

JOURNAL OF THE OPTICAL SOCIETY OF AMERICA VOLUME 35, NUMBER 11 NOVEMBER, 1945

The Significance of Emittance* in Radiation Pyrometry

THOMAS R. HARRISON
The Brown Instrument Company, Philadelphia, Pennsylvania.
(Received June 5, 1945)

"EMITTANCE" COMPARED TO THE SETTING OF SHUTTERS AT A WINDOW

A HEATED body, such as a block of steel, emits radiant energy at a rate dependent upon its temperature and upon the freedom with which its surface allows radiant energy to escape. Surfaces of different materials vary in the latter respect. Imagine, for example, a certain area on the surface of a steel block as similar to a window without glass but with shutters. If the shutters are completely removed, radiant energy, such as light or infra-red heat waves, can pass into or out of the room through the window with perfect freedom. Sunshine from without can freely enter the room or conversely, light from an electric lamp within the room can pass outward through the window without hindrance or diminution. If the shutters are half closed, only half of the light approaching the window in either direction will pass through it. Considering the steel block in place of the room (the interior of the block being equivalent to the interior of the room), radiant energy falling upon its surface meets the equivalent of partly closed shutters, so that only part of it passes inward through the surface and is absorbed. Somewhat like a lighted lamp within the room, the steel block tends to radiate its own energy. This energy may be thought of as "taxiing" up to the surface by conduction and "taking off" (i.e., being emitted) through the "shutters" by radiation. The nature of the surface, like the setting of shutters, governs the relative rate of emission of this energy.

Corresponding to shutters that are about 79 percent open, the surface of the steel block would be said to have an emittance of 0.79, that is, within a given time 79 percent as much radiant energy would be emitted from the surface of the heated metal as would be emitted if the "shutters" were absent.

BLACKBODY, BLACKBODY RADIATION, AND BLACKBODY CONDITIONS

Certain cold objects appear black to the eye because all light falling upon them passes inward and is absorbed, leaving none to be reflected to the eye for observation. This is as if no "shutters" were present. Soot or lampblack are good examples (though strictly speaking they are not perfect in this respect). The same effect is encountered when looking through a small opening into a large, unlighted cavity, such as into a cave or a cold muffle furnace. Light can pass inward through the opening perfectly freely and, if not absorbed by the first internal surface that it strikes, is successively reflected from surface to surface until it is practically all absorbed and very little gets back out through the opening. The opening, therefore, appears to an observer to be black.[1]

Conversely, when the soot or lampblack is heated, it radiates energy at the maximum rate possible for its temperature because its surface, in effect, has no shutters. Likewise, a cavity such as a muffle furnace, having its inner walls uniformly heated to the same temperature, will emit radiant energy through a relatively small opening at this same maximum rate. The hole is actually completely open, of course, and even though the materials of the inner walls may have a low emittance, the walls will reflect enough of the energy coming to them from other walls to make up for what they lack in their own emission so that the total is the same as if the walls emitted energy at the maximum possible rate.

Such a uniformly heated cavity, with appropriately small opening, or a material that emits its energy without hindrance is known as a *blackbody*. Radiant energy emitted from such a source due to its temperature is known as

* See footnote 1 of following paper by T. R. Harrison, "Industrial Use of Radiation Pyrometers under Non-Blackbody Conditions," J. Opt. Soc. Am. **35**, 708 (1945).
Editor's Note: This simplified explanation of emittance, as a factor in radiation pyrometry, is presented as an introduction to the following article. It is designed for those readers who may desire a brief review of the subject before considering the more technical details.

[1] This subject is treated in greater detail by Robert B. Sosman in *The Pyrometry of Solids and Surfaces* (American Society for Metals, Cleveland, Ohio, 1940), pp. 15–18.

blackbody radiation. Also, any conditions that enable *blackbody radiation* to be emitted are known as *blackbody conditions*. These conditions might be the result of the use of a uniformly heated enclosure, or of the nature of the material employed, or of the presence of suitable fine indentations, crevices, etc., in the surface of the material.

In the above-mentioned case of the heated enclosure or cavity, the total energy emanating from the opening within a given unit of time is the sum of that emitted by, and that reflected from, the opposite walls. If the emittance of the material of the wall is high enough, the reflected energy will be negligible so that the portion of the wall in question might as well be in the open so far as blackbody radiation is concerned. However, if the emittance is low, more dependence is placed upon reflection from the other walls, thus requiring the cavity to be nearly closed. Where the emittance of the wall material is fairly high, only a moderate amount of equally heated enclosing wall is required to render practically full blackbody conditions. The above factors are involved in establishing the proper depth to which a radiation pyrometer target tube should be inserted into a furnace. Figure 1 shows how the spectral radiancy (rate of emission of radiant energy at a given wave-length per unit area) of a blackbody varies from one wave-length to another. The point of maximum spectral radiancy is seen to shift toward the shorter wave-lengths with increasing temperature. The wave-length at which this maximum occurs is $\lambda_{max} = 2892/T°K$ microns. The total radiancy of the blackbody (rate of emission at all wave-lengths per unit area), represented for each temperature by the area beneath the corresponding curve, is proportional to the fourth power of the absolute temperature.

SPECTRAL EMITTANCE AND TOTAL EMITTANCE

Emittance is defined as the ratio of radiant energy emitted per unit time and per unit area by a body to that emitted by a blackbody at the same temperature. Total emittance refers to radiation of all wave-lengths and spectral emittance refers to the radiation in a very narrow wave-length interval.

Tables of values of spectral emittance for wave-length $\lambda = 0.65\mu$, for use with the usual optical pyrometer, and of total emittance for use with radiation pyrometers, are given for many materials, in the following article. Where the spectral emittance for a given substance has a substantially uniform value for all wave-lengths throughout the blackbody spectrum the total emittance has the same value as that of spectral emittance. Where spectral emittance varies from one wave-length to another the total emittance is a composite of the spectral emittances. The spectral emittance at each wave-length contributes to the composite value in proportion to the relative radiancy of a blackbody at that wave-length. The variation of relative radiancy of a blackbody with change in wave-length and in temperature is shown in Fig. 1. Thus it is seen that the spectral emittance at 1.92μ contributes more strongly toward determining total emittance for a body at 2240°F than it does for a body at 1340°F. Likewise spectral emittances at all other wave-lengths contribute toward the composite value comprising total emittance to relative extents that vary with the object temperature. It follows that where spectral emittance is not uniform from one wave-length to another the total emittance of an object will vary with its temperature. Some of the differences between the total emittance values, for the same sub-

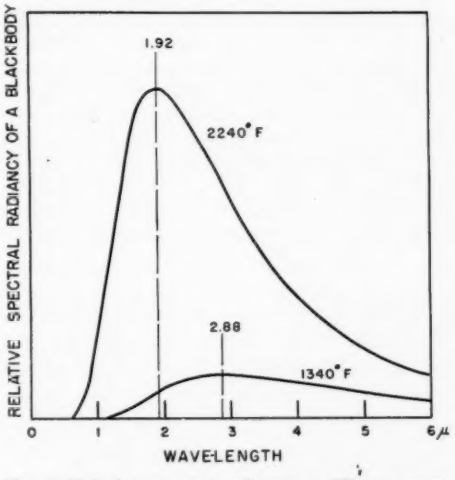

FIG. 1. Relative spectral radiancy at different wave-lengths, of a blackbody at 1340°F and at 2240°F.

stance at different temperatures, as listed in the tables referred to above, are accounted for on this basis.

Referring again to Fig. 1, it is seen that the radiant energy of a blackbody at even a rather high temperature is distributed principally throughout wave-lengths longer than 1 micron. The human eye is sensitive to that portion of the spectrum roughly between 0.4μ and 0.7μ. Obviously, if the characteristics of a substance vary from one wave-length to another they can be very different in the visible portion of the spectrum from what they are over the range of wave-lengths important in transmitting the main portion of the energy that the substance radiates. Accordingly, visual appearance is not a dependable indication of total emittance. An instance of this is that of painted radiators for heating buildings. Usually the color of paint makes little difference in the emittance of the radiator.

JOURNAL OF THE OPTICAL SOCIETY OF AMERICA VOLUME 35, NUMBER 11 NOVEMBER, 1945

Industrial Use of Radiation Pyrometers under Non-Blackbody Conditions

THOMAS R. HARRISON
The Brown Instrument Company, Philadelphia, Pennsylvania

(Received June 5, 1945)

The principles of non-blackbody radiation and of the application of emittance corrections is discussed for various industrial conditions. Beside the commonly treated case of radiation from a non-blackbody in the open, others discussed are radiation from a heated object surrounded by walls at a higher or lower temperature, radiation from an object viewed through flame, smoke, and furnace gases, and radiation from glass. A table and curves are given for obtaining emittance corrections applicable for a radiation pyrometer having a Pyrex glass lens and another table and other curves are given for a radiation pyrometer with fused silica lens. The use of an optical pyrometer as a "checking instrument" is discussed, and a table and curves are given for emittance corrections where $\lambda=0.65\mu$. Comparisons are drawn between the readings of the optical pyrometer and radiation pyrometers having the two types of lens, for the condition $e_\lambda=e_t$. For certain cases data and procedures are given by means of which emittance corrections are obtainable. For other cases, only the underlying principles are discussed. A bibliography is given.

A LARGE portion of the industrial processes to which radiation pyrometers are applicable embody so-called blackbody conditions. There are many applications, however, in which non-blackbody conditions exist but to which radiation pyrometers are being applied successfully. In many cases, the pyrometer may be usefully employed as a gauge or controller of the uniformity of conditions without an attempt being made to ascertain the true temperatures.

The present article discusses the principles of non-blackbody radiation and gives various relations between emittance, the readings of radiation pyrometers, of optical pyrometers, and the corresponding true temperatures of the object whose temperature is being measured. Consideration is given to the case of a heated object surrounded by walls at a higher temperature, and to other special cases.

PRINCIPLES OF RADIATION PYROMETRY

A heated body emits radiant energy at a rate dependent upon its temperature. When a suitable sensitive element is subjected to this radiant energy, a rise in temperature of the element is produced which may be utilized to provide an indication of the temperature of the body. The radiation pyrometer is based upon this principle. Many such instruments make use of several thermocouples, assembled to form a unit called a thermopile, as the sensitive element. The electromotive force developed by the thermopile is representative of the temperature of the heated body from which the radiant energy is received. When measuring elevated temperatures, the temperature attained by the thermopile is much lower than the temperature being measured.

BLACKBODY, NON-BLACKBODY, AND EMITTANCE[1] DEFINED

If the surface of an opaque body possesses the ability to allow energy to pass perfectly freely from within the body, the radiant energy emerges at a maximum rate possible for any body at that temperature. Radiant energy is emitted at this maximum rate through a relatively small hole in the side of an opaque chamber, the walls of which are at a uniform temperature. Such a surface or enclosure is known as a *blackbody*. *Blackbody conditions* are those conditions under which radiant energy flows from any given area at the maximum rate possible for that temperature.

A substance may emit radiant energy at a lower rate than that of a blackbody at the same temperature. Such a substance is a non-blackbody. The "emittance" of a body is the ratio between its rate of emission per unit of area and that of a blackbody at the same temperature. When considering the total radiant energy at all the wave-lengths that are emitted (caused by temperature alone) the ratio is called *total emittance* and is indicated by the symbol e_t. Total emittance is used in dealing with the usual types of radiation pyrometers.

Where the ratio applies to a comparatively narrow band of wave-lengths the ratio is called "spectral emittance" and written e_λ. Where an optical pyrometer using a narrow band of wave-lengths around 0.65 micron is under consideration, the spectral emittance is designated as $e_{0.65\mu}$. For a blackbody $e_t = 1$ and $e_\lambda = 1$.

RADIATION FROM A NON-BLACKBODY IN THE OPEN

As explained above, radiation from a non-blackbody is reduced with respect to that from a blackbody by a ratio indicated by its emittance. Values of total emittance and spectral emittance for various substances are given in tables included with this article. These values range from 0.05 or less for some substances to over 0.95 for others. Additional tables and several sets of curves show, for various values of emittance, the relations between true temperatures and the readings of two types of radiation pyrometers and of the usual optical pyrometer using a band of wave-lengths around 0.65μ.

In the tables for total emittance, several values of total emittance are given for one substance, each value corresponding to a different temperature. One reason for such variation with temperature is dependent upon the fact that, for materials presenting such variation, the spectral emittance is different at different wave-lengths. As the temperature increases the predominating wave-lengths become shorter. This causes the emittances at shorter wave-lengths to become of increasing importance with rising temperature, contributing an increasing share toward establishing the corresponding value of total emittance.

RADIATION FROM A NON-BLACKBODY WITHIN A HEATED ENCLOSURE

When a non-blackbody is enclosed within heated walls, such, for example, as a steel object in a furnace, some of the radiant energy coming from the walls is reflected by the object. For an understanding of such a case, reference is made to Fig. 1. When radiant energy from an external source impinges upon a body, part is reflected from the surface, part enters the body and is absorbed as heat, and, unless the body is opaque, part is transmitted and emerges from the body just as light is transmitted through glass. Part of the energy absorbed may go to raise the temperature of the body; part is subsequently re-radiated from the body.

Arrow L represents radiant energy impinging upon body B. R represents the portion of L that

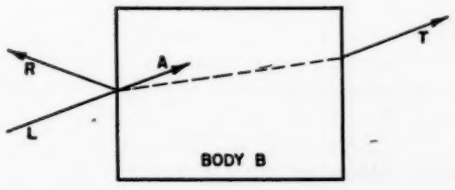

FIG. 1.

[1] The term "emittance" is used here in the sense in which "emissivity" is commonly used. As recommended by Professor A. G. Worthing, the term "emissivity" is reserved for a more restricted meaning. See page 1164 of *Temperature, Its Measurement and Control in Science and Industry* (American Institute of Physics, 1941) published by the Reinhold Publishing Company, New York. The Committee on Colorimetry of the OSA (J. Opt. Soc. Am. **34**, 183–218 (1944)) continues to apply the original definition of the term "emissivity" and gives a different meaning to the term "emittance."

is reflected, A the portion that is absorbed, and T the portion that is transmitted. Reflectance, r, equals R/L; absorptance, a, equals A/L, and transmittance, t, equals T/L. The terms r, a, and t, can be taken to represent either "spectral" or "total" reflectance, absorptance, and transmittance according to the spectral composition of the incident radiation as indicated by the subscripts t and λ. Since the sum of the parts must equal the whole,

$$r_t+a_t+t_t=1 \quad \text{and} \quad r_\lambda+a_\lambda+t_\lambda=1.$$

For opaque bodies, t equals zero, and the above relations become

$$r_t+a_t=1 \quad \text{and} \quad r_\lambda+a_\lambda=1.$$

The ease with which a body or substance can radiate or emit its own heat energy is precisely equivalent to the ease with which that same body or substance can absorb *like* radiant energy impinging upon it. This relationship is easily explained, since, if a completely enclosed body were able to absorb radiant energy more freely than it could emit or re-radiate that energy, the body would become hotter than its surroundings. Reverse conditions would cause the body to cool below the surrounding temperature. Neither of these resulting conditions, of course, is possible. Hence, when a body is surrounded by walls at the same temperature, energy must be emitted by the body at the same rate that it is absorbed from the walls. Accordingly, total absorptance a_t equals total emittance e_t, and spectral absorptance a_λ equals spectral emittance e_λ when body and surrounding walls are at the same temperature; that is,

$$e_t=a_t$$

and by substitution,

$$e_t+r_t+t_t=1$$

or, for opaque bodies,

$$e_t+r_t=1;$$

and also

$$e_\lambda=a_\lambda,$$

and by substitution,

$$e_\lambda+r_\lambda+t_\lambda=1$$

or, for opaque bodies,

$$e_\lambda+r_\lambda=1.$$

Therefore, under these conditions, a radiation pyrometer or an optical pyrometer, calibrated for blackbody conditions, would read temperature correctly when sighted upon a non-blackbody in such manner as to receive both the energy emitted by the body and that reflected by it from surrounding walls at the same temperature as that of the object. Where the object and walls are at different temperatures, the pyrometer reading will lie between the temperature of the object and that of the walls. An object with a *high* emittance (total or spectral) tends to decrease the difference between the object temperature and the pyrometer reading. *Surrounding walls* of *low* emittance also tend to decrease the difference. Conversely, the condition of an object having low emittance surrounded by walls of high emittance tends to increase the difference between the object temperature and the pyrometer reading.

The radiant energy received by the pyrometer per unit of time will be the sum of two components, as follows:

(*a*) That radiated by the object itself. This equals the total or spectral emittance of the object (for radiation or optical pyrometer, respectively) multiplied by the radiant energy that would be received per unit of time from a similarly located blackbody at the same temperature as the object.

(*b*) That received from the surrounding walls by transmission through the object, if transparent, and by reflection from its surface. This equals unity minus total or spectral emittance[2] multiplied by the radiant energy that would be received per unit of time from a blackbody at the same temperature as the walls. This component depends upon the temperature of the walls instead of that of the object.

If the walls of the furnace are composed of materials having practically blackbody characteristics it is obvious that the above-mentioned energy impinging upon the object from the surrounding walls is blackbody radiation corresponding to the wall temperature. Even if the

[2] Since $e_t+r_t+t_t=1$, then $r_t+t_t=1-e_t$, or, where $t_t=0$, $r_t=1-e_t$. Likewise $r_\lambda+t_\lambda=1-e_\lambda$, or where $t_\lambda=0$, $r_\lambda=1-e_\lambda$. It is noted that, in certain cases, total emittance varies with temperature. Likewise, in such cases, "total" transmittance or "total" reflectance values, or both, vary with temperature. The values of the latter factors are based upon the temperature of the source of the transmitted and reflected energy (the furnace walls in the case under consideration) while emittance is based upon the object temperature. Accordingly, the above relation of r_t, t_t, and e_t is not necessarily rigorous for all cases. For most practical industrial cases, however, it is sufficiently true to be used in the examples given.

walls have low emittance, multiple reflections from wall to wall would build up the total to the value of blackbody radiation for that temperature, provided the enclosed object fills a relatively small fraction of the internal volume of the furnace. When the wall emittance is low and the object is relatively large in size, a good portion of the energy impinging upon the object from the wall will have been previously emitted by the object and reflected by the wall. In this latter case, the object temperature tends to have a predominant effect upon the pyrometer reading. In the examples given in Table VIII, the surrounding wall will be assumed to be composed of a substance having unit emittance so that the wall temperature has maximum effect upon the reading of a radiation pyrometer sighted upon the enclosed object. With walls of lower emittance and the object largely filling the space within the enclosure, the temperature reading will be closer to the temperature of the object than the examples indicate.

RADIATION FROM AN OBJECT VIEWED THROUGH FLAME, SMOKE, OR FURNACE GASES

Conditions which otherwise might be considered as perfect blackbody conditions may be upset by the presence of flame, smoke, or furnace gases. In installations where these latter conditions exist, the radiation pyrometer generally indicates a temperature between that of the furnace atmosphere and that temperature which would be indicated if such an atmosphere were not present. Where cooler gases and smoke intervene between the pyrometer and the object sighted upon, the reading will be lowered.

A thick luminous flame may shield the object almost completely, and the reading of the radiation pyrometer will be affected markedly by the flame. Non-luminous flames radiate and absorb energy only in certain wave-length bands, principally because of the presence of carbon dioxide and water vapor. The greater portion of this radiation is within the wave-length bands transmitted by a fused silica lens. A Pyrex lens does not transmit some of these wave-lengths and, therefore, a radiation pyrometer equipped with a Pyrex lens should read the temperature of an object more accurately when sighted upon it through non-luminous flames than one equipped with a fused silica lens. Where appreciable flame, smoke, and furnace gases are present, unless a closed-end tube can be used, it is generally advisable to provide a purged sighting path in connection with an open-end sighting tube.

The subject of measuring temperatures where flames are present is too complex to consider more fully in this article. Readers who are interested in pursuing the subject further are referred to articles listed in the bibliography appended hereto.

RADIATION FROM GLASS

Glass reflects, absorbs, and transmits light and other radiant energy; its spectral absorptance at any given wave-length equals its spectral emittance at that wave-length. A thin layer of glass lying at a depth t beneath the surface will both absorb and emit radiant energy of a given wave-length in direct relation to the spectral absorption coefficient k_λ of the substance. In its transit toward the surface the radiant energy emitted from such a thin layer is reduced by absorption by the intervening mass. The fraction of the original energy reaching the surface is given by the expression e^{-x} where $x = k_\lambda t$. Thus, from a layer relatively close to the surface practically all of the radiant energy arising within the layer and directed toward the surface will reach the surface; from a layer at a depth $t = 0.7/k_\lambda$, for which $x = 0.7$, half reaches the surface; from a depth $t = 1/k_\lambda$, for which $x = 1$, about 37 percent reaches the surface; and from a depth giving $x = 4.61$, only about one percent reaches the surface. Thus the term e^{-x} determines the relative extents to which layers at various depths contribute to the entire spectral radiation from the mass, and the numerical value of $1/k_\lambda$ fixes the actual depths within the glass for which the specified fractions apply.

If it is desired to have a pyrometer to respond as largely as possible to the temperature of layers deep within the mass, it follows that the pyrometer response should be limited, as far as practicable, to those wave-lengths for which k_λ is relatively small, so that correspondingly large values of t are required to give any chosen value of x.

TABLE I. Total emittances of miscellaneous materials.* (Most values are uncertain by ten percent to thirty percent. In many cases value depends upon particle size.)

Material	Temperature °C	Emittance ϵ_t
Aluminum (oxidized)	200	0.11
	600	0.19
Brass (oxidized)	200	0.61
	600	0.59
Calorized copper	100	0.26
	500	0.26
Calorized copper (oxidized)	200	0.18
	600	0.19
Calorized steel (oxidized)	200	0.52
	600	0.57
Cast iron (strongly oxidized)	40	0.95
	250	0.95
Cast iron (oxidized)	200	0.64
	600	0.78
Copper (oxidized)	200	0.6
	1000	0.6
Fire brick	1000	0.75
Gold enamel	100	0.37
Iron (oxidized)	100	0.74
	500	0.84
	1200	0.89
Iron (rusted)	25	0.65
Lead (oxidized)	200	0.63
Monel (oxidized)	200	0.43
	600	0.43
Nickel (oxidized)	200	0.37
	1200	0.85
Silica brick	1000	0.80
	1100	0.85
Steel (oxidized)	25	0.80
	200	0.79
	600	0.79
Steel plate (rough)	40	0.94
	400	0.97
Wrought iron (dull oxidized)	25	0.94
	350	0.94
20Ni-25Cr-55Fe (oxidized)	200	0.90
	500	0.97
60Ni-12Cr-28Fe (oxidized)	270	0.89
	560	0.82
80Ni-20Cr (oxidized)	100	0.87
	600	0.87
	1300	0.89

* This table was prepared by Wm. F. Roeser and H. T. Wensel of the Pyrometry section of the National Bureau of Standards and is taken from the appendix of *Temperature, Its Measurement and Control in Science and Industry* (American Institute of Physics, 1941), Reinhold Publishing Company, New York.

TABLE II. Total emissivities of metals, surface unoxidized.*

Material	Emissivity ϵ_t 25°C	100°C	500°C	1000°C	1500°C	2000°C
Aluminum	0.022	0.028	0.060			
Bismuth	0.048	0.061				
Carbon	0.81	0.81	0.79			
Chromium		0.08				
Cobalt			0.13	0.23		
Columbium					0.19	0.24
Copper		0.02		(Liquid 0.15)		
Gold		0.02	0.03			
Iron		0.05				
Lead		0.05				
Mercury	0.10	0.12				
Molybdenum				0.13	0.19	0.24
Nickel	0.045	0.06	0.12	0.19		
Platinum	0.037	0.047	0.096	0.152	0.191	
Silver		0.02	0.035			
Tantalum					0.21	0.26
Tin	0.043	0.05				
Tungsten	0.024	0.032	0.071	0.15	0.23	0.28
Zinc	(0.05 at 300°C)					
Brass	0.035	0.035				
Cast iron		0.21		(Liquid 0.29)		
Steel		0.08		(Liquid 0.28)		

* Source—same as Table I.

A Pyrex lens about 5 mm thick transmits radiant energy in the wave-length band between about 0.3 micron and 2.6 microns though it transmits relatively little radiant energy at longer wave-lengths. A fused silica lens of similar thickness transmits equally well throughout the band transmitted by the Pyrex lens, and in addition it transmits fairly freely in the wave-length band from 2.6 microns to around 3.8 microns. Most glasses are rather good emitters within the latter band of wave-lengths, though many are poorer emitters at wave-lengths below 2.6 microns unless the emitting mass is appropriately thick.

Thus where it is desirable to measure temperatures at a considerable depth within a large mass of glass, the use of a radiation pyrometer having a Pyrex lens has the advantage that its transmission is limited more to those wave-lengths for which usually k_λ has a small value, so that a large fraction of the radiant energy received by the pyrometer arises from appreciable depths within the glass.

In many industrial applications the mass of glass whose temperature is to be measured is not thick enough to make it completely opaque to radiation of all wave-lengths. In order to

TABLE III. Spectral emittances of oxides.*

Material	Emittance $\epsilon_{0.65\mu}$ Range of observed values	Probable value for the oxide formed on smooth metal
Aluminum oxide	0.22 to 0.40	0.30
Beryllium oxide	0.07 to 0.37	0.35
Cerium oxide	0.58 to 0.80	
Chromium oxide	0.60 to 0.80	0.70
Cobalt oxide		0.75
Columbium oxide	0.55 to 0.71	0.70
Copper oxide	0.60 to 0.80	0.70
Iron oxide	0.63 to 0.98	0.70
Magnesium oxide	0.10 to 0.43	0.20
Nickel oxide	0.85 to 0.96	0.90
Thorium oxide	0.20 to 0.57	0.50
Tin oxide	0.32 to 0.60	
Titanium oxide		0.50
Uranium oxide		0.30
Vanadium oxide		0.70
Yttrium oxide		0.60
Zirconium oxide	0.18 to 0.43	0.40
Alumel (oxidized)		0.87
Cast iron (oxidized)		0.70
Chromel P (90 Ni-10 Cr) (oxidized)		0.87
80 Ni—20 Cr (oxidized)		0.90
60 Ni—24 Fe-16 Cr (oxidized)		0.83
55 Fe—37.5 Cr-7.5 Al (oxidized)		0.78
70 Fe—23 Cr-5 Al-2 Co (oxidized)		0.75
Constantan (55 Cu-45 Ni) (oxidized)		0.84
Carbon steel (oxidized)		0.80
Stainless steel (18–8) (oxidized)		0.85
Porcelain	0.25 to 0.50	

* Source—same as Table I.

obtain pyrometer readings as representative as possible of the true temperature of glass under such conditions it is preferable to use a pyrometer responsive to the wave-lengths for which the absorption coefficient k_λ of the specimen is relatively high, so that the pyrometer responds largely to radiant energy emitted by layers of glass relatively close to the surface sighted upon. Thus for such cases the use of a radiation pyrometer equipped with a fused silica lens is preferable to one having a Pyrex lens. Another advantage of the fused silica lens is that at the relatively low temperatures usually involved in glass temperature measurement a very considerable fraction of total blackbody radiant energy has wave-lengths between 2.6 and 3.8 microns. A good portion of this energy, being passed by the fused silica lens, causes appreciably higher e.m.f. to be developed by the pyrometer.

TABLE IV. Spectral emissivities of materials, surface unoxidized.*

Material	Temp. °C	Emissivity $\epsilon_{0.65\mu}$ Solid state	Liquid state
Beryllium		0.61	0.61
Carbon		0.80–0.93	
Chromium		0.34	0.39
Cobalt		0.36	0.37
Columbium		0.37	0.40
Copper		0.10	0.15
Erbium		0.55	0.38
Gold		0.14	0.22
Iridium		0.30	
Iron		0.35	0.37
Manganese		0.59	0.59
Molybdenum		0.37	0.40
Nickel		0.36	0.37
Palladium		0.33	0.37
Platinum		0.30	0.38
Rhodium		0.24	0.30
Silver		0.07	0.07
Tantalum		0.49	
Thorium		0.36	0.40
Titanium		0.63	0.65
Tungsten		0.43	
Uranium		0.54	0.34
Vanadium		0.35	0.32
Yttrium		0.35	0.35
Zirconium		0.32	0.30
Steel		0.35	0.37
Cast iron		0.37	0.40
Constantan		0.35	
Monel		0.37	
Chromel P (90 Ni-10 Cr)		0.35	
80 Ni-20 Cr		0.35	
60 Ni-24 Fe-16 Cr		0.36	
Alumel (95 Ni; Bal. Al, Mn, Si)		0.37	
90 Pt-10 Rh		0.27	
Stainless steel**			
27 Cr, or 18-10 Cb and Ti	2750		0.64
	2875		0.69
	3000		0.75
16 Cr	2750		0.59
	2875		0.65
	3000		0.70
12 Cr, or 16-2	2750		0.56
	2875		0.62
	3000		0.67
27-20	2750		0.51
	2875		0.56
	3000		0.62
18-9 Sulfur	2750		0.44
	2875		0.49
	3000		0.54
12 Cr Sulfur	2750		0.39
	2875		0.44
	3000		0.50
18-9 Se	2750		0.37
	2875		0.43
	3000		0.48

* Source—same as Table I except as noted for stainless steel.
** These values are taken from curves by George N. Goller; transactions of A.S.M. Vol. 32, pp. 239–49, 1944.

When the thickness of the specimen is ample for complete opaqueness of all of the wave-lengths affecting the pyrometer, spectral emis-

TABLE V. Corrections to be added corresponding to various emittances and various brightness temperatures observed with an optical pyrometer. The temperatures and corrections, in °F, are for $\lambda = 0.65$ and $C_2 = 1.432$ cm deg. K.

Spectral emittance	Observed temperature in headings—corrections in the body of the table																							
	1200	1300	1400	1500	1600	1700	1800	1900	2000	2100	2200	2300	2400	2500	2600	2700	2800	2900	3000	3100	3200	3300	3400	3500	3600
0.05	237	269	303	339	378	420	464	510	560	612	666	724	785	849	917	987	1061	1139	1220	1304	1393	1486	1582	1683	1789
0.10	177	200	224	251	279	309	340	373	409	445	484	525	568	612	659	708	758	811	867	924	984	1046	1111	1178	1248
0.15	143	161	181	202	224	248	273	299	327	356	387	418	452	487	523	561	600	641	684	728	774	822	871	922	975
0.20	120	135	151	169	187	207	227	249	272	296	321	347	374	403	432	463	495	529	563	599	636	675	715	756	798
0.25	102	115	129	144	159	176	193	212	231	251	272	294	317	341	365	391	418	446	475	504	535	567	600	634	669
0.30	88	99	111	124	137	151	166	182	198	215	233	252	271	291	312	334	357	380	405	430	456	483	511	539	569
0.35	76	86	96	107	118	131	143	157	171	186	201	217	234	251	269	288	307	327	348	369	391	414	438	462	487
0.40	66	74	83	93	103	113	124	136	148	161	174	188	202	217	232	248	265	282	300	318	337	357	377	398	419
0.45	57	64	72	80	89	98	107	117	128	139	150	162	174	187	200	214	228	243	258	274	290	307	324	342	360
0.50	50	56	62	69	77	85	93	101	110	120	129	139	150	161	172	184	196	209	222	235	249	264	278	294	309
0.55	43	48	54	60	66	73	79	87	94	103	111	119	128	138	148	158	168	179	190	201	213	225	238	251	264
0.60	36	41	46	51	56	62	68	74	80	87	94	101	109	117	125	134	142	152	161	171	181	191	201	212	223
0.65	30	34	38	43	47	52	57	62	67	73	79	85	91	98	105	112	119	127	135	143	151	160	168	177	187
0.70	25	28	31	35	39	43	47	51	55	60	65	70	75	81	86	92	98	104	111	117	124	131	138	146	153
0.75	20	23	25	28	31	34	38	41	45	48	52	56	60	65	69	74	79	84	89	94	100	105	111	117	123
0.80	16	18	20	22	24	26	29	32	35	37	40	43	47	50	53	57	61	64	68	73	76	81	86	90	95
0.85	11	13	14	16	17	19	21	23	25	27	29	31	34	36	39	41	44	47	50	53	56	59	62	65	68
0.90	7	8	9	10	11	12	14	15	16	17	19	20	22	23	25	27	28	30	32	34	36	38	40	42	44
0.95	4	4	4	5	5	6	7	7	8	8	8	9	10	11	12	13	14	15	16	16	17	18	19	20	21
1.00	00	00	00	00	00	00	00	00	00	00	00	00	00	00	00	00	00	00	00	00	00	00	00	00	00

sivity and total emissivity equal unity minus the reflectance of the material. For most glasses reflectance equals about 0.04 for such wavelengths, so that $e_\lambda = 0.96$ and $e_t = 0.96$ for masses of most kinds of glass when of ample thickness.

For thinner masses of glass contained in a crucible a portion of the energy at those wavelengths for which k_λ is relatively small will emanate from the walls beyond the glass. For such a case a composite reading of glass and crucible temperatures is obtained.

When sighting upon glass in the open, such as in a container plant, a radiation pyrometer equipped with a fused silica lens should be employed in preference to one having a Pyrex lens. The instrument should be calibrated under actual plant-operating conditions. As an example, in the measurement of temperature in a glass feeder, a thermocouple is immersed in the glass at a point upon which the radiation pyrometer is sighted, or at a nearby point and the readings obtained from the thermocouple are used as a basis for calibrating the radiation pyrometer.

TOTAL AND SPECTRAL EMITTANCES OF OXIDIZED AND UNOXIDIZED SURFACES

The emittances of various substances often involved in industrial measurements made with radiation pyrometers and optical pyrometers are given in Tables I through IV.

The values listed in Table I are given as uncertain by 10 percent to 30 percent in many cases, depending upon the particle size of the material concerned. In general these values may be used with comparable accuracy in connection with radiation pyrometers equipped with fused silica or Pyrex glass lenses. Technically, the emittances applying to pyrometers whose wavelength band is limited by these lenses may differ somewhat from the "total" emittances.

Where it is important to use the best possible value, it may be desirable to make a special check, employing a thermocouple inserted into a sample specimen, or so located as to provide the desired reading. Such checks are often possible where the continual use of thermocouples is impossible or undesirable. As later shown, the use of an optical pyrometer as a checking instrument is helpful.

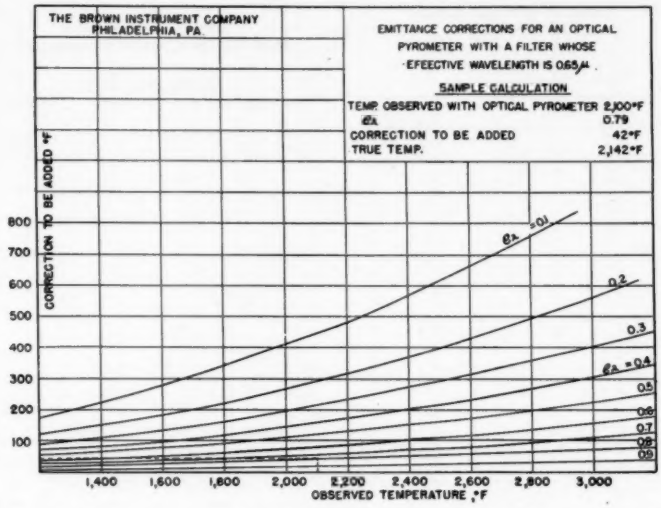

FIG. 2. Emittance corrections for an optical pyrometer with a filter whose effective wave-length is 0.65μ. Where greater accuracy is required than the scale of this figure permits, use Table V.

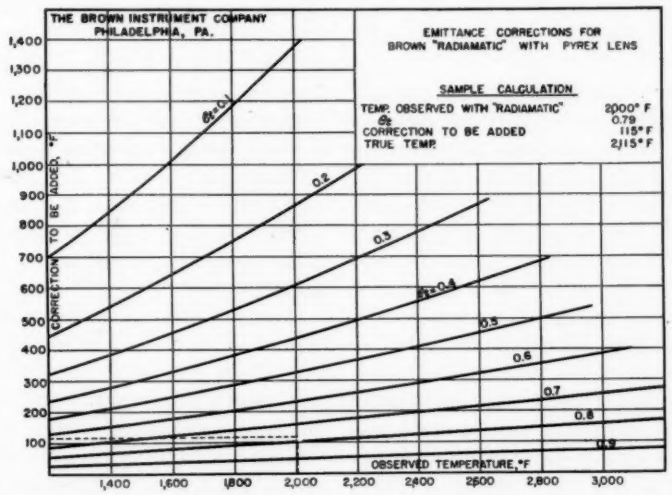

FIG. 3. Emittance corrections for radiation pyrometer having Pyrex lens. Corrections may be obtained also by use of Table VI as illustrated by Example 1.

The values in Table II are presented for comparison with Table I to show the contrast between the emittance of oxidized and unoxidized metals. From the extremely low values of ϵ_t, given in Table II, it is evident that a radiation pyrometer is not well adapted for measuring the temperatures of totally unoxidized metals.

In Table I, considerable differences in the emittances of cast iron, iron, steel, and steel plate—all oxidized—and wrought iron, dull oxidized, may be seen. These differences probably depend chiefly upon the roughness of the surface and the degree of oxidation. The values presented in the tables were determined by various observers and undoubtedly the surface conditions were not uniform. For many industrial installa-

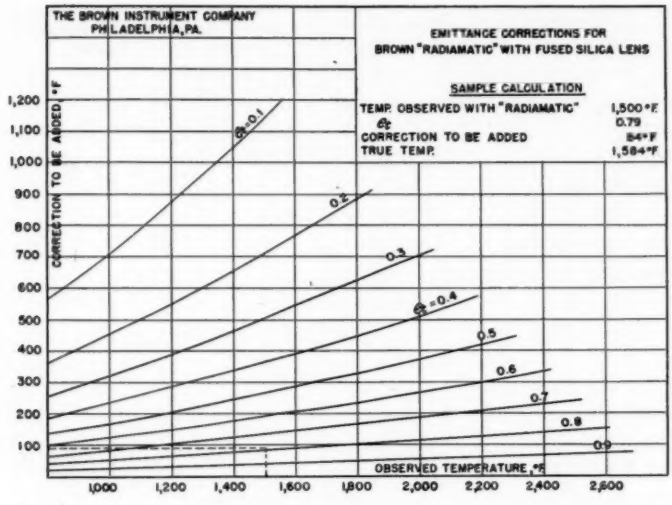

FIG. 4. Emittance corrections for radiation pyrometer having fused silica lens. Corrections may be obtained also by use of Table VII as illustrated by Example 1.

tions where oxidizing conditions are present, a value of $e_t = 0.95$ is believed to be of reasonable accuracy.

Except in those processes employing strongly reducing atmospheres such as those used for bright annealing, etc., practically all industrial furnaces have oxidizing atmospheres so that the surfaces of materials within them are oxidized. In the majority of cases, therefore, the emittance values given in Tables I and III must be used rather than those given in Tables II and IV.

When a heavy oxide scale is loosened from a body, the temperature of the scale tends to become higher or lower than that of the underlying surface, depending upon the temperature of the surrounding walls, atmosphere, etc. Loose scales which cover only a small fraction of the area sighted upon produce only negligible effects upon the reading of a radiation pyrometer sighted upon the body. In extreme cases where scale is involved, it may be best to sight the pyrometer upon a location where the metal has passed through a scale breaker.

TOTAL AND SPECTRAL EMITTANCE CORRECTIONS AND COMPARISON OF READINGS FOR PYROMETERS OF DIFFERENT TYPES

Optical pyrometer readings are corrected for spectral emittances other than unity by use of Table V or the curves of Fig. 2. The curves of this figure are drawn to the same scale as those of Figs. 3 and 4 for ease of comparison of the figures. Table V should be used where dictated by requirements for accuracy.

Readings of a radiation pyrometer having a lens consisting of Pyrex No. 774 glass are corrected for total emittances other than unity by use of the curves of Fig. 3 or by applying values from Table VI as explained below and illustrated by Example 1.

Readings of a radiation pyrometer having a fused silica lens are corrected for total emittances other than unity by use of the curves of Fig. 4 or by applying values from Table VII as explained below and also illustrated by Example 1.

Tables VI and VII are the blackbody millivolt *versus* temperature equivalents for the Brown "Radiamatic" pyrometer with Pyrex lens and fused silica lens, respectively. The design of this pyrometer is such that the radiant energy received from a heated source by the receiver of the thermopile (the flattened hot junctions) is dissipated mainly by thermal conduction, so that the relation of temperature rise of the receiver with respect to the rate at which radiant energy is received is linear to within from one percent to five percent over different temperature ranges covering an e.m.f. ratio of one to four (used for

TABLE VI. Temperature-millivolt equivalents for Brown "Radiamatic" radiation pyrometer with Pyrex lens sighted on a blackbody.

Degs. Fahr.	700	800	900	1,000	1,100	1,200	1,300	1,400	1,500
	Millivolts								
0	0.03	0.08	0.11	0.17	0.28	0.44	0.67	0.99	1.42
10						0.46	0.70	1.02	1.47
20						0.48	0.73	1.06	1.52
30						0.50	0.78	1.10	1.57
40						0.52	0.79	1.14	1.62
50	0.04	0.08	0.14	0.21	0.36	0.54	0.82	1.18	1.67
60						0.56	0.85	1.22	1.73
70						0.58	0.88	1.27	1.79
80						0.61	0.92	1.32	1.85
90						0.64	0.96	1.37	1.91
100	0.06	0.11	0.17	0.28	0.44	0.87	0.99	1.42	1.97
Degs. Fahr.	1,600	1,700	1,800	1,900	2,000	2,100	2,200	2,300	2,400
	Millivolts								
0	1.97	2.66	3.49	4.51	5.74	7.20	8.95	10.99	13.35
10	2.03	2.74	3.59	4.62	5.88	7.36	9.14	11.21	13.60
20	2.09	2.83	3.69	4.74	6.02	7.53	9.33	11.44	13.85
30	2.16	2.90	3.79	4.86	6.16	7.70	9.53	11.67	14.11
40	2.23	2.98	3.89	4.98	6.30	7.87	9.73	11.91	14.37
50	2.30	3.06	3.99	5.10	6.44	8.05	9.93	12.15	14.64
60	2.37	3.14	4.09	5.22	6.59	8.23	10.14	12.39	14.91
70	2.44	3.22	4.19	5.34	6.74	8.41	10.35	12.63	15.18
80	2.51	3.31	4.29	5.47	6.89	8.59	10.56	12.87	15.46
90	2.58	3.40	4.40	5.60	7.04	8.77	10.77	13.11	15.74
100	2.66	3.49	4.51	5.74	7.20	8.95	10.99	13.35	16.03
Degs. Fahr.	2,500	2,600	2,700	2,800	2,900	3,000	3,100	3,200	3,300
	Millivolts								
0	16.03	19.08	22.48	26.26	30.43	34.98	39.96	45.34	51.02
10	16.32	19.40	22.84	26.66	30.86	35.47	40.48	45.90	51.61
20	16.62	19.73	23.21	27.06	31.30	35.96	41.00	46.46	52.20
30	16.92	20.06	23.58	27.46	31.76	36.45	41.53	47.02	52.80
40	17.22	20.40	23.95	23.87	32.20	36.94	42.06	47.58	53.41
50	17.52	20.74	24.33	28.29	32.64	37.44	42.60	48.15	54.02
60	17.82	21.08	24.71	28.71	33.09	37.94	43.14	48.72	54.64
70	18.13	21.42	25.09	29.14	33.55	38.44	43.69	42.29	55.26
80	18.44	21.77	25.48	29.57	34.02	38.94	44.24	49.86	55.88
90	18.76	22.12	25.87	30.00	34.50	39.45	44.79	50.44	56.50
100	19.08	22.48	26.26	30.43	34.98	39.96	45.34	51.02	57.12

total emittances down to 0.25). For higher total emittances the linearity would be proportionately better.[3]

If the object sighted upon has low total emittance, its total radiancy is proportionately lower than that of a blackbody. If, further, the total emittance is non-selective[4] with respect to wave-length, the rate at which radiant energy is received by the thermopile, and accordingly the e.m.f. of the thermopile, are likewise proportionately lower than those values applying for a blackbody.

Where the above conditions are met the e.m.f. of the pyrometer for which the table applies can be corrected for the low emittance of the object

[3] For a discussion of the basis upon which this relation is developed, see Appendix on page 720.

[4] If a pyrometer equally sensitive to all wave-lengths were under consideration and its blackbody calibration data were used, it would be unnecessary to specify that the emittance be non-selective.

as follows:

$$\text{Corrected e.m.f.} = \frac{\text{Observed e.m.f.}}{\text{Total emittance}}.$$

The true temperature is then taken from Tables VI or VII corresponding to this corrected e.m.f.

For radiation pyrometers calibrated to read in terms of temperature, an e.m.f. value corrected for use with the table is obtained as follows:

TABLE VII. Temperature-millivolt equivalents for Brown "Radiamatic" radiation pyrometer with fused silica lens sighted on a blackbody.

Degs. Fahr.	900	1,000	1,100	1,200	1,300	1,400	1,500
	Millivolts						
0	0.33	0.50	0.76	1.11	1.57	2.16	2.90
10		0.52	0.79	1.15	1.62	2.23	2.98
20		0.54	0.82	1.19	1.67	2.30	3.07
30		0.56	0.85	1.23	1.73	2.37	3.16
40		0.59	0.88	1.27	1.79	2.44	3.25
50	0.41	0.62	0.91	1.32	1.85	2.51	3.34
60		0.65	0.95	1.37	1.91	2.58	3.43
70		0.67	0.99	1.42	1.97	2.66	3.53
80		0.70	1.03	1.47	2.03	2.74	3.63
90		0.73	1.07	1.52	2.09	2.82	3.73
100	0.50	0.76	1.11	1.57	2.16	2.90	3.83
Degs. Fahr.	1,600	1,700	1,800	1,900	2,000	2,100	2,200
	Millivolts						
0	3.83	4.93	6.25	7.82	9.65	11.77	14.19
10	3.93	5.05	6.40	7.99	9.85	12.00	14.45
20	4.03	5.17	6.55	8.16	10.05	12.23	14.71
30	4.14	5.30	6.70	8.34	10.25	12.47	14.98
40	4.25	5.43	6.85	8.52	10.46	12.71	15.25
50	4.36	5.56	7.00	8.70	10.67	12.95	15.53
60	4.47	5.69	7.16	8.89	10.88	13.19	15.81
70	4.58	5.83	7.32	9.08	11.10	13.44	16.10
80	4.69	5.97	7.48	9.27	11.32	13.69	16.39
90	4.81	6.11	7.65	9.46	11.54	13.94	16.68
100	4.93	6.25	7.82	9.65	11.77	14.19	16.97
Degs. Fahr.	2,300	2,400	2,500	2,600	2,700	2,800	
	Millivolts						
0	16.97	20.11	23.63	27.89	32.36	37.04	
10	17.26	20.44	24.05	28.33	32.82	37.52	
20	17.56	20.78	24.47	28.77	33.28	38.00	
30	17.87	21.12	24.89	29.21	33.74	38.48	
40	18.18	21.47	25.31	29.65	34.21	38.97	
50	18.50	21.82	25.74	30.10	34.68	39.46	
60	18.82	22.18	26.16	30.55	35.15	39.95	
70	19.14	22.54	26.59	31.00	35.62	40.44	
80	19.46	22.90	27.02	31.45	36.09	40.93	
90	19.78	23.26	27.46	31.90	36.56	41.43	
100	20.11	23.63	27.89	32.36	37.04	41.93	

$$\text{Corrected e.m.f.} = \frac{\text{e.m.f. taken from table corresponding to temperature indicated by pyrometer}}{\text{Total emittance}}.$$

Example 1 illustrates the application of this method of applying emittance corrections:

Example 1

Known conditions:

Object sighted upon	Steel with oxidized surface
Instrument used	Radiation pyrometer with fused silica lens
Temperature indicated by pyrometer	1953°F

Calculations:

(1) e.m.f. from Table VII for the indicated temperature	= 8.757 millivolts
(2) Total emittance[5] for steel (oxidized)	= 0.79
(3) Equivalent e.m.f. for a blackbody = 8.757/0.79	= 11.085 millivolts
(4) True temperature from Table VII	= 2069°F

Reference to Tables I–IV discloses a number of instances in which e_λ is higher than e_t.

In the case of oxidized steel and oxidized iron both e_λ and e_t vary over considerable ranges and the data are insufficient to indicate definitely whether or not for any given specimen of these materials e_λ and e_t would be materially different.

Obviously, it is impractical to consider in detail all the cases of unequal values of e_λ and e_t, though it is useful to compare the readings of an optical pyrometer with a filter whose effective wave-length is 0.65μ, a radiation pyrometer having a Pyrex lens, and a radiation pyrometer having a fused silica lens, for the case in which $e_\lambda = e_t$.

Referring to Figs. 2–4 it is noted that, for curves having the same value for e_λ or e_t, the difference between true temperature and pyrometer reading is least for the optical pyrometer, larger for the radiation pyrometer with Pyrex lens, and still larger for the radiation pyrometer with fused silica lens. For a radiation pyrometer responsive to all wave-lengths (total radiation pyrometer), the necessary corrections are largest of all.

[5] Where the total emittance of steel is higher than 0.79, the radiation pyrometer reading is proportionately nearer to the true temperature of the steel.

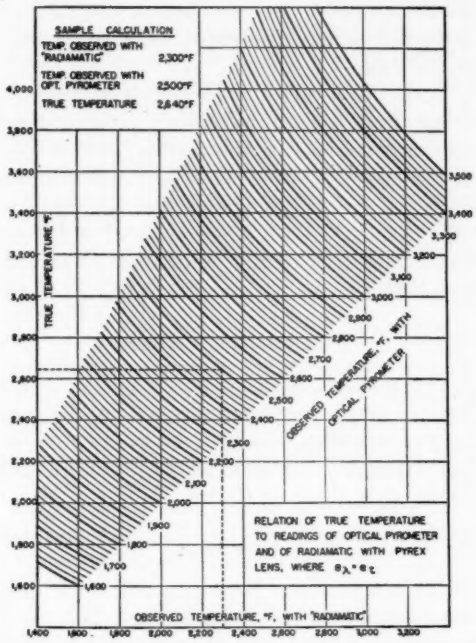
SAMPLE CALCULATION
TEMP. OBSERVED WITH "RADIAMATIC" 2,300°F
TEMP. OBSERVED WITH OPT. PYROMETER 2500°F
TRUE TEMPERATURE 2,640°F
TRUE TEMPERATURE, °F
OBSERVED TEMPERATURE, °F, WITH OPTICAL PYROMETER
RELATION OF TRUE TEMPERATURE TO READINGS OF OPTICAL PYROMETER AND OF RADIAMATIC WITH PYREX LENS, WHERE $e_\lambda = e_t$
OBSERVED TEMPERATURE, °F, WITH "RADIAMATIC"

FIG. 5. Relation of true temperature to readings of an optical pyrometer with a filter whose effective wave-length is 0.65μ and of a radiation pyrometer with a Pyrex lens. For use when $e_\lambda = e_t$.

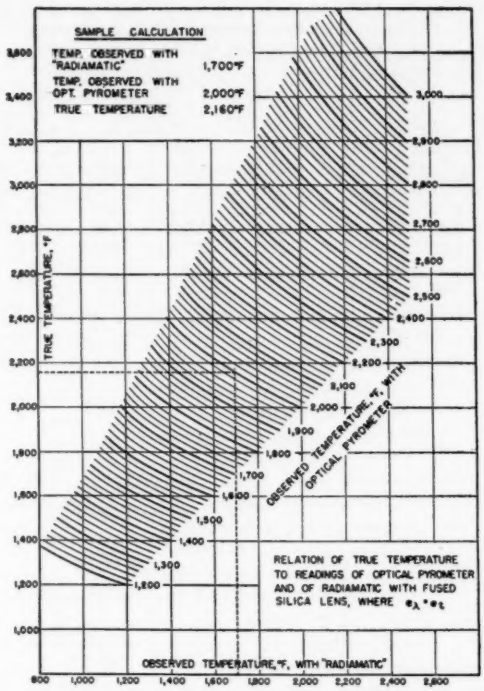
SAMPLE CALCULATION
TEMP. OBSERVED WITH "RADIAMATIC" 1,700°F
TEMP. OBSERVED WITH OPT. PYROMETER 2,000°F
TRUE TEMPERATURE 2,160°F
TRUE TEMPERATURE, °F
OBSERVED TEMPERATURE, °F, WITH OPTICAL PYROMETER
RELATION OF TRUE TEMPERATURE TO READINGS OF OPTICAL PYROMETER AND OF RADIAMATIC WITH FUSED SILICA LENS, WHERE $e_\lambda = e_t$
OBSERVED TEMPERATURE, °F, WITH "RADIAMATIC"

FIG. 6. Relation of true temperature to readings of an optical pyrometer with a filter whose effective wave-length is 0.65μ and of a radiation pyrometer with a fused silica lens. For use when $e_\lambda = e_t$.

Another comparison of pyrometer readings is given in Figs. 5 and 6, which are applicable only when $e_\lambda = e_t$.

By means of these curves true temperature can be obtained from simultaneous readings of an optical pyrometer and a radiation pyrometer for the special conditions indicated.

Readings of Pyrometers Sighted Upon an Object within a Heated Enclosure

The principles applying for radiation from a non-blackbody within a heated enclosure have been explained in an earlier section of this article. As already explained, the assumption is made that the enclosure walls have high emittance for purposes of determining the maximum corrections that may be required.

In order to determine the pyrometer reading that would be obtained under this assumption, an extension of the previously described use of Tables VI and VII is employed as follows:

(1) For item (*a*) defined on page 710, find from Table VI or VII (according to type of lens used) the e.m.f. corresponding to the true temperature of the heated object and multiply this quantity by the total emittance of the object.

(2) For item (*b*) also defined on page 710, find the e.m.f. corresponding to the wall temperature and multiply this quantity by (one minus the total emittance of the object).

(3) Add the products obtained for items (*a*) and (*b*) and from the table of millivolt equivalents, find the corresponding temperature. This is the temperature which would be indicated by the pyrometer.

Example 2 illustrates this process.

Example 2

Known Conditions:

Object sighted upon	Steel with oxidized surface
Instrument used	Radiation pyrometer with Pyrex lens
Temperature of object sighted upon	2000°F
Temperature of furnace walls (made of blackbody materials) surrounding object	2400°F

TABLE VIII. Comparative pyrometer readings of objects within an enclosure having walls at higher temature than the object. When $e_\lambda = e_t$.

Emittance of object	Object temp. °F	Wall temp. °F	Pyrometer reading, °F: Radiation pyrometer, Fused silica lens	Radiation pyrometer, Pyrex lens	Optical pyrometer
0.94	2300	2500	2314	2314	2315
0.79	2300	2500	2346	2346	2350
0.75	2300	2500	2354	2355	2360
0.60	1500	1750	1613	1617	1641

Calculations:

(1) Total emittance[5] for steel (oxidized) from Table I = 0.79

(2) Blackbody e.m.f. from Table VI for object at 2000°F = 5.74 millivolts

(3) Blackbody e.m.f. from Table VI for walls at 2400°F = 13.35 millivolts

(4) e.m.f. produced due to emission from the object = 5.74×0.79 = 4.53 millivolts

(5) e.m.f. produced due to reflection from walls = 13.35×(1−0.79) = 2.80 millivolts

(6) Total e.m.f. developed = 4.53+2.80 = 7.33 millivolts

(7) Indicated temperature from Table VI = 2108°F.

Table VIII, constructed by using the above method to determine radiation pyrometer readings, shows a comparison between object temperature, wall temperature, and pyrometer reading for several equal values of total and spectral emittances of the object and the corresponding readings of radiation pyrometers with Pyrex lens and fused silica lens and of an optical pyrometer using 0.65μ wave-length. Where flame is present, its effect should be taken into account also. In this table, an indication is given as to the extent to which pyrometer readings may vary from the temperature of objects sighted upon within heated enclosures.

Referring to the "Pyrometer reading" columns, it will be noted that, unlike the case of viewing an object in the open, here, when $e_\lambda = e_t$, the optical pyrometer reads further from the true *object* temperature than do the radiation pyrometers. At the lower temperature, the radiation pyrometer with a fused silica lens shows a slight advantage over the pyrometer with a Pyrex lens. This relation, which is the reverse of that applying when the object sighted upon is in the open, should be taken into account in checking radiation pyrometers by comparison with the optical pyrometer.

If the walls were cooler than the object, the order of the type of pyrometer giving the most accurate reading is again reversed and is similar to the case of viewing the object in the open. Of course, as already pointed out for blackbody conditions, where body and walls are at the same temperature, all of the pyrometers should read true temperature.

CONCLUDING NOTE

The relative scarcity of complete data on spectral emittances of solids within the wavelength band from 0.7μ to 7μ or 8μ is noted. It is hoped that physicists will be able to improve this condition in the near future.

APPENDIX

The design of the Brown "Radiamatic" radiation pyrometer is discussed by Thomas R. Harrison and William H. Wannamaker.* The following theoretical analysis is useful in showing the relation that exists between the e.m.f. developed by the thermopile and the rate at which radiant energy from a source whose temperature is to be measured is received by the thermopile through the fused silica lens of the pyrometer under consideration. The principles are applicable for the Pyrex lens also.

Equation (3) of that article should be corrected by inserting the term σ ahead of T_2^4; it can then be put into the form

$$0.92(\phi_1 T_1^4 - \phi_3 T_3^4) = (T_2 - T_3) \times \left[Q + (T_2 + T_3)(T_2^2 + T_3^2) \frac{1+e}{\sin^2 \theta_2} \right], \quad (1)$$

Q being the conduction factor for the pyrometer as defined by Eq. (6) of the article cited.

The terms T_1, T_2, and T_3 refer to the absolute temperatures in degrees K of the source of radiation whose temperature is to be measured, of the hot junctions of the thermopile, and of the cold junctions of the thermopile together with the pyrometer housing, respectively.

* Thomas R. Harrison and William H. Wannamaker, Rev. Sci. Inst. **12**, 20–32 (1941).

The terms $0.92\,\phi_1$ and $0.92\,\phi_3$ are the fractional parts of blackbody radiant energy falling upon the lens that would pass through it. The constant 0.92 allows for about 4 percent reflection from the front and rear surfaces of the lens. The subscripts indicate the temperatures for which the fractions apply.

The term e represents the total emittance of the rear side of the receiver and θ_2 is the angle from the optic axis to a limiting element in the cone of radiant energy rays falling upon the thermopile.

For a fused silica lens, $\phi_1 T_1^4$ for 900°F or more is four thousand or more times as large as $\phi_3 T_3^4$ so that for the range covered by the tables the latter term may be dropped from Eq. (1).

Using the value 0.2 for e and 0.048 for $\sin\theta_2$ as in the original article, $(1+e)/\sin\theta_2$ equals 25.

Computation from the calibration data of the pyrometer renders a value for Q of about 9.65×10^{10} while the value of the term added to Q in Eq. (1) varies from 0.272×10^{10} to 0.328×10^{10} with the increase in hot junction temperature T_2. This accounts for less than one percent change in value of the term within the brackets for the full range given for object temperature in Table VII.

As indicated by Eq. (6) of the original article, the term Q is subject to change with change in temperature of portions of the thermopile and the surrounding air accompanying a rise in T_2. No actual determination has been made to show such change but from the foregoing considerations it may be assumed that such a change in the value of Q with change in T_2 would be the principal reason for such non-linearity as might exist between (T_2-T_3) and $\phi_1 T_1^4$.

Computation of Lens Absorption

In order to determine the effect of lens absorption, use is made of the absorption coefficients k for fused silica given by Drummond.[6]

The ratio of incident radiant energy of a given wave-length, $R_{\lambda 0}$, to that transmitted, R_λ is

$$R_\lambda/\rho R_{\lambda 0}=\exp(-k_\lambda t), \tag{2}$$

where ρ allows for reflection at the lens surfaces and t is lens thickness in mm. With a plano-convex lens having radius of curvature r, the thickness t parallel to the axis at a point where the normal to the spherical surface makes angle α with the optic axis is

$$t=t_1-r(1-\cos\alpha), \tag{3}$$

where t_1 is the thickness at the center of the lens. The projected area of the lens perpendicular to the axis, within angle α is

$$A=\pi r^2\sin^2\alpha. \tag{4}$$

It was found that within the limits of the dimensions used, the relation of t and A is reasonably linear and for the purpose at hand may be represented by the relation

$$t=t_1-bA, \tag{5}$$

where b is a constant.

Substituting this into Eq. (2) gives, for such a lens

$$\frac{R_\lambda}{\rho R_{\lambda 0}}=\exp\left[-k_\lambda(t_1-bA)\right]$$
$$=\exp(-k_\lambda t_1)\cdot\exp(k_\lambda bA). \tag{6}$$

The ratio of the radiant energy of wave-length λ transmitted through an elemental area dA of the lens, having thickness t, to that incident upon the entire lens within the same time interval is

$$\frac{dA}{A_{\max}}\cdot\exp(-k_\lambda t_1)\cdot\exp(k_\lambda bA),$$

from which we have

$$\frac{R_\lambda}{R_{\lambda 0}}=\frac{\exp(-k_\lambda t_1)}{A_{\max}}\int_0^{A_{\max}}\exp(k_\lambda bA)\,dA$$

for the entire lens. Noting from Eq. (5) that $t_1-bA_{\max}=t_2$, the minimum thickness, and that $bA_{\max}=t_1-t_2$ the above becomes

$$\frac{R_\lambda}{\rho R_{\lambda 0}}=\frac{1}{k_\lambda(t_1-t_2)}\left[\exp(-k_\lambda t_2)-\exp(-k_\lambda t_1)\right] \tag{7}$$

when the integration is carried out.

For the lens in question the values 6.77 mm and 3.05 mm are used for t_1 and t_2, respectively (though there is a slight indefiniteness in the value of t_2 owing to the fact that the limiting diaphragm is not in contact with the lens).

[6] D. G. Drummond, Proc. Roy. Soc. **153**, 328–329 (1935–36).

TABLE IX. Equivalent cut-off wave-length λ for fused silica lens of "Radiamatic" pyrometer.

Blackbody temperature	λ	Blackbody temperature	λ
300°K	3.987	1000°K	3.775
600	3.847	1200	3.753
700	3.823	1400	3.737
800	3.805	1800	3.712

Taking Drummond's values of k_λ for every tenth of a micron wave-length from $\lambda=2.1\mu$ to $\lambda=4.8\mu$, the corresponding values of $R_\lambda/R_{\lambda 0}$ were calculated from Eq. (7).

Relative Blackbody Radiant Energy Transmitted by Lens

A series of fractional portions $R_{\Delta\lambda}/R_{0-\infty}$ (lying within wave-length increment $\Delta\lambda$) of the total radiancy $R_{0-\infty}$ of a blackbody at a chosen temperature T were obtained by taking suitable differences from a table[7] giving values of the ratio of blackbody radiancy in the wave-length interval 0 to λ with respect to that for all wave-lengths.

Wave-length intervals of one-tenth micron were taken from 2.05μ to 4.85μ and the value obtained for $R_{\Delta\lambda}/R_{0-\infty}$ obtained for each interval was multiplied by the value obtained from Eq. (7) for $R_\lambda/\rho R_{\lambda 0}$ for the wave-length at the middle of the interval in question.

Summation of these products, added to $R_{0-2.05\mu}/R_{0-\infty}$ gave the portion of the blackbody radiancy for the chosen temperature that is transmitted.

From the table the corresponding value for λT indicated the "effective cut-off" wave-length λ (defined by the above derivation) of the lens for radiation of a blackbody at the chosen temperature.

Similar computations were made for a number of blackbody temperatures with the results listed in Table IX. Using the values of Table IX plotted into a suitable curve, λT is determined for any chosen value of T_1. The corresponding value of $R_{0-\lambda}/R_{0-\infty}(=\phi_1)$ is taken from the above mentioned tables[7] of Planck's Radiation Functions. Values of $\phi_1 T_1^4$ thus obtained were used in connection with Eq. (1) for calculating the value of Q and for comparison to the corresponding e.m.f. developed by the thermopile.

[7] Table I given in *Miscellaneous Physical Tables, Planck's Radiation Functions and Electronic Functions*, prepared by the Federal Works Agency, Work Projects Administration, Arnold N. Lowan, Ph.D., Technical Director, Sponsored by National Bureau of Standards.

BIBLIOGRAPHY

Emittance Values, Etc.

G. K. Burgess and P. D. Foote, "The Emissivity of Metals and Oxides," Part 4, Bull. Bur. Stand. **12**, 83 (1916).

G. K. Burgess and R. G. Waltenberg, "The Emissivity of Metals and Oxides," Part 2, Bull. Bur. Stand. **11**, 591 (1915).

W. W. Coblentz, "Absorption and Reflection Spectra," Bull. Bur. Stand. **2**, 457 (1906).

W. W. Coblentz, "Selective Radiation from Various Solids," Bull. Bur. Stand. **5**, 159 (1908).

W. W. Coblentz, "Selective Radiation from Various Solids," Part 2, Bull. Bur. Stand. **6**, 301 (1909).

W. W. Coblentz, "The Reflecting Power of Various Metals," Bull. Bur. Stand. **7**, 197 (1911).

W. W. Coblentz, W. B. Emerson, and M. B. Long, "Spectroradiometric Investigation of the Transmission of Various Substances," Bull. Bur. Stand. **14**, 653 (1918–19).

W. W. Coblentz, "Absorption, Reflection and Dispersion Constants of Quartz," Bull. Bur. Stand. **11**, 471 (1915).

W. W. Coblentz, "The Diffuse Reflecting Power of Various Substances," Bull. Bur. Stand. **9**, 283 (1913).

W. W. Coblentz, "Selective Radiation from Various Substances," Part 3, Bull. Bur. Stand. **7**, 243 (1911).

P. D. Foote, "The Emissivity of Metals and Oxides," Part 3, Bull. Bur. Stand. **11**, 607 (1915).

J. N. Greenwood, *Carnegie Scholarship Memoirs* (Spon and Chamberlain, 1923), Vol. 12, Iron and Steel Institute, p. 27, "Determination of the Corrections to Optical Pyrometer Readings Taken During Steel Making and Casting."

H. C. Hottel, *Chemical Engineer's Handbook* (McGraw-Hill Book Company, Inc., New York, 1941), second edition, pp. 1002–1029. (Contains additional emissivity tables.)

W. T. Reid and R. C. Corey, "Errors in Temperature Measurement by Radiametric Methods," Combustion **15**, 30 (Feb., 1944).

R. B. Sosman, *The Pyrometry of Solids and Surfaces* (American Society for Metals, Cleveland, Ohio, 1940).

R. E. Stephens, "The Spectral Emissivity and the Relation of True Temperatures and Brightness Temperatures of Platinum," J. Opt. Soc. Am. **29**, 158–161 (1939).

A. G. Worthing, "Temperature and Radiation Emissivities and Emittances," J. App. Phys. **11**, 421 (1940).

Radiation from Flames and Gases

E. Eckert, "Messung der Gesamtstrahlung von Wasserdampf und Kohlensaure in Mischung mit nichtstrahlenden Gasen bei Temperaturen bis zu 1300°C," VDI—Forschungsheft, Ed. B, **8**, n. 387 (Nov.–Dec., 1937).

D. H. Fax, "Non-Luminous Radiation to Tube Banks," Mech. Eng. **63**, 657 (Sept., 1941).

R. T. Haslam and M. W. Boyer, "Radiation from Luminous Flames," Ind. Eng. Chem. **19**, 4 (1927).
G. Hettner, "Ueber das Ultrarote Absorptionsspektrum des Wasserdampfes," Part 2, Ann. d. Physik [4F] **55**, 476 (1918).
H. C. Hottel, "Heat Transmission by Radiation from Non-Luminous Gases," Ind. Eng. Chem. **19**, 888 (1927).
H. C. Hottel and F. P. Broughton, "Determination of True Temperature and Total Radiation from Luminous Gas Flames," Ind. Eng. Chem. Anal. Ed. **4**, 166 (April 15, 1932).
H. C. Hottel and R. B. Egbert, "The Radiation of Furnace Gases," Trans. A.S.M.E. **63**, 297 (May 1941).
B. Lewis and G. von Elbe, "Flame Temperature," J. App. Phys. **11**, 698 (1940).
A. Schack, "Die Strahlung der Feuergase," Archiv für das Eisenhüttenwesen **13**, 241 (Dec., 1939).
C. Schaefer and B. Philipps, "Das Absorptions spektrum der Kohlensaure und die Gestalt der Co_2—Molekel," Zeits. f. Physik n. 36 (March 5, 1926), p. 641.
E. Schmidt and E. Eckert, "Die Warmestrahlung von Wasserdampf in Mischung mit nichtstrahlenden Gasen," Forsch. auf dem Gebiete des Ing. Ed. A. **8**, 87 (1937).
H. Schwiedessen, Archiv für das Eisenhüttenwesen **14**, "Die Strahlung von Kohlensaure und Wasserdampt mit besonderer Berucksichtingung hoher Temperaturen," Part 1: no. 1, p. 9 (July 1940); Part 2: n. 4, p. 145 (Oct. 1940).
W. M. Vaidya, "Spectroscopic Investigation of Hydrocarbon Flames," Proc. Roy. Soc. **A178**, 356 (1941).
J. P. Vollrath, "The Measurement of Flame Radiating Characteristics," Instrumentation **1**, 23–25 (1945).
Max Wimmer, "Beeinflussung ultraroter Kohlensaureabsorptionsbande," Ann. d. Physik [4F] **81**, 1091 (1926).

JOURNAL OF THE OPTICAL SOCIETY OF AMERICA VOLUME 35, NUMBER 11 NOVEMBER, 1945

Two Criteria for the Selection of Color Vision Test Plates

EARL L. GREEN AND LOUISE L. SLOAN
AAF School of Aviation Medicine, Randolph Field, Texas
(Received August 17, 1945)

TESTS of color vision utilizing pseudo-isochromatic charts have proved very useful as rapid screening tests which will detect a high percentage of subjects with red-green color deficiency regardless of the type or the degree of the defect. There are a number of versions of this type of test.[1] The Stilling test produced in Germany and the Ishihara test produced in Japan have been widely used in this country. The American Optical Company test is composed of 46 charts, some copied from the Stilling and some from the Ishihara series. A relatively recent test developed by Rabkin (1936) in Russia has been used by a few American investigators but has been difficult to obtain in this country. In 1944 Dvorine[2] introduced the first test having origin in America, but unfortunately made little use of the well-established facts about color deficiency. One series of the Dvorine charts is for training individuals to read charts of this type, the other is for testing and for assessing the results obtained by training. A 36-plate test has been developed by the U. S. Navy, the plates of which are similar to those of the American Optical Company test, but embody certain modifications in the formation of the digits, the choice of colors, etc. A limited edition was produced and issued for experimental study in 1945.

A series of charts to be known as the IOPH Charts is under development by Hardy and Rand[3] at the Institute of Ophthalmology, New York. These charts, unlike those of previous tests, are designed to be of graded difficulty for the color deficient subject. They use only two pairs of confusion colors, one for the protanopic and one for the deuteranopic type of defect. The saturation of the colors in different plates is varied in order to introduce graded degrees of difficulty. If successful, a test composed of such plates should be of value, not only as a dichotomous test to differentiate between normal and color deficient subjects, but also as a quantitative test to measure degree of defect.

[1] Elsie Murray, "Evolution of Color Vision Tests," J. Opt. Soc. Am. **33**, 316–334 (1943).
[2] Israel Dvorine, "A New Diagnostic Method of Testing and Training Color Perception," Am. J. Optom. Arch. Am. Acad. Optom. **21**, 225–235 (1944).
[3] G. Rand, personal communication to the authors.

Charts of the type now available are suitable primarily for use in constructing simple pass-or-fail tests. For this purpose, the only requirement is that the range of error scores of normal subjects be differentiated from the range of errors of color deficient subjects. The extent to which a given group of charts fulfills this requirement obviously depends upon the number of charts used and upon what may be called the diagnostic efficiency of the individual charts. Fewer charts will be needed if those selected have a relatively high diagnostic efficiency.

Data on the efficiency of the individual charts composing the various tests can serve a double purpose as a guide in devising better tests from existing charts, and as a guide in the development of new charts. The diagnostic efficiency of individual charts may be evaluated by testing two groups of subjects classified respectively as normal and color deficient on the basis of one or more tests of color vision. If one is interested only in the detection of red-green color deficiency and not in determining the type or the degree of defect, it is permissible to classify individuals into one of two and only two categories, normal or color deficient. It is not necessary to specify further the color deficient group as protanopic or deuteranopic, nor is it necessary to distinguish degrees of defect.

THE RATES OF MISCLASSIFICATION

Some normal subjects may be misclassified as color deficient by any particular pseudo-isochromatic plate, and some color deficient subjects may be misclassified as normal. In general, for a plate to have any diagnostic value whatsoever, somewhat more than half of the normal and color deficient subjects must be classified correctly. If about one-half of the subjects are misclassified, the plate is obviously no better than chance in discriminating the two categories of subjects.

The rate of misclassification may be found simply by dividing the number of subjects misclassified by the number exposed to any given plate. The rate for normal subjects is thus

$$q_N = a_N/n_N, \tag{1}$$

and for color deficient is

$$q_D = a_D/n_D, \tag{2}$$

where N refers to the subjects with normal color vision, D refers to the subjects with deficient color vision, n is the total number of subjects, a is the number misclassified, and q is the proportion misclassified.

After technical requirements in the construction of a pseudo-isochromatic plate have been satisfied, judgment of the plate's diagnostic efficiency must be based upon the rates of misclassification of normal and color deficient subjects. These are the raw materials.

The use of the two misclassification rates to evaluate a plate assumes that there has been a prior separation of a certain group of experimental subjects into normal and color deficient. This separation may not be performed perfectly by any one test, but the use of several color vision tests of different types already in existence will provide a definite classification for all but a trivial number of the subjects.

TWO CRITERIA OF SELECTION

The two criteria which we propose for the selection of color vision test plates may be called (1) minimal average misclassification rate, and (2) minimal difference in misclassification rates. The first has formerly been used in various ways, the second is an innovation. The application of the two criteria *jointly* will be illustrated and its advantage pointed out.

1. Minimal average misclassification.—The ideal plate is the plate which correctly classifies all the normal and all the color deficient individuals. Available plates satisfy this ideal in different degrees. As a first measure of the departure of any given plate from the ideal, we may take the average of the two misclassification rates. That is:

$$\bar{q} = (q_N + q_D)/2. \tag{3}$$

To illustrate, let us say that, for a particular plate, it is found that six of 150 normal subjects are misclassified as color deficient ($q_N = 0.04$); and 15 of 75 color deficient subjects are misclassified as normal ($q_D = 0.20$). The average rate of misclassification is thus $\bar{q} = 0.12$.

Averaging the misclassification rates in this manner assumes that they are equally important in judging the value of the plate. This may be far from so. On a scale of importance, $q_N = 0.04$

may be equal to $q_D = 0.20$. In consequence, we may multiply q_D by an "importance ratio," k, in order to give q_N and q_D appropriate weight in the average, $\bar{q}$. The value of k may be chosen as $\frac{1}{5}$ or $\frac{1}{4}$ or any suitable fraction. Introducing this concept of importance into the average misclassification rate,

$$\bar{q} = (q_N + kq_D)/2, \tag{3a}$$

where $0 < k < 1$ by choice. (If q_N were regarded as less important than q_D, then kq_N may be substituted in (3) instead of kq_D.)

2. Minimal difference in misclassification.— Several plates may turn out to have the same average misclassification rate, yet in fact be quite different. As shown in Table I, these five plates have equal $\bar{q}$'s, assuming $k = 1$. Similarly, if $k = .2$, these five have equal $\bar{q}$'s. (See Table II.) Obviously, the average rate of misclassification alone is an incomplete description of a plate. When misclassification of either normal or color deficient or both does in fact occur, the standard deviation (σ_q), which measures the amount of discrepancy between q_N and q_D, may be taken as a second measure of a plate's value. Thus

$$\begin{aligned} \sigma_q^2 &= \tfrac{1}{2}((q_N - \bar{q})^2 + (kq_D - \bar{q})^2), \\ &= \tfrac{1}{4}(q_N - kq_D)^2. \end{aligned} \tag{4}$$

If the positive root is always taken, then

$$\sigma_q = |q_N - kq_D|/2, \tag{4a}$$

where the vertical lines indicate that the sign of the difference is to be neglected, and k is an "importance ratio" as before.

The usefulness of this second criterion may be illustrated by a few artificial examples. Suppose that misclassification of normal subjects is regarded as equal in importance to misclassification of color deficient subjects, i.e., $k = 1$. Then only those plates which have $\sigma_q = 0$ or $q_N = q_D$ will satisfy the requirement of not misleading the investigator more often (proportionally) in one direction than in the other. The third plate in the group above with $\bar{q} = 0.12$ is such a plate.

TABLE I.

	q_N	q_D	$\bar{q}$	σ_q
(1)	.00	.24	.12	.12
(2)	.04	.20	.12	.08
(3)	.12	.12	.12	.00
(4)	.20	.04	.12	.08
(5)	.24	.00	.12	.12

TABLE II.

	q_N	q_D	$\bar{q}$	σ_q
(1)	.00	.40	.04	.04
(2)	.02	.30	.04	.02
(3)	.04	.20	.04	.00
(4)	.06	.10	.04	.02
(5)	.08	.00	.04	.04

If no plates available have $\sigma_q = 0$, then those with the least σ_q will be preferred, which is the same as preferring those with most nearly equal rates of misclassification.

For the selection of actual plates to include in a color vision test, the misclassification of normal subjects may be regarded as much more serious than the misclassification of color deficient subjects. Suppose one is led to choose $k = 0.2$. The requirements will best be satisfied by those plates which have standard deviations (σ_q) most nearly equal to zero, or $q_N = kq_D$. Such plates are the best balanced with respect to the conditions we may impose. In the group of plates, with $\bar{q} = 0.04$, the third plate is the best balanced. This plate will be preferred to plate 2 of the same group, even though plate 2 actually misclassified fewer normal subjects.

These two measures of a plate's value are not independent. If the average rate of misclassification, $\bar{q}$, is low, the discrepancy in the rates, σ_q, must necessarily be small also. It is apparent, therefore, that if a sufficient number of plates with low values for $\bar{q}$ is available for the construction of a color vision test, the second criterion will automatically have been satisfied. Its chief usefulness will occur when choices must be made among plates which have intermediate or high average misclassification rates.

We defer until later a discussion of the conditions which may lead to choosing particular values of the "importance ratio," k.

JOINT APPLICATION OF CRITERIA

If the two criteria, minimal average and minimal difference, are applied singly in the selection of color vision test plates, many cases will arise which leave the experimenter in doubt. For example, three plates are exposed to each person in two groups of subjects, *N* and *D*, with the results given in Table III, assuming for simplicity that $k = 1$.

TABLE III.

Plate	Group	n	a	q	$\bar{q}$	σ_q	r
1	N	200	24	.120	.1335	.0135	.1342
	D	75	11	.147			
2	N	200	18	.090	.0915	.0015	.0915
	D	75	7	.093			
3	N	200	13	.065	.1125	.0475	.1221
	D	75	12	.160			

Which plate is best? If a low rate of misclassification of normal subjects is the sole standard of judgment, then plate 3 with $q_N = .065$ is the best. However, the additional expense of using this plate will be to classify 16 of every 100 color deficient subjects as normal. If we are willing to assume that the rates of misclassification of normal and color deficient are equally important, then plate 3 on the average will misclassify 11.25 percent of the experimental subjects to whom it is exposed. Plate 2, with $\bar{q} = 0.0915$, is apparently better than plate 3, and for that matter is also better than plate 1, with respect to the average rate of misclassification. Plate 2 also satisfies the criterion of least difference in misclassification rates more closely than either plate 1 or plate 3. Plate 2 is obviously the best plate.

Which plate is next best? Plate 3 misclassifies fewer subjects on the average than plate 1, but is not as nearly balanced with respect to the sources of misclassification. To view the problem diagrammatically, a point for each of the three plates may be located in a plane with coordinates $\bar{q}$ and σ_q, as in Fig. 1. The point for an ideal plate will be located at the origin. To measure the departure of any plate from the ideal, and thus to provide a means of comparing plates, the distance (r) of the point from the origin may be computed. We use the relationship

$$r^2 = \bar{q}^2 + \sigma_q^2. \tag{5}$$

From (5) we find the distances (r) are 0.1221 unit for plate 3 and 0.1342 unit for plate 1. If there is a necessity for choosing one of these plates in preference to the other, plate 3 is the better plate. Plate 2, with $r = 0.0915$, is better than either plate 1 or 3. This conclusion, however, is reached only by joint application of the two criteria; in fact, the criteria have been combined so that a single figure, r, represents the value of a plate. This value (r) may be regarded as an index of the diagnostic efficiency of the plate.

For this example, we have assumed that q_N and q_D are equal in importance, i.e., $k = 1$. If we choose $k = 0.2$, we may arrive at quite different choices of plates, because in this circumstance the misclassification of a color deficient subject is much less important than the misclassification of a normal subject. In fact, by easy computation, we find the distances (r) are now 0.0874 for plate 1, 0.0650 for plate 2, and 0.0465 for plate 3. Plate 3 will now be regarded as the best plate, with plate 2 next best.

SIMPLIFIED PROCEDURE

The combination of the two criteria, measured by $\bar{q}$ and σ_q, into a single standard of judgment provides a simplification in the arithmetic of evaluating individual plates. We find by substituting (3a) and (4a) in (5),

$$r^2 = \bar{q}^2 + \sigma_q^2, \tag{5}$$

$$= \tfrac{1}{4}(q_N + kq_D)^2 + \tfrac{1}{4}(q_N - kq_D)^2,$$

$$= \tfrac{1}{2}(q_N^2 + (kq_D)^2). \tag{5a}$$

Two possibilities are presented for graphical procedure as a result of (5a). The first of these requires a restatement of (5a) as follows:

$$r^2 = [q_N/2^{\frac{1}{2}}]^2 + [kq_D/2^{\frac{1}{2}}]^2. \tag{5b}$$

Thus, by scaling q_N and kq_D as multiples of $2^{\frac{1}{2}}$, and by plotting $q_N/2^{\frac{1}{2}}$ and $kq_D/2^{\frac{1}{2}}$ as coordinates of points in a plane, values of r may be estimated graphically. Since division by $2^{\frac{1}{2}}$ may be somewhat tedious, and since the chief use of the r values is for comparing plates, another statement of (5a) seems more suitable.

$$R^2 = 2r^2 = q_N^2 + (kq_D)^2. \tag{5c}$$

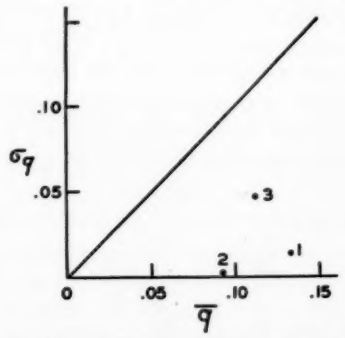

FIG. 1. Diagram of pairs of values of $\bar{q}$ and σ_q for three pseudo-isochromatic plates.

This relationship permits us to plot q_N and kq_D directly as coordinates of points in a plane. The distances (R) from the origin may be used in place of the distances (r) to compare plates. From (5c), it is readily seen that $r=0.7071R$. The joint application of the two criteria for the selection of color vision test plates thus becomes a very simple direct procedure of graphing points for pairs of q_N and kq_D.

When knowledge of the average ($\bar{q}$) and standard deviation (σ_q) for a given plate is desired, these values must be computed directly from q_N and kq_D by use of (3a) and (4a). A diagram such as Fig. 1 will assist in a visual appraisal of the data. When plates are to be evaluated only by joint application of the two criteria, the distances either as r or R may be computed directly from the data without finding $\bar{q}$ and σ_q. Figure 2 represents geometrically why this is so. The distance (r) between the point (P') and the origin is actually the common hypotenuse of two different right-angle triangles. For one of these triangles, OTP',

$$r^2=[q_N/2^{\frac{1}{2}}]^2+[kq_D/2^{\frac{1}{2}}]^2, \qquad (5b)$$

and for the other, OSP',

$$r^2=\bar{q}^2+\sigma_q^2. \qquad (5)$$

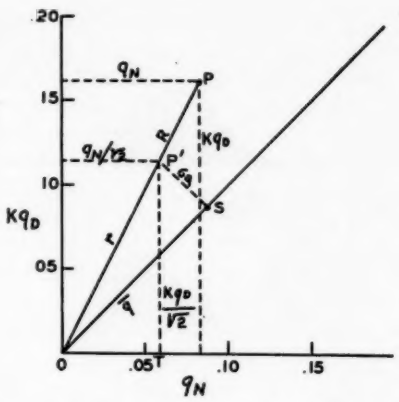

FIG. 2. Diagram of the location of a point (P') for a particular plate according to two systems of coordinates. $q_N=0.0825$, $q_D=0.1625$, $k=1.0$.

EFFECT ON ENTIRE TEST

For several reasons, single plates are inadequate for a routine screening test of color vision. No single plate, now in existence, that has been exposed to large numbers of subjects, has been proved to give perfect separation of normal and color deficient subjects. Furthermore, for mass testing when there is a premium upon the correct response, the subjects may memorize the intended response and so circumvent the purpose of the test. It is necessary, therefore, to choose a number of plates for inclusion in a color vision test. Attention must be given to the desiderata of fairness and economy discussed by Murray.[1] But the question still remains, of about 100 different color vision test plates now in existence, what combination of, say, 20 of these plates will yield the best discrimination of normal and color deficient vision?

We mention 20 plates as a possible number to include in a color vision test because at least 20 plates of fairly high efficiency are now in existence, because 20 is a large enough number of plates to minimize learning effects, and because a 20-plate test may be administered in a reasonable length of time in mass testing.

If the test has 20 plates, and a score made up of the number of errors is recorded for each individual, normal individuals will score 0, 1, $\cdots$, x_N, $\cdots$, x_s errors, and color deficient individuals will score x_t, $\cdots$, x_D, $\cdots$, 19, 20 errors, where $s<t$. If $s>t$, the test may still be used, but a number of (artificially) doubtful cases will appear. The frequency of these doubtful cases will depend on the extent of the overlapping of the x_N and x_D distributions.

Depending upon how the individual plates are chosen, several different types of color vision tests may be constructed. These tests may be described in qualitative terms as follows.

1. q_N's and q_D's all high ($\bar{q}$'s high, σ_q's low). This would be a least satisfactory test. Practically no discrimination of normal and color deficient vision could be achieved. In the limit when all the q_N's and all the q_D's are equal to one-half, the expected distributions of errors for the N and D groups coincide with a mean error of $\bar{x}_N=\bar{x}_D=10$ and a standard deviation of $\sigma_{xN}=\sigma_{xD}=2.2$ (Fig. 3A).

2. q_N's low, q_D's high ($\bar{q}$'s intermediate, σ_q's high). Discrimination of normal and color deficient vision would still be quite inefficient. A large number of artificially doubtful cases

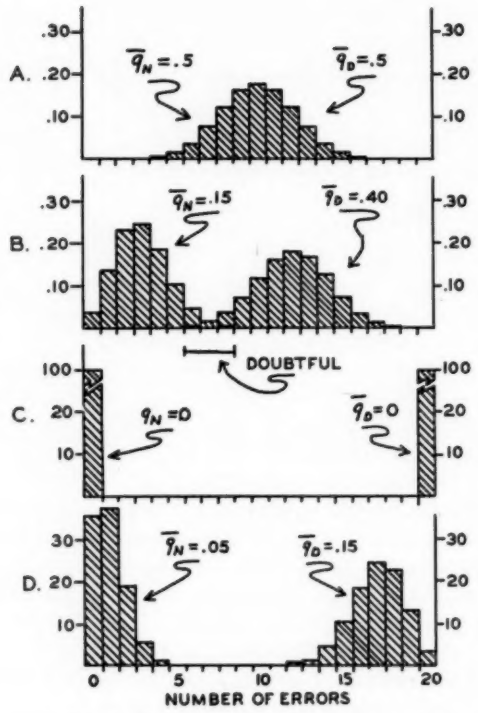

FIG. 3. Distributions of number of errors for tests composed of various sets of pseudo-isochromatic plates.

would occur due to the overlapping distributions of the error scores, x_N and x_D, of the two groups of individuals (Fig. 3B).

3. q_N's high, q_D's low ($\bar{q}$'s intermediate, σ_q's high). The reverse of the previous type of test and equally unsatisfactory.

4. q_N's and q_D's all low ($\bar{q}$'s low, σ_q's low). Obviously, this is the desired type of test. In the limiting case, when the q_N's and q_D's are all zero, it follows that $\bar{x}_N=0$ and $\bar{x}_D=20$ (Fig. 3C). The practical question, of course, is what magnitude of q_N's and q_D's may be permitted before the distribution of errors among normal and color deficient subjects overlap and so give artificially doubtful subjects. Figure 3D represents a separation of normal and color deficient subjects that may be attainable. If the chance for error by N subjects for each plate of a 20-plate test is about 5 percent (i.e., $\bar{q}_N=0.05$), then less than one percent of the N subjects will make more than four errors. Seventy percent or more will make no more than one error. If for the same plates the chance for error by D subjects is about 85 percent (i.e., $\bar{q}_D=0.15$), then less than one percent of the D subjects will make fewer than 13 errors. A wide gap in error scores exists from approximately 6 up to 11 errors. Any individual who, upon exposure to the test, makes 6 to 11 errors, may be regarded as a true doubtful as distinguished from an artificial doubtful. A low error score for such a subject is not the result of chance but is an indication that his color deficiency differs in some way from that of a majority of those classed as color deficient.

The simplified model, represented in Fig. 3D, departs from fact in several respects. These departures require slight modifications in the expectations. In the first place, it will never be possible to obtain 20 different plates, each of which misclassifies exactly 5 percent of N and 15 percent of D, or for that matter any other pair of percentages. Plates which do have the same q_N will probably not have the same q_D, and *vice versa*. Therefore, we shall have to accept some variation in the q_N's from plate to plate, and likewise in the q_D's. The effect of these variations will be to yield a slightly smaller dispersion in the error scores of each group of subjects. In consequence of this effect, the gap between the two distributions of error scores will be slightly larger. In the second place, not all differences in error scores among the normal individuals (N) or among the color deficient individuals (D) may be explained by chance alone. Some N individuals may not misidentify any of the charts, whereas others may misidentify several, because of variations in motivation, training, and other causes. Among D individuals, there may be still greater variation in the number of errors owing to the great differences between the subjects in color perception. In any case, the effect of these variations is to cause a wider dispersion of the error scores in each of the two groups, and consequently to narrow the gap between the distributions. The variation in the probability for error from subject to subject is thus seen to affect the error scores in a direction opposite to the variation in misclassification rate from plate to plate.

In addition to these two circumstances, the number of plates in the test is a third circumstance which affects the width of the gap between

the distributions of errors for the N and the D subjects. These three circumstances interact in such a way that, for a given amount of variability within the two groups of subjects, the number of plates in a test may be reduced only by improving the individual plates, if the same width of gap is to be preserved.

CHOICE OF IMPORTANCE RATIO

The numerical value of the importance ratio, k, which enters into the computations for the average misclassification rate, $\bar{q}$, and the difference in misclassification rates, σ_q, may be decided only by policy. There are several considerations that may influence the choice of a specific value for k.

Because of differences in kind and in degree of color deficiency, it may be anticipated that some individuals who are in fact color deficient will nevertheless identify some plates correctly more often than expected by chance alone. The protanope may identify correctly plates having a higher diagnostic efficiency for deuteranopes and *vice versa*. The color deficient individual with only a mild defect will be more likely to identify a plate correctly than the one with a marked defect.

The causes of misclassification of normal subjects are less numerous. The occasional errors made by this group are presumably not related in any way to color discrimination. The normal individual may, for example, give the correct response but exceed the time limit allowed, may misread a 3 as an 8, or may fail to trace a path correctly through carelessness.

The misclassification rate of color deficient subjects (q_D) for many plates may be larger than the misclassification rate of normal subjects (q_N). Owing to the composite nature of the D group and to the fact that misclassification in this group is related to the type and degree of color deficiency, a large q_D might be regarded as less serious than a large q_N. We might therefore choose to rate q_N and q_D as equivalent on a scale of importance if, for example, q_D is no more than three times q_N.

The choice of the value of k will affect the symmetry and the dispersion of the error scores of an entire test made of, say, 20 plates. If $k=1$, the two distributions, x_N and x_D, will be approximately mirror images, one centering about the sum of the q_N's, the other centering about 20 minus the sum of the q_D's, where the sum of the q_N's approximately equals the sum of the q_D's. If $k=\frac{1}{3}$, say, the x_D distribution will center at a point nearer the middle of the range of errors with an increased dispersion about its center. The sum of the q_N's will be about equivalent to 20 minus three times the sum of the q_D's in this case.

ILLUSTRATION

For the purpose of a simple numerical example of the methods outlined in the foregoing sections, data obtained by exposing 12 pseudo-isochromatic plates of the American Optical Company to a group of 200 normal subjects and to a group of 73 color deficient subjects are given in Table IV. These data are part of a much larger series collected under the supervision of one of us (L.L.S.) at the AAF School of Aviation Medicine, Randolph Field, Texas. Since we have no interest in the nature of the individual plates, they are identified only by letter. Assume that our ob-

TABLE IV. Misclassification rates, $\bar{q}$, σ_q, r, and rank for 12 different pseudo-isochromatic plates for two different importance ratios.

Plate	Number misclassified		Misclassification rate		$k=1$				$k=1/5$			
	a_N	a_D	q_N	q_D	$\bar{q}$	σ_q	r	Rank	$\bar{q}$	σ_q	r	Rank
A	7	5	.035	.068	.0515	.0165	.0541	1	.0243	.0107	.0265	3
B	16	1	.080	.014	.0470	.0330	.0574	2	.0414	.0386	.0566	9
C	15	8	.075	.110	.0925	.0175	.0941	6	.0485	.0265	.0553	8
D	46	4	.230	.055	.1425	.0875	.1672	10	.1205	.1095	.1628	12
E	7	23	.035	.315	.1750	.1400	.2197	12	.0490	.0140	.0510	7
F	0	8	.000	.110	.0550	.0550	.0778	4	.0110	.0110	.0156	1
G	37	0	.185	.000	.0925	.0925	.1308	9	.0925	.0925	.1308	10
H	14	6	.070	.082	.0760	.0060	.0762	3	.0432	.0268	.0508	6
I	22	5	.110	.068	.0890	.0210	.0914	5	.1230	.0482	.1321	11
J	5	10	.025	.137	.0810	.0560	.0985	7	.0262	.0012	.0262	2
K	2	22	.010	.301	.1555	.1455	.2129	11	.0351	.0251	.0432	5
L	7	11	.035	.151	.0930	.0580	.1096	8	.0326	.0024	.0327	4

jective is to construct a screening test for color vision composed of six of these 12 plates.

Let us try two different importance ratios to observe this effect upon the distribution of error scores. First, take $k=1$, which we should do if we regard the errors among N as equal in importance to the errors among D. This leads to the selection of plates A, B, C, F, H, and I as the best. The average rate of misclassification of N by these plates is $\bar{q}_N=0.062$, and of D is $\bar{q}_D=0.075$. Figure 4A shows the expected distribution of error scores among N and D subjects, using the observed probabilities of misclassification for each plate, but assuming that the individuals within the N and D groups differ only by chance. As expected when $k=1$, the mean number of errors among N, $\bar{x}_N=0.37$, is about the same as six minus the mean number of errors among D, i.e., $6-5.55=0.45$. The two distributions are approximately mirror images. The separation of the N and D subjects is accomplished at an error score of $x=3$. Several subjects may obtain error scores of 3, however, so it is obvious that this illustrative test of six plates would not be suitable for practical use.

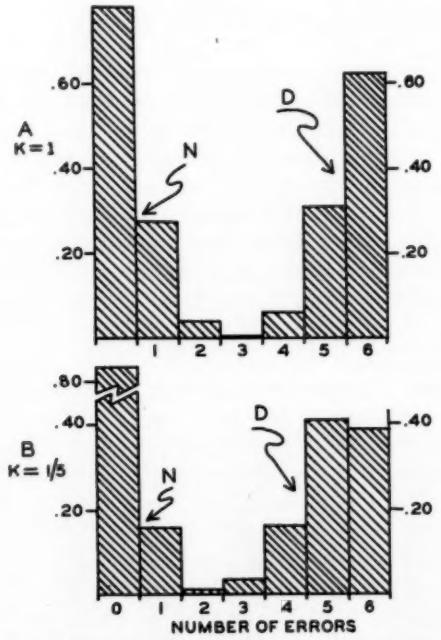

FIG. 4. Distributions of number of errors among normal (N) and color deficient (D) subjects for two illustrative 6-plate tests.

Next, take $k=\frac{1}{5}$, which we should do if we regard correct scores by D subjects as about $\frac{1}{5}$ as important as error scores among N subjects. This weighting appears to be more satisfactory intuitively because correct responses by some D subjects may occur as a result of real differences in color perception. The effect of this weighting, in any case, is to select plates which have the very smallest values of q_N, even though some fairly large values of q_D may have to be accepted. Plates A, F, H, J, K, L appear to be best for this circumstance as seen in Table IV. The average of the misclassification rates for N is $\bar{q}=0.029$, but this was accomplished at the sacrifice of raising $\bar{q}_D$ to 0.142. The expected distribution of error scores is shown in Fig. 4B. Separation now occurs at an error score of $x=2$ and there is a marked tendency for the N subjects to make no errors. The average number of errors by N subjects is found as $\bar{x}_N=0.18$, whereas the average for D subjects has become $\bar{x}_D=5.15$. Obviously, the gap between the two distributions is not wide enough to make such a six-plate test useful in practice.

SUMMARY

A procedure is presented for selecting pseudo-isochromatic plates for constructing screening tests for red-green color deficiency. The procedure consists of finding an index of diagnostic efficiency for each available plate, either numerically or graphically, and choosing the plates with the lowest index (highest efficiency). The index is shown to be a function of the sum and of the difference of the rates of misclassification of normal and color deficient subjects. To arrive at the index, the two rates of misclassification may be weighted equally or unequally, depending upon policy.

Tests composed of several plates separate the color deficient from the normal with an efficiency which depends upon the efficiency of the individual plates and upon the number of plates in the test. The distribution of errors among normal and color deficient subjects depends upon the manner in which the two rates of misclassification have been balanced in the computation of the index of efficiency.

A numerical illustration is provided in which the best six plates of 12 are selected for a screening test of color deficiency.

JOURNAL OF THE OPTICAL SOCIETY OF AMERICA VOLUME 35, NUMBER 11 NOVEMBER, 1945

Unusual Colors Produced by Uranium in Glasses

W. COLBERT
Glass Science, State College, Pennsylvania

AND

N. J. KREIDL
Bausch and Lomb Optical Company, Rochester, New York

(Received August 27, 1945)

IN this study uranium was introduced into several base glasses of uncommon composition and glasses with unusual transmission spectra were obtained. Uranium containing glasses can be conveniently divided into the following three groups:

I. The faint yellow glasses characterized by a strong green fluorescence visible even in daylight. Glasses of this type are obtained by introducing uranium into ordinary soda lime silicate glasses under oxidizing conditions.

II. The non-fluorescent yellow glasses obtainable under oxidizing conditions in very alkaline silicates and borates as well as in lead containing glasses.

III. The non-fluorescent brown and green glasses obtained under strongly reducing conditions.

The most common uranium glasses contain the uranyl group as color centers and belong to Type I of this classification. In the present study, variations of the second and third types were made, and the base glasses were extended to include less common fields of glass composition. In this way several series of new and unusual uranium colors were obtained. One of these glasses exhibits a truly red color. Hitherto, red colors were obtainable only in glasses of the gold, copper, antimony sulfide, and cadmium sulfoselenide ruby type. These glasses containing non-ionic colorants are strongly affected by heat treatment. The new red uranium glass has color centers which are ionic in character and therefore remain unaffected by thermal treatment; consequently, this red glass is strictly reproducible.

A variety of unusual transmission curves was obtained in the field of reduced uranium glasses

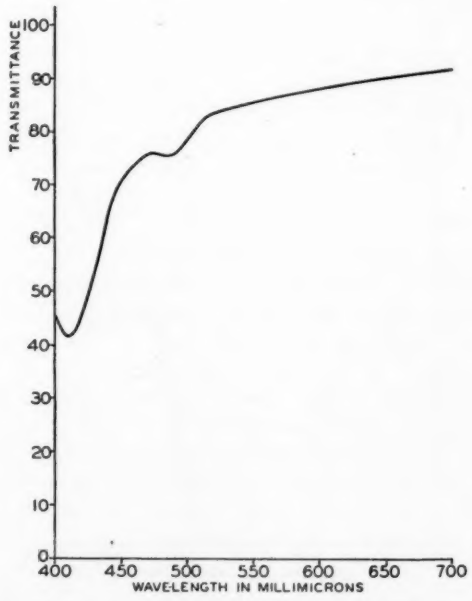

FIG. 1. The transmission of the uranyl group in a Na_2O, $4SiO_2$ glass.

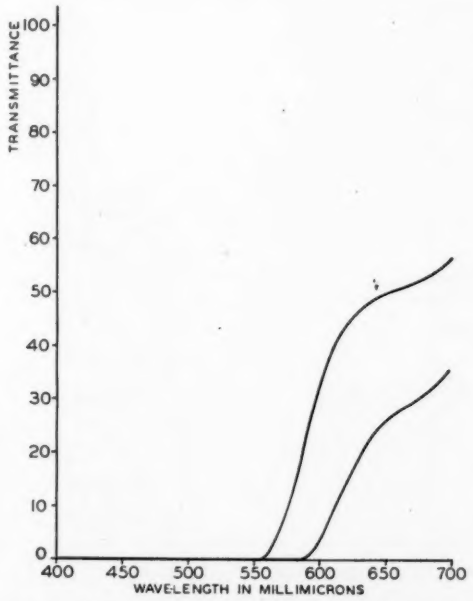

FIG. 2. The transmission of uranium containing lead glasses with a low silica content.

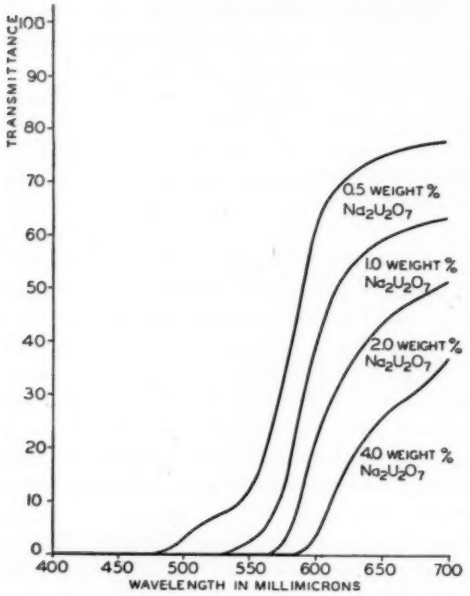

FIG. 3. The influence of uranium concentration on the transmission of lead metasilicate ($PbSiO_3$) glass.

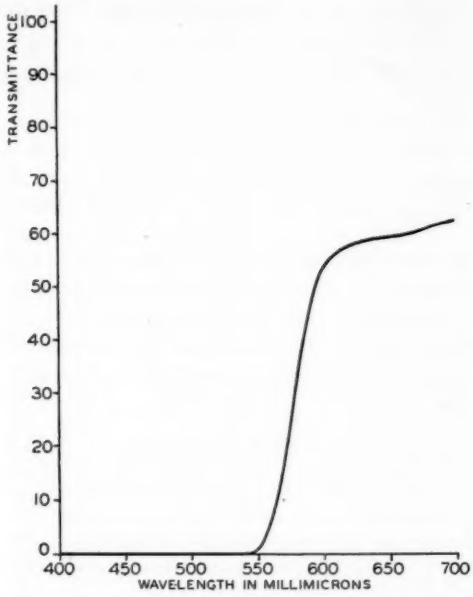

FIG. 5. The transmission of a uranium containing barium crown (25 percent silica, 5 percent lead oxide, 50 percent barium oxide by weight).

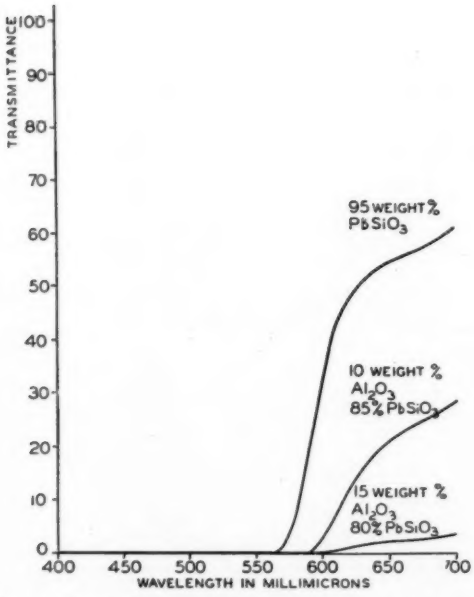

FIG. 4. The influence of aluminum oxide on the transmission of uranium containing lead metasilicate glass.

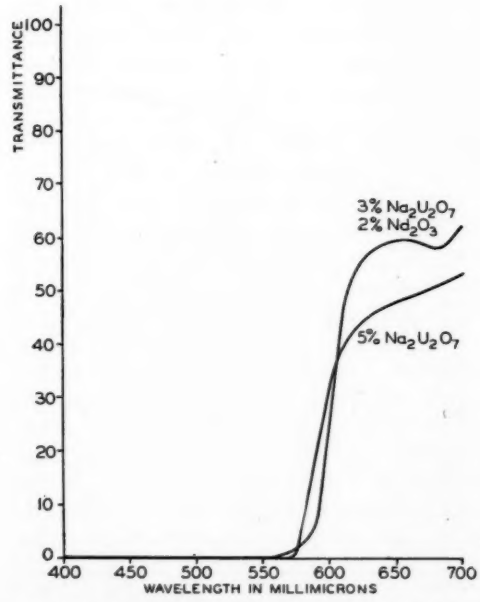

FIG. 6. The influence of neodymium oxide on the cut-off of a uranium containing barium crown (20 percent silica, 17 percent lead oxide, 46 percent barium oxide by weight).

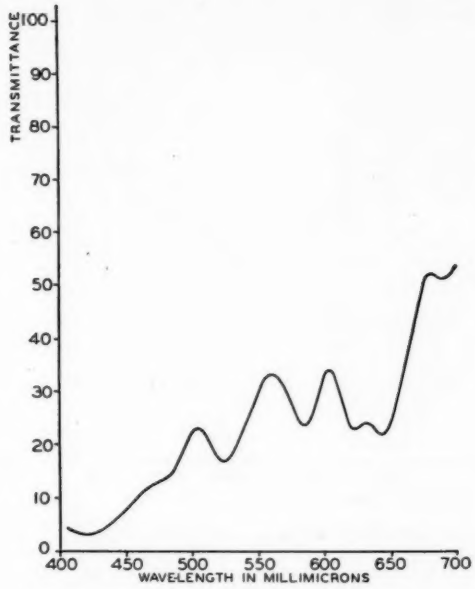

FIG. 7. The transmission of the uranous ion in a Na_2O, $4SiO_2$ glass.

which are characterized by sharp bands similar to those of the rare earths.

The analogy between the color and fluorescence of uranium glasses and the corresponding crystallized uranium compounds has been used by Weyl and Thuemen[1,2] to draw conclusions in regard to the forms in which uranium is present in glasses. These forms are the uranyl group, the uranate group, and the uranous ion.

URANYL GLASSES

The color and fluorescence center of those glasses which show a yellow color and a strong green fluorescence is the hexavalent uranium ion, U^{6+}, in the so-called uranyl $(UO_2)^{2+}$ group. In this group two oxygens are so close to the uranium that the excess positive charge makes this group act like a divalent cation. These color centers usually form when uranium is introduced into normal soda lime silicate or into alkali borosilicate glasses. They seem to be stable in all glasses having a sufficient supply of glass forming oxides such as silica and boric oxide. These glasses exhibit the same yellow color and the same strong green fluorescence as most crystallized hydrated uranyl salts. A transmission spectrum of a glass containing the uranyl group as color centers is given in Fig. 1.

URANATE GLASSES

The transmission of the uranate group in glass is shown in Fig. 2. As the amounts of glass forming constituents such as silica and boric oxide decrease and those of other constituents such as alkali increase, the hexavalent uranic ion changes from the cationic uranyl to the anionic uranate group. In this respect the arrangement becomes analogous to that in a crystallized uranate such as sodium uranate. If, for example, alkali or lead oxide is added to a uranium containing glass, its fluorescence decreases and the yellow color characteristic of the uranate group becomes more pronounced. This does not mean that lead or alkali uranate is present in these glasses in the form of defined molecules, but only that the arrangement of the uranium in the entire glass structure is similar to the anion in the sodium uranate lattice. If the concentration of these uranate groups increases beyond the solu-

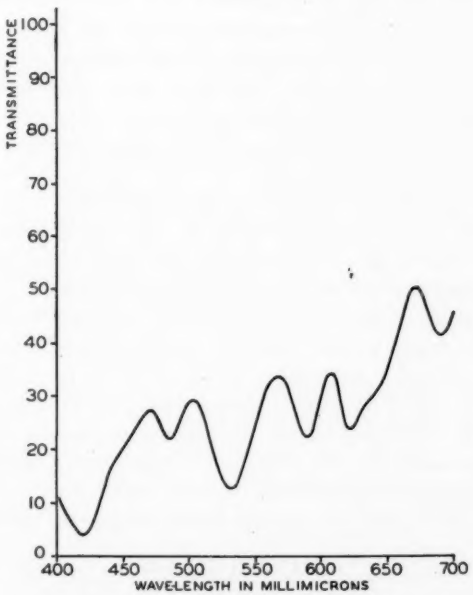

FIG. 8. The transmission of the uranous ion in a borosilicate glass.

[1] W. Weyl and E. Thuemen, Sprechsaal **67**, 95–97 (1934).
[2] W. Weyl, J. Soc. Glass Tech. **28**, 240–245 (1944).

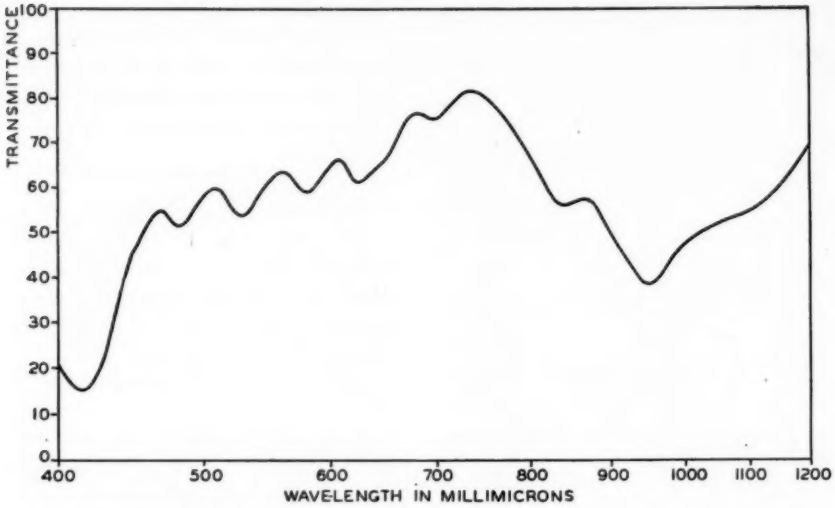

FIG. 9. The transmission in both the visible and the infra-red regions of a borosilicate glass containing uranous ion. (The authors are indebted for this curve to Mr. J. M. Moran, Radio Research Laboratory, Harvard University, Cambridge, Massachusetts and E. I. Stearns of the Calco Chemical Company, Bound Brook, New Jersey.)

bility limit, crystalline uranates of defined chemical composition will precipitate. Opaque systems of this type containing crystallized lead uranates dispersed in a glassy matrix are used for tomato red glazes.

Among the few stable glasses of extremely low silica content, the heavy lead and barium silicate glasses were found to be particularly suitable for stabilizing the uranate group (Figs. 3–6). It was found that in high lead silicate glasses, especially some alumino-silicates of lead, the absorption edge of the uranate group is shifted to longer wave-lengths. This leads to a group of glasses whose colors vary from orange to deep red. If the lead content of the glass becomes very high, the environment of the uranium ion becomes similar to that in lead uranate crystals. Basic lead uranate is red, and a red color can be produced in high lead silicate glasses apparently because of the loosening of the outer electrons of the uranium by the lead ion. Those glasses which contain less lead oxide than the lead metasilicate, $PbSiO_3$, show an orange rather than a red color.

URANOUS GLASSES

In the presence of reducing agents, the hexavalent uranic ion can be reduced to the tetravalent uranous ion, U^{4+}. The color changes to green, brown, or gray, and the fluorescence characteristic of the uranyl group disappears. Weyl and Thuemen[1] describe the absorption

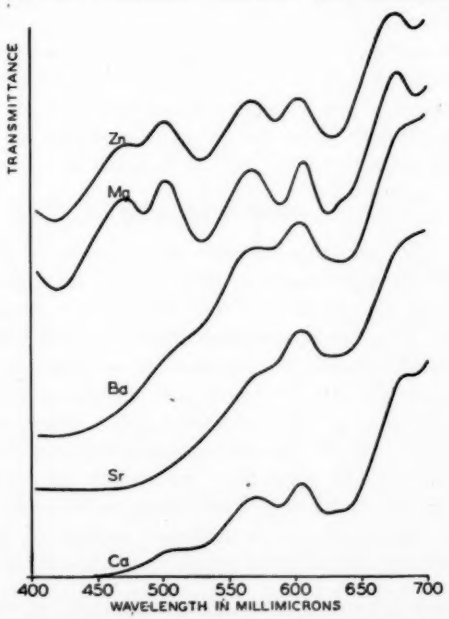

FIG. 10. The transmission of the uranous ion in Na_2O, RO, $4SiO_2$ glasses (R = Ca, Sr, Ba, Mg, Zn).

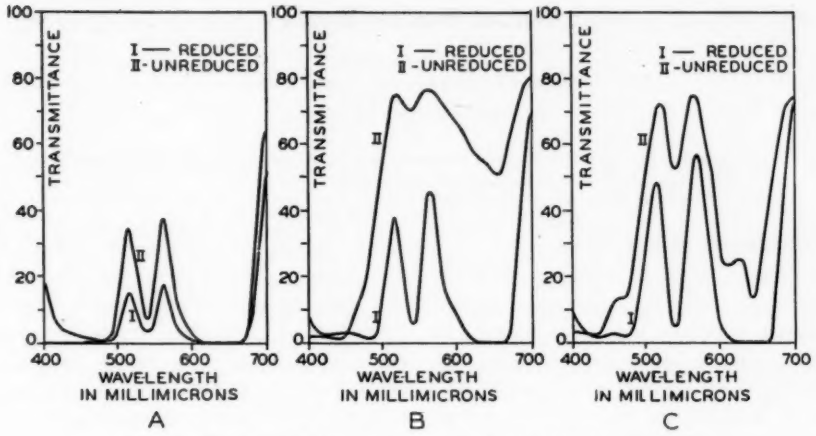

FIG. 11. The transmission of the uranous ion in phosphate glasses.

spectra of sodium tetrasilicate, potassium tetrasilicate, and a borosilicate glass with uranous ions as color centers. The reduced uranium forms cations and it becomes evident from the experimental results that it is particularly stable in those glasses which are rich in glass forming oxides. In the present investigation various silicate, borosilicate, and phosphate glasses containing reduced uranium were prepared. The transmission curves of a green sodium tetrasilicate and a grayish pink sodium borosilicate glass are given in Figs. 7 and 8 (for transmission to 1200 millimicrons see also Fig. 9). The colors of silicate glasses of the type $Na_2O \cdot RO \cdot 4SiO_2$, where R represents a divalent ion, vary from green to brown (Fig. 10); this shift in color is caused by a change in the equilibrium between uranic and uranous ions. From the light absorption at 540 millimicrons, one may judge the concentration of uranous ions in the glass. As the uranous ions possess an absorption band having a maximum at 540 millimicrons, the transmission at this wave-length decreases with increasing uranous ion concentrations. In phosphate glasses (Fig. 11) the bands are particularly sharp and the transmission is limited almost exclusively to the two wave-lengths in the yellow and green and to the boundaries of the visible range. This type of absorption was observed in glasses which had been reduced with sodium cyanide. The influence of the base glass on the reducibility of the uranium ion, and more particularly on the equilibrium between hexavalent and tetravalent uranium, is brought out in Fig. 11. Figure 11-A gives the light absorption of uranium in a barium aluminum phosphate glass with and without a reducing agent. Figure 11-B shows the same for a potassium barium glass, and Fig. 11-C for a potassium zinc glass. In the presence of aluminum or zinc oxides, both of which strengthen the network of phosphate glasses, the uranous ion is favored even in the absence of a reducing agent.

Sunset Shadow Bands

RONALD L. IVES
Dugway Proving Ground, Tooele, Utah
(Received September 12, 1945)

Shadow bands, occasionally observed at sunset when flat desert terrain is observed from above, are here described, and an explanation attempted.

OBSERVED PHENOMENA

AT sunset, when looking eastward over flat barren terrain, from a point having a higher angular elevation than the sun, faint, eastward-moving shadow bands, several miles wide, and extending an unknown, but relatively great, distance to the north and south, have been observed on several occasions. These bands were seen, in each instance, just as the sun dipped below the local horizon. Duration of the phenomena was less than 30 seconds. Estimated rate of eastward motion of the nearest shadow band was 40 miles per hour. Recession of the bands seemed to accelerate with distance. Conditions extant at time of observation are shown in Fig. 1. General similarity of these shadow bands to those occurring during a solar eclipse is notable.

FIELD CONDITIONS

Sunset shadow bands have been observed six times in fifteen years—once from the Pinacate Peaks, Sonora, Mexico; once from the summit of Navajo Peak (Boulder County), Colorado; twice from an airliner approaching El Paso, Texas, from the west; and twice from high points in the Dugway Mountains (Tooele County), Utah.

Astronomical, topographic, and meteorological conditions were substantially identical in each instance. The angular elevation of the observation point was greater than that of the sun: there were high mountains to the west of the location of the shadow bands, which were seen on level, treeless land, with either sparse or no vegetative cover. The sky was absolutely clear (C.A.V.U.), the relative humidity very low, the temperature high, the wind speed near zero, and the lapse rate steep (nearly adiabatic).

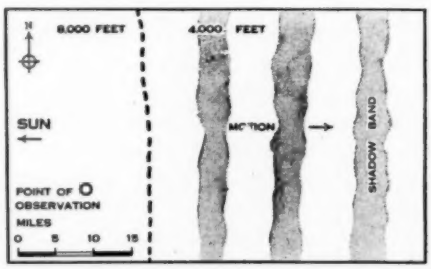

FIG. 1. Plan view showing relative location of sun, point of observation, and sunset shadow bands. The heavy dotted line is the western boundary of the flatlands upon which the shadow bands were seen.

As shadow bands were seen rarely even under these conditions, it is believed that other critical conditions, still unknown, must exist.

EXPLANATORY HYPOTHESIS

Because of their general similarity to eclipse shadow bands, sunset shadow bands are believed to be caused by diffraction of sunlight across mountain crests. Discrepancy between computed diffractive effects and observed phenomena is considerable, and led to a search for other possible causes.

Rather extensive field meteorologic investigations in the Salt Lake Desert failed to disclose any meteorologic cause for the shadow bands. Specifically investigated were air motion patterns, both normal wind and katabatic; regional variations in temperature and relative humidity; and the possibility of interference between thermally differing air strata.

Absence of other plausible explanations, and qualitative, but not quantitative, agreement of diffraction theory with field observations, lead to the belief that sunset shadow bands are a diffraction phenomenon.

CONCLUSIONS

Field observations suggest that sunset shadow bands are of infrequent occurrence, even under supposedly favorable conditions. Theoretical considerations, and the absence of a better explanation, indicate that they may be diffraction phenomena. Additional attempts to observe them, where terrain and meteorological conditions are supposedly favorable, seem desirable.

JOURNAL OF THE OPTICAL SOCIETY OF AMERICA VOLUME 35, NUMBER 11 NOVEMBER, 1945

Note on MacAdam's Determination of Chromaticity Sensibilities

R. H. SINDEN
Wolcott, New York

(Received March 29, 1945)

IN his recent determination of visual sensitivities to color differences, or *chromaticity sensibilities*,[1] MacAdam used filters to produce illuminants of the desired chromatic qualities. Undoubtedly there are valid practical reasons for doing so, one of the most important of them being the avoidance of the disturbing effects due to refractive defects of the eye which are present when viewing a mixture composed of "monochromatic" illuminants of widely different refrangibility. The use of filters has, on the other hand, the disadvantage that results obtained with their use are not independent of the effects of selective absorption occurring in the optical media of the observer's eye. The errors arising from this cause could be very considerable if the individual observer's retinal pigmentation happened to differ widely from that assigned to the "1931 I. C. I. Standard Observer," whose data form the basis for MacAdam's computation of the chromatic values of the various illuminants. It would be possible, however, to introduce corrections for such errors, should they exist, but only if additional colorimetric data pertaining to the individual observers were available.

Very appreciable differences are shown by the results of MacAdam's two observers, DLM and PGN. Wright,[2,3] who likewise carried out a determination of chromaticity sensibilities upon several observers, and whose results, having been obtained with the use of monochromatic illuminants, are independent of macular pigmentation, points out that the data of observer PGN differ more widely from his own than do those of DLM. There are therefore at least grounds for suspicion that the retinal pigmentation of PGN, who furnished the bulk of the observations in MacAdam's investigation, differs materially from the normal retinal pigmentation as specified (indirectly) by the colorimetric data of the Standard Observer. Taking for granted that sufficient care was used in balancing the densities of the paired filters to suit the individual observer's vision so that fluctuations of brightness (luminance) played no part in the ultimate result, MacAdam's data, owing to the superior efficacy of his method and the immense number of separate observations made by his observers, should be potentially of unique value and usefulness in both their practical and theoretical aspects; therefore it would seem to be a matter of prime importance that additional data be obtained for these observers, particularly observer PGN, such as would serve to establish the amounts of their retinal pigmentation and permit corrections to be applied to their results if found necessary.

The manner and the extent to which MacAdam's results would be affected by a departure of the individual observer's retinal pigmentation from the normal or Standard Observer pigmentation are indicated by the diagram shown in Fig. 1, which represents the central portion of Judd's "uniform chromaticity scale" projection[4] of the Newtonian *color chart*[5] constructed from the 1931 I. C. I. Standard Observer's data.[6] Parts of the spectral and blackbody loci are shown, by means of which the reader who is familiar with the uniform-chromaticity-scale color chart should be able to orient himself with respect to the diagram. At *A* in Fig. 1 is shown one of the *chromaticity cells* determined experimentally by MacAdam.[7] This cell, drawn ten

[1] D. L. MacAdam, "Visual Sensitivities to Color Differences in Daylight," J. Opt. Soc. Am. **32**, 247–274 (1942).
[2] W. D. Wright, Proc. Phys. Soc. **53**, 93 (1941).
[3] W. D. Wright, "The Graphical Representation of Small Color Differences," J. Opt. Soc. Am. **33**, 632–636 (1943).
[4] D. B. Judd, "A Maxwell Triangle Yielding Uniform Chromaticity Scales," J. Opt. Soc. Am. **25**, 24–35 (1935).
[5] Sir Isaac Newton's descriptive term for the "center-of-gravity" type color diagram, of which he was the originator, is adopted in this discussion in preference to either of the currently used terms *color triangle* or *chromaticity diagram*. The former has little meaning unless the diagram is plotted in trilinear coordinates, while the latter, it is felt, is not sufficiently distinctive for the purposes of the present context wherein reference must continually be made to a number of similar diagrams and there is danger of confusing the reader as to which is meant.
[6] D. B. Judd, "The I. C. I. Standard Observer and Coordinate System for Colorimetry," J. Opt. Soc. Am. **23**, 359–374 (1933).
[7] Cf. D. L. MacAdam, "The Graphical Representation of Small Color Differences," J. Opt. Soc. Am. **33**, 675–679 (1943).

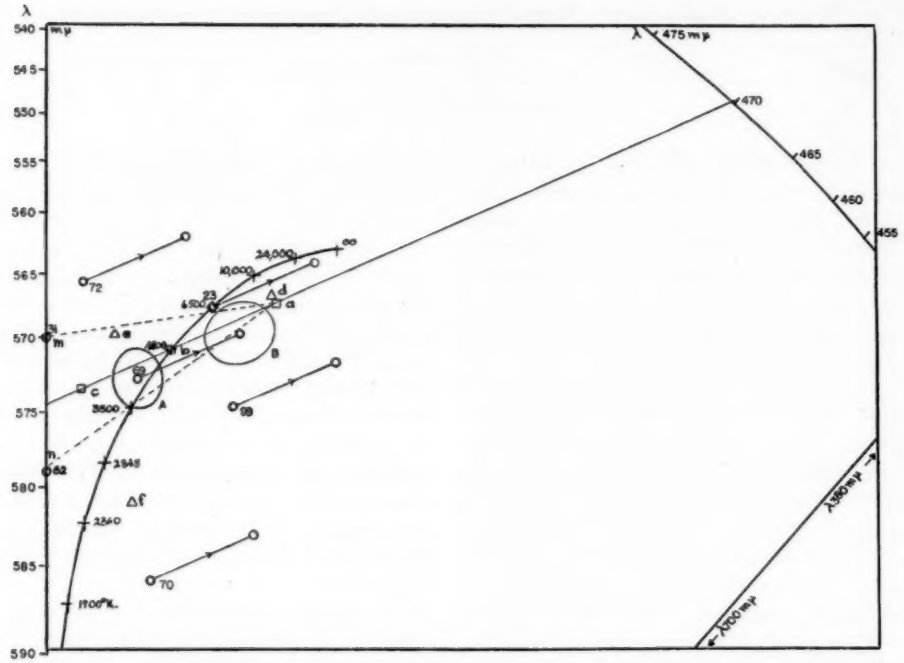

FIG. 1. Uniform-chromaticity-scale diagram illustrating the possible effects of anomalous retinal pigmentation of the observer upon one of MacAdam's chromaticity cells.

times its true size, is the one shown in Fig. 36 of MacAdam's original paper.[1] The given coordinates were of course transformed to the uniform-chromaticity-scale projection, this projection having been used for the diagram because the magnitudes of the chromaticity differences involved are more readily apparent on it than on the standard projection.

Also indicated on the diagram is the locale of the "white points" (corresponding to an illuminant of approximately 4800°K distribution) of 37 observers tested by Wright.[8] Wright found that the white points of these observers were scattered over a V-shaped area on the color chart bounded by the lines *am* and *an* in Fig. 1. The scattering is in all probability caused almost wholly by variations in the density and selectivity of the observers' macular pigmentation,[9] with variations of the former type greatly predominating. The white points of Wright's observers with least, average, and greatest amounts of pigmentation are represented respectively by the small squares *a*, *b*, and *c* on the diagram. The point *b* coincides with the point (4800°K) on the Standard Observer's blackbody locus.

A comparison of the chromaticity sensibility data of MacAdam's observer PGN (the author of the chromaticity cell shown in the figure) with the similar data of other observers appears to indicate that this individual has less than the usual amount of pigmentation. Be it assumed, therefore, for purposes of illustration, that the pigmentation of observer PGN coincides with that of Wright's observer with least pigmentation. Were that the case, an actual physical measurement would show that PGN's white

[8] W. D. Wright, "A Redetermination of the Trichromatic Coefficients of the Spectral Colors," Trans. Opt. Soc. **30**, 141–164 (1928–29).

[9] For the sake of simplifying the discussion it is assumed that these white-point variations are caused wholly by differences in pigmentation of the macula lutea or "yellow spot" of the retina. Other factors may, of course, enter in, although probably only to a very limited extent. Other transparent parts of the eye may possess a variable selectivity. Intrinsic variations of the color sense may play some small part. Whatever their complete explanation, these individual variations in the interior of the color chart are matters of experimental fact, and their effects so far as the present discussion is concerned would be the same regardless of their cause.

(4800°K) point lay at *a*, Fig. 1, instead of at *b*. The reason, of course, is that the radiant energy reaching the sensitive layer of his retina, having been less modified upon passage through the outer pigmented layer, would be actually different in spectral constitution than as if the observer's pigmentation were normal, and hence would excite a different color in his sensory mechanism. Similarly, an experimental determination upon this observer of points in the interior of the color chart corresponding to the colored illuminants produced with the filters used for the purpose by MacAdam would in general give different points from those arrived at by calculation with the Standard Observer data. The entire configuration of chromaticity cells in MacAdam's Fig. 48,[1] being based on the calculated positions of these *filter points* in the color chart, would be in error. Not only would the locations of the chromaticity cells be affected, but also, because of the method of calculating their coordinates, the sizes and shapes of the individual cells as well.

The exact displacement which any given filter point would undergo as a result of anomalous pigmentation of the observer depends on the spectral distribution of the illuminant transmitted by the filter. Thus, two illuminants of different spectral distribution might appear the same color to an observer with normal pigmentation, but differently colored to an observer with anomalous pigmentation, or *vice versa*. This effect may be quite pronounced if the illuminants in question are composed of narrow, sharply defined spectral bands, and in fact constitutes the only present means of gauging the macular absorption of the living eye. It would seldom be noticeable, on the other hand, where the colored illuminants are of the "natural" type (i.e., produced by modification through selective absorption of the distribution of energy emitted by an incandescent radiator), due fundamentally to the combined circumstances that illuminants of the latter type generally comprise sizable portions of the visible spectrum, and the contour of the macular transmission curve is very nearly flat throughout most of the spectrum. Computations based on the average macular transmissivities as determined by post-mortem spectrophotometric examination of human retinae indicate that even in instances when matched illuminants of this type have widely divergent spectral energy distributions and are viewed by observers whose difference of retinal pigmentation is extreme, the effect is marginal or wholly subliminal. It is therefore justifiable to conclude that filter points lying near one another on the color chart would be similarly displaced as a result of variations of retinal pigmentation. Specifically, filter points in the vicinity of point (4800°K) on the Standard Observer's blackbody locus would be displaced similarly to that point, a fact which provides a means of estimating with reasonable assurance what would become of the chromaticity cell shown at *A* in Fig. 1, were PGN's pigmentation as assumed.

Before proceeding to do so, however, it will first be necessary to review briefly the process by which the cell was originally determined. A number of filters having different transmissivities were used in the determination. Employing the known transmissivities of the filters, the spectral distribution of the light emitted by the source, and the standard tri-stimulus specifications of the spectral colors, the color corresponding to each filter was located on the color chart by the accepted calculative method.[6] The given locations of several of these filters are indicated in Fig. 1 by the heavily inked small circles. The numbers beside the circles refer to the filters listed opposite the same numbers in MacAdam's Table 1.[1]

The first step in the determination of a chromaticity cell was to select a filter that in conjunction with the light source produced a color around which the cell was to be constructed. Several pairs of filters were then selected, such that mixtures in suitable proportions of the colored illuminants transmitted by them could be made to match, or nearly match, the central color. Thus, for the center of the cell shown in Fig. 1, filter (69) was chosen. Mixtures produced with paired filters (31) and (99), (62) and (23), and (70) and (72) would each approximately match the color of filter (69).

Having established as close a match as possible between one of the mixtures and the central color, the mixture was allowed to remain fixed on one side of the comparator field, while on the other side a similar mixture was altered by

varying the relative intensities of its components, the observer then readjusting the relative intensities until the two halves of the field appeared identical. The experimental arrangements were such that brightness remained constant. The mean deviation of a large number of settings was therefore a measure of chromaticity sensibility. The deviations of the settings were read on an angular scale on the instrument, and afterwards translated into terms of distances on the color chart by the formula,

$$\Delta s = \Delta\theta(ds/d\theta),$$

where $\Delta\theta$ is the deviation measured on the angular scale of the comparator, and Δs is the corresponding line segment on the color chart. The differential $ds/d\theta$ was evaluated by an approximation method in which use was made of the ratio $f=s/S$, where S is the distance on the color chart between the two points corresponding to the pair of filters that was in the comparator at the time the setting was made, and s is a variable distance along the line joining the two filter points, measured from the end corresponding to $\theta=0$, to the point representing the mixture when the instrument scale reading is θ, both distances being measured in the same unit of length as the scale of the rectangular coordinate network of the color chart. Substituting in the above equation the approximation for $ds/d\theta$ used by MacAdam would give

$$\Delta s = \Delta\theta\left[S\frac{(f_2-f_1)}{(\theta_2-\theta_1)}\right], \qquad (1)$$

in which θ_1 and θ_2 are neighboring values of θ, and f_1 and f_2, corresponding values of f. When $\Delta\theta$ is assigned the value of the *standard deviation* of a group of settings, Δs as given by this equation is taken as the measure of the semi-diameter parallel to its own direction of the chromaticity cell being constructed about the point first chosen. The dimensions of the cell are therefore dependent upon the distances on the color chart between the colors corresponding to the paired filters.

Resuming now the assumption that the retinal pigmentation of observer PGN is anomalous in the manner specified, the resultant effect upon these distances and consequently upon the dimensions and location of the chromaticity cell A, Fig. 1, will be examined. Filter points (69), (23), and (99), lying in the neighborhood of point (4800°K) on the blackbody locus of the Standard Observer, would move in directions approximately parallel to the displacement of that point, and about the same distance. Their displacements are indicated on the diagram by the lines connected with the numbered circles, and their new positions by the lightly inked circles in which the lines terminate. Filter points (31) and (62), lying on the spectral locus, would remain stationary. The exact displacements of points (70) and (72) are less certain since they are more remote from point (4800°K) whose displacement is known, but they would move in directions not far from parallel to the latter. Measurements on the color chart show that as a result of the displacements the distances between the paired points (31) and (99), and (62) and (23), are increased about 50 percent, while the distance between points (70) and (72) would remain practically unchanged. On the diagram the displacements of all the interior numbered points are represented as being equal, although actually they would not be: in this general region of the color chart, points lying closer to the long-wave limb of the spectral locus would be displaced less than points farther away; so that in every direction the ratio $f=s/S$ would remain about as it was. Hence, by Eq. (1) above, the diameter of the chromaticity cell in any given direction would change proportionally to S in that direction.

Thus it is seen that the cell receives a lateral shift from position A to position B, Fig. 1, accompanied by an increase of about 50 percent in its diameter in the direction of the displacement but no change in its transverse diameter.[10] Not only is the center of the cell removed a considerable distance in terms of unit chromaticity steps, its area increased by about 50 percent, its eccentricity altered, but also the direction of the major axis of the presumably elliptical cell has

[10] In the original determination of this chromaticity cell, seven pairs of filters were used. The three pairs considered here are sufficient to establish the outline of the displaced cell. The others were left out of account to simplify the argument, and also because the points on the color chart corresponding to some of these other filters lie too far away from the Standard Observer's 4800°K point to be able to predict safely their displacements.

been oriented through something like 90°, a circumstance that might be of much theoretical importance. It is likely that the contours of other parts of MacAdam's Fig. 48 would be equally altered, some places perhaps more so.

In appraising these very appreciable alterations of the diagram in terms of chromaticity differences, it must be remembered that the chromaticity cell in Fig. 1 is shown ten times its real size. On the scale to which it is drawn in the figure, any diameter of the cell is equivalent to about seven unit chromaticity steps (i.e., just perceptible differences of chromaticity). An objective idea of the chromaticity differences involved may be had by comparing the displacement of the center of the cell with the Standard Observer's blackbody locus. It may be seen that the separation of the centers of position *A* and position *B* of the cell almost equals the distance between the blackbody points (4800°K) and (2848°K); in other words, the chromaticity difference corresponding to the displacement is practically as great as that between "average noon sunlight" and the light of the ordinary gas-filled incandescent lamp. Even a much smaller anomaly of retinal pigmentation than that which has been assumed would give rise to substantial error unless taken into account.

The assumption was here made, for purposes of illustration, that PGN had less than the normal amount of retinal pigmentation. If in fact he has more than the normal amount, the pigment differences and the consequent aberrations in MacAdam's results could be even greater than those demonstrated. Before Wright's investigation of white point variations, the writer made a series of complementary color determinations upon eight individuals with trichromatic vision, the results of which revealed similar variations among those observers.[11] The white points of three of the writer's observers, determined by the complementary color method, are shown in Fig. 1 by the small triangles *d*, *e*, and *f*. The remaining observers' white points, not shown, all lie approximately on a line connecting points *d* and *e*. It will be seen that point *d*, belonging to the writer's observer with least pigmentation, nearly coincides with point *a*, belonging to Wright's observer with least pigmentation. There was a slight but not significant difference in the neutral illuminants used in the two investigations. The remaining white points of the writer's observers all lie within the area bounded by the lines *am* and *an*, that is, within the area over which the white points of Wright's observers are distributed, with the exception of point *f*. This fully authenticated point lies far outside the bounds of the region where all the other white points are to be found, and obviously not only did the observer to whom it belonged possess much more than the normal amount of pigmentation, but the pigment had unusual selective characteristics. Although only one such individual has been found among the very limited number of persons so far examined, that one is proof that exceptionally wide variations of pigmentation can occur, and the uncompensated effects of a pigmentation anomaly of this magnitude upon the outcome of an investigation similar to MacAdam's would be profound indeed.

The occurrence of individuals whose retinal pigmentation differs from normal sufficiently to cause serious error in the results of an investigation such as MacAdam's, unless taken into account, is by no means infrequent. Among the eight examined by the writer, three (those whose white points are shown in Fig. 1) fall definitely into this category, and at least one other is in the doubtful class. As to MacAdam's observer PGN, no proof, of course, has been offered nor any attempted that he is anomalous in retinal pigmentation. It may be that his pigmentation is close enough to that assigned to the Standard Observer so as not to give rise to any significant error in his results, and that the differences noted between his chromaticity sensibility data and those of other observers are altogether caused by inherent differences of the color sense. On the other hand, in view of these differences, the preponderance of probability would appear to favor a marked anomaly in PGN's pigmentation. The question can only be settled by experimental means.

Two experimental methods have been de-

[11] R. H. Sinden, "Studies Based on the Spectral Complementaries," J. Opt. Soc. Am. and Rev. Sci. Inst. **7**, 1123–1153 (1923).

scribed whereby the degree of an observer's pigmentation can be established, and also, if found necessary, corrective factors can be determined. These are the three-color method of Wright[8] and the complementary color method used by the writer.[11] Should PGN's retinal absorption be found significantly anomalous, it would be necessary to relocate on the color chart the colors corresponding to nearly all the 120 filters used in the investigation, and then to recalculate the coordinates of the 25 chromaticity cells shown on MacAdam's diagram. The relocation of the filter points could be accomplished experimentally either by Wright's method or by a method analogous to the determination of spectral complementaries. Wright's trichromatic method would have the advantage that only one observation would be necessary for each filter, while the "complementary color method" would require two. In a special case, namely, if the observer's (4800°K) point is found experimentally to lie on the line through points *a* and *c* in Fig. 1, or not far from this line, it might be possible to estimate the requisite corrections closely enough by calculative means without the necessity of an extended series of experimental observations, by using as a norm the average values for macular transmissivities found experimentally by Sachs,[12] although this method would have to be checked experimentally to find out whether it was applicable in any particular case.

Until PGN's retinal pigmentation has been experimentally established, it would seem unsafe to place too much dependence upon any apparent theoretical implications of this observer's chromaticity sensibility data as they now stand. For example, the agreement of these data with Judd's uniform-chromaticity-scale construction is not as close as one would have been led to expect by the agreement of the latter with the similar though less comprehensive data of other observers;[4] yet to discount this rationalized color system for that reason would hardly be justifiable, for, as has been shown, the configuration of MacAdam's chromaticity-cell aggregate might have to undergo major readjustments with reference to the uniform-chromaticity-scale diagram, should it eventuate that his observer has anomalous retinal absorption, and this might conceivably alter the over-all relationship between the two very materially. Various inferences of a theoretical nature which have already been deduced from these data may possibly require modification if the readjustment should prove necessary.

[12] See L. T. Troland, Trans. I. E. S. **11**, 956 (1916), for retinal transmission data.

Errata: Uses of Retardation Plates in Spectrophotometry

III. Measurement of Dichroic Samples

GEORGE L. BUC AND E. I. STEARNS
Research Department, Calco Chemical Division, American Cyanamid Company, Bound Brook, New Jersey

[J. Opt. Soc. Am. **35**, 521 (1945)]

MR. E. F. SMITH of Bakelite Corporation, Bound Brook, New Jersey has kindly pointed out that on page 523 in Eq. (6) the sign of the second term in line one should be + instead of −, the sign of line two should be − instead of +, and the sign of line four should be + instead of −.

The conclusions drawn from Eq. (6) in the original article need not be changed.